Dissertation zur Erlangung des Doktorgrades
der Fakultät für Chemie und Pharmazie
der Ludwig-Maximilians-Universität München

Evaluation of the natural compound Archazolid and its target V-ATPase for treatment of T-cell acute lymphoblastic leukemia

&

Evaluation of Cdk5 as target for breast cancer treatment

Siwei Zhang

Changchun, Jilin Province, P.R.China

2014

Erklärung

Diese Dissertation wurde im Sinne von §7 der Promotionsordnung vom 28. November 2011 von Frau Prof. Dr. Angelika M. Vollmar betreut.

Eidesstattliche Versicherung

Diese Dissertation wurde eigenständig und ohne unerlaubte Hilfe erarbeitet.

München, den _____

Siwei Zhang

Dissertation eingereicht am:

1. Gutachter:	Prof. Dr. Angelika M. Vollmar
2. Gutachter:	Prof. Dr. Stefan Zahler
Mündliche Prüfung am:	22.09.2014

To my family and friends

Contents

1 Introduction

1.1 Evaluation of the V-ATPase inhibitor Archazolid for treatment of T-cell acute lymphoblastic leukemia

1.1.1 Background

T-cell acute lymphoblastic leukemia (T-ALL) is an aggressive hematopoietic malignancy that is characterized by infiltration of the bone marrow with immature lymphoblasts that express T-cell surface markers (1). T-ALL accounts for 10%-15% of pediatric and 25% of adult acute lymphoblastic leukemia (ALL). T-ALL patients suffer from huge tumor burden, mediastinal enlargement and also have high risk of central nervous system (CNS) infiltration (1). These aggressive features in T-ALL make the treatment difficult and often result in poor prognosis. Thus, the cure rate of T-ALL had been lower than 10% for a long time due to high rate of relapse (1). Nowadays, various treatment approaches including aggressive-intensified combinational chemotherapy, radiotherapy, and stem cell transplants have improved the outcome of T-ALL treatment, with a 5-year event-free rate up to 75% in children and more than 50% in adults (1). However, the treatment of T-ALL remains a problem in the clinic due to resistance and relapse (1). Although the detailed mechanisms that contribute to poor outcome of the disease remain elusive, activating mutations in Notch1 were found in more than 50% of T-ALL cases, highlighting Notch1 as a key player in T-ALL (1, 2).

1.1.2 The Notch1 signaling pathway

The Notch signaling pathway requires the binding of Notch ligand [Delta/Serrate/Lag2 (DSL) in invertebrates and Delta-like/Jagged in mammals] on the signal-sending cell to the Notch receptor on the receiving cell for activation. Ligand binding triggers two subsequent proteolytic cleavages of the Notch receptor: 1) the first cleavage, so called S2-cleavage, is mediated by ADAM family (also called TNF-α converting enzyme, TACE) metalloprotease and generates a short-lived truncated fragment NEXT (Notch extracellular trunction) (3); 2) the second cleavage, i.e. S3-cleavage of the membrane-bound NEXT fragment, is mediated by the γ-secretase complex and results in release of the Notch intracellular domain (NICD) from the plasma membrane. NICD translocates into the nucleus where it initiates transcription of Notch target genes. Afterwards, NICD is rapidly targeted by the FBW7-SCF ubiquitin ligase complex resulting in proteosomal degradation (4).

1.1.3 Notch1 as a target for T-ALL treatment

Since γ-secretase is required for the S3-cleavage and thus Notch signaling activation, it is used as target to effectively block this oncogenic pathway. Inhibitors of γ-secretase (GSIs) have been developed for the treatment for Alzheimer's disease as the protease is implicated in the processing of Amyloid precursor protein (APP) which mediates the pathogenesis of the disease (1). Several studies have shown that GSIs effectively inhibit Notch signaling and induce cell cycle arrest in T-ALL cells harboring Notch1 activation mutations (2, 5, 6). However, several clinical trials investigating GSIs in T-ALL have shown that they exert mainly cytostatic effects and mostly failed to induce apoptosis (1, 2, 5) . Moreover, primary resistance to GSI treatment has been described (2, 7). As resistance is a major problem in T-ALL therapy, novel strategies to inhibit Notch1 signaling with alternative mechanisms different from GSIs could represent promising approaches for T-ALL therapy.

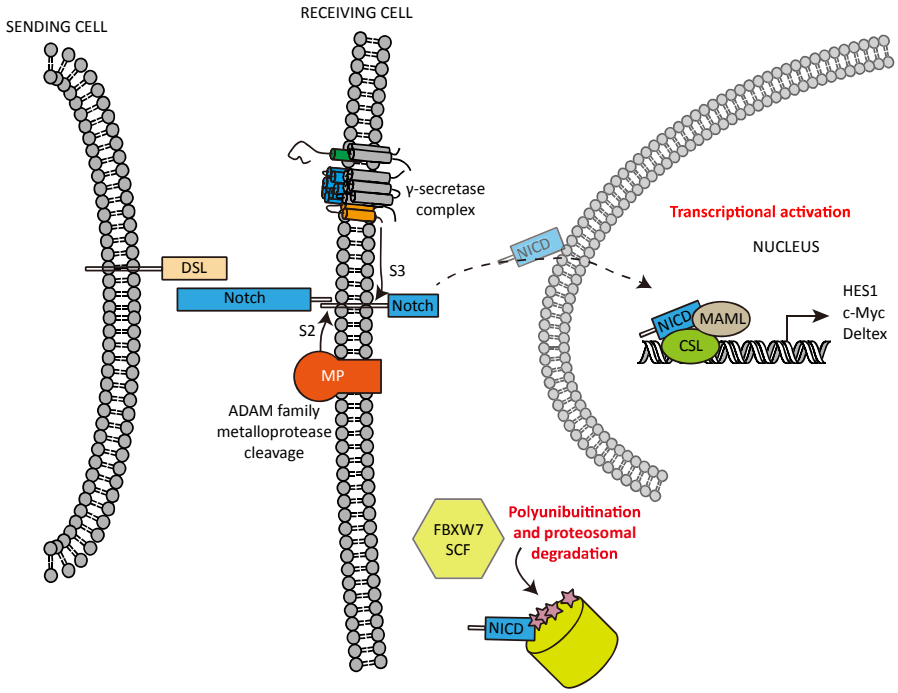

Figure 1.1 The Notch signaling pathway.

Binding of Notch ligand DSL initiates proteolytic cleavage of the Notch receptor. The ADAM family metalloprotease mediates S2-cleavage, generating the substrate for S3-cleavage by γ-secretase complex, which releases Notch intracellular domain (NICD). Subsequently, NICD translocates into the nucleus where it interacts with DNA-binding protein CSL (CBF1, Su(Human) and LAG-1). The co-activator Mastermind like (MAML) is recruited to the NICD-CSL complex mediating transcription of Notch downstream targets. Image adapted from Jon C. Aster, 2008(4).

1.1.4 The V-ATPase as cancer target

1.1.4.1 V-ATPase function and structure

Vacuolar (V)H+-ATPase (V-ATPase) is a multimeric membrane protein complex that ATP-dependently pumps protons across membranes and thereby regulates the pH of intracellular compartments as well as the cytoplasm (8). The organellar pH is strictly regulated and acidic pH is fundamental to various biological events such as membrane trafficking, the processing of receptor-ligand complexes and the maintenance of lysosomal enzymatic activities (8-10). V-ATPase is located at the plasma membrane where it can either acidify extracellular environments such as around osteoclasts and renal cells (8, 11-13), or modulate cytoplasmic pH as in neutrophils and macrophages (8, 14, 15).

Although the structure of V-ATPase (shown in Figure 1.2) is similar to that of F_0F_1-ATP-synthase (F-ATPase) (10), V-ATPase is not required for ATP synthesis. Eukaryotic V-ATPase is a membrane complex that consists of two domains working in a rotary mechanism (10, 16). The peripheral soluble V1 domain is located at the cytoplasmic side of the membrane, and possesses ATPase activity, i.e. it uses ATP as energy source to promote rotary movement. V1 consists of 8 different subunits (A-H) with multiple copies of some subunits. Three copies of each A and B subunits form a hexamer in a "ring-like" structure and the ATP binding site is located at the interface of the two subunits. The remaining subunits in the V1 domains are distributed between the peripheral (C, E, G, H) and central stalks (D, F) which connect V1 and V0 domains. They either pass the ATP-derived energy to a ring of proteolipid subunits in V0 serving as rotor or stabilize A3H3 hexamer-ring as a stator.
The membrane bound V0 domain is responsible for translocation of protons across the membrane (9, 11, 15). The V0 domain contains six different subunits (a,d,e,c,c' and c''). The hydrophobic membrane-embedded proteolipid subunits (c, c' and c'') form a ring (17) and each contains a buried Glu residue which is important for proton transport (10). Another crucial player of proton transport is the subunit a which hypothetically provides two H+ half channels that work together with the c, c'and c'' subunits (18). Protons enter the inner half channel and bind to buried Glu residues in the c-subunits. This is followed by rotation of the c subunits for nearly 360 degree and protons get transferred to a buried Arg (R735) residue within subunit a. Subsequently, the protons get then transferred to the outer half channel which is lined by buried charged residues on the C-terminal domain of subunit a and exit the membrane (10, 11).

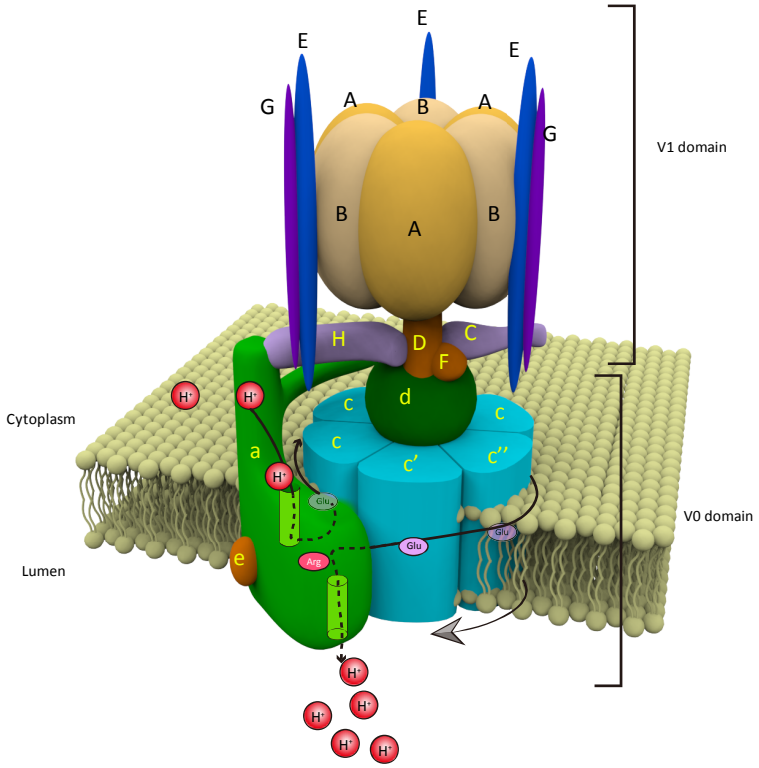

Figure 1.2: Structure of the V-ATPase

V-ATPase is a membrane-bound multimeric proton-translocating protein complex. V-ATPase is mainly composed of two domains, a peripheral V1 domain and a membrane integrated V0 domain. The V1 domain mediates ATP hydrolysis which provides energy for the rotary motion that is subsequently passed to the c-ring. Protons can enter the half-channel of the a-subunit in the V0 domain and thereafter bind to a Glu residue in the c-subunit. Rotation of the c-ring passes protons to the outer half-channel on the a-subunit, resulting in release of protons into the lumen. Image is adapted from Forgac, 2007(11).

1.1.4.2 V-ATPase inhibitors

Recent studies have demonstrated that V-ATPase is overexpressed in some types of cancer (19-21) and contributes to tumor metastasis, survival and growth (22, 23) . Therefore, V-ATPase inhibition represents an interesting anti-tumor target. Nowadays, only few V-ATPase inhibitors are known. Achieving a better understanding in the mode of action of the enzyme and its inhibitors would help to develop new drugs that might be promising anti-tumor therapeutics (24).

Class ONE: Plecomacrolides.

The plecomacrolide V-ATPase inhibitors bafilomycin and concanamycin were isolated from *Streptomyces* species in the early 1980s (25-28). The investigation of their structure-activity relationships has been intensively conducted (29-33). In the early 1990s, several studies

demonstrated that their V-ATPase binding site is located in the V0 domain (34). These findings were further corroborated by amino exchanges and radioactive labeling (cross-linking) studies, proving that plecomacrolides interact with the V0 c-subunit (35, 36).

Class TWO: Benzolacton Enamides

A new class of compounds, sharing a benzolactone enamide core structure, had entered the field in the late 1990s. Benzolacton enamides were found in different natural sources ranging from marine macroorganisms such as *Haliclona sp.* (salicylinhalamides) or *Aplidium lobatum* (lobatamides) to microorganisms such as the gram negative bacterium *Pseudomonas* sp. (oximidines) or the myxobacterium *Chondromyces sp.* (apicularens) (24, 37-40). These substances were demonstrated to be highly cytotoxic and showed a V-ATPase inhibition pattern similar to that of the plecomacrolides (24, 37-41).

Class THREE: Indolyls

Structure activity studies based on bafilomycin led to the discovery of major structural elements for V-ATPase inhibition (32) which allowed the identification of indole derivatives as structurally simplified V-ATPase inhibitors (42). The most potent one in this class of substances, referred to as INDOL0, showed V-ATPase inhibition in chicken osteoclast with an IC_{50} of 30 nM (43). INDOL0 has been shown to interact with subunit c of V-ATPase (44, 45) with a similar mode of inhibition as bafilomycin.

Class FOUR：New players: Archazolids

Archazolid was first isolated from myxobacteria *Archangium gephyra* and *Cystobacter violaceus* (46, 47). Archazolid contains a macrocyclic lactone ring bearing a thiazole side chain (24, 46, 47). Initial screening of biological activity of novel antibiotics originated from myxobacteria led to the discovery of Archazolid that later showed highly growth inhibitory effect in a set of mammalian cell lines due to V-ATPase inhibition (24, 47). Further studies confirmed V-ATPase as target of Archazolid with an IC_{50} in the nanomolar range (48).

Even though F-ATPases and Na+/K+-ATPases share structural similarity with V-ATPase, the effect of Archazolid was proved to be specific for V-ATPase. Moreover, Archazolid competes with the concanamycin binding site located in the V0 subunit c (48).

During recent years, our group has studied the function of Archazolid in invasive metastatic cancer cells and has elucidated that Archazolid A inhibited cell motility and induced apoptosis (49-51). Archazolid has attracted attention as highly potent V-ATPase inhibitor that exerts promising anti-tumor and anti-metastatic effects (49-51).

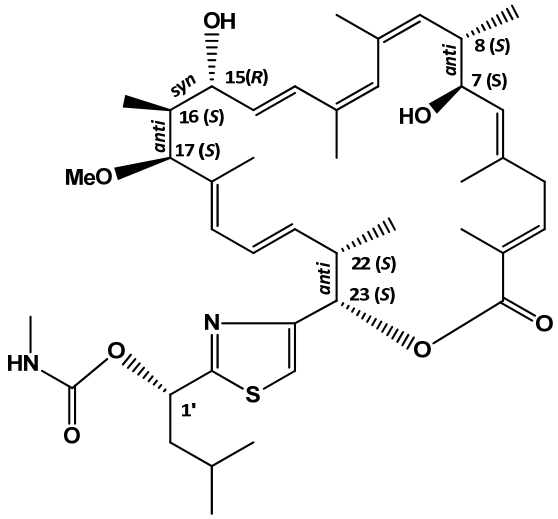

Figure 1.3 Chemical structure of Archazolids.
Image was adapted from Hassfeld, J. *et al* 2006 (52).

1.1.4.3 Aim of the study

It was shown recently that γ-secretase-mediated S3 cleavage of the Notch receptor occurs at endosomal compartments and requires low pH (53, 54). Moreover, reduced acidification of the endo-lysosomal system by inhibition of the vacuolar H+-ATPase (V-ATPase) impaired Notch processing and signaling activity (53, 55).

Interestingly, lysosome disruption has been shown to exert anti-leukemic effects which were based on increased lysosomal size and biogenesis in acute myeloid leukemia (AML) (56).

Along this line, this study aimed to investigate whether inhibition of V-ATPase by Archazolid A could inhibit Notch signaling in a way different from GSI and therefore might be an alternative strategy for leukemia treatment.

1.2 Evaluation of Cdk5 as target for breast cancer treatment

1.2.1 Breast cancer and its treatment

Breast cancer represents one of the most common cancer types among women, and its incidence is increasing every year. For many years, the treatment of breast cancer had solely depended on cytotoxic chemotherapy (57). Nowadays, conventional treatment of breast cancer involves surgery, radio- and chemotherapy leading to markedly reduced mortality (58). Notably, the treatment of breast cancer has evolved to a more tailored, target-directed therapy, based on the presence of estrogen receptors, progesterone receptors, and human epidermal growth factor receptor 2 (HER2/Neu, also known as ErbB2, a member of the epidermal growth factor receptor family) (57, 59, 60). The blockade of EGF to HER2/Neu receptor by the therapeutic monoclonal antibody Trastuzumab (Herceptin®, Roche) increased survival of patients with HER2-overexpressing breast cancer (61-63). However, response to Herceptin therapy is limited due to its requirement for HER2 expression.
Despite the major progress achieved in breast cancer treatment in the past years, the treatment of "triple-negative" breast cancer, which lacks the expression estrogen receptor, HER2/Neu and progesterone receptors, was rather unsuccessful. Triple-negative breast cancers are very aggressive, and have the poorest prognosis amongst the different subtypes. Due to the absence of these three major targets of conventional treatment, fighting this type of breast cancer requires combined therapies and effective treatment options are strongly limited. Therefore, it is of great importance to identify alternative novel targets for the treatment of breast cancer.

1.2.2 Breast cancer stem cells

During recent years, research indicated that the high relapse rate of aggressive breast cancers is associated with a small subpopulation of breast cancer cells, i.e. breast cancer stem cells (CSCs). Breast CSCs have the characteristic of $CD44^{+}/CD24^{-/low}$ mesenchymal phenotype, undergo asymmetric cell division, show high tumor-initiating potential, and are resistant to common therapies(64). There is growing evidence that CSCs are the main cause for cancer relapse and metastasis formation. It was shown that "successful" metastasis formation requires the CSC to migrate from the primary tumor followed by establishment of metastasis in a secondary site (65).
The epithelial to mesenchymal transition (EMT) is a well-coordinated and multistep process during which epithelial cells lose their epithelial properties and acquire mesenchymal characteristics (65). This process is critical for embryonic development when cells change their morphology, lose cell-cell adhesion and cell polarity, and acquire migratory and invasive characteristics (66). There is

growing body of evidence that the abnormal activation of the EMT developmental program contributes to tumor metastasis and that this process enables tumor cells to migrate from their primary site and also promotes their ability of self-renewal(66-68). Thus, EMT was reported to be essential for CSCs formation and maintaining "stemness" (69-71).
Thus, EMT plays a fundamental role in metastasis, therapy resistance, and tumor recurrence by causing CSC formation(65). After chemotherapy, residual tumors have been shown to be enriched in CSCs and possess gene signatures with hallmarks of EMT like properties (64, 72, 73).

Therefore, targeting breast CSCs/EMT may be an attractive strategy to treat resistant and recurrent breast cancers and might improve breast cancer therapy and patient prognosis.

1.2.3 Cyclin dependent kinase 5 (Cdk5)

1.2.3.1 Cdk5 and its functions

Cyclin-dependent kinase 5 (Cdk5) is a proline-directed serine/threonine kinase which was discovered in 1992 and is structurally related to Cdc2/Cdk1, sharing approximately 60% sequence identity (74-77). Cdk5 is a unique member of the Cdk family. Unlike classical mitotic Cdks, Cdk5 is not mainly involved in controlling cell cycle transitions, but is highly expressed in neuronal tissues where it exerts important functions. Cdk5 is important for the layering of the CNS during development (78), i.e. Cdk5 knockout mice die perinatally and show severe defects in neuronal positioning. In a cellular context, Cdk5's function in neurons is well studied: Cdk5 regulates actin dynamics, neuronal migration, adhesion, membrane transport and synaptic processes (79, 80). Deregulation of neuronal Cdk5 contributes to neurodegenerative diseases, amongst them Alzheimer's disease, where constitutively active Cdk5 results in hyper-phosphorylation of tau (81, 82). Due to its high abundance and importance in the CNS, Cdk5 was thought to be neuron-specific for a long time. However, recently, non-neuronal functions of Cdk5 gained attention and Cdk5 has been shown to be implicated in regulating cell migration, cell death and survival in peripheral tissues (83-85).

1.2.3.2 Cdk5 inhibitor (*R*)-Roscovitine

Characterization of 2,6,9-trisubstituted purines led to the discovery of Cdk inhibitors (86-88), amongst them Roscovitine. It is a close analogue to olomoucine, one of the first 2,6,9-trisubstituted purine Cdk inhibitors, but exerts increased potency and selectivity towards Cdk5 (88). Roscovitine acts only on Cdk1, Cdk2, Cdk5, Cdk7 and Cdk9 (IC_{50} below 1μM) to a relevant degree (88). Further structure-activity studies have shown that (*R*)-Roscovitine (Seliciclib, CYC202) is more potent than

its (*S*)-stereoisomer in inhibiting cdc2/cyclin B (87). Since it was discovered, studies have shown that Roscovitine exerts anti-mitotic and pro-apoptotic effects in various types of tumors (89). Also, by inhibiting Cdk5 activity, Roscovitine functioned cell cycle-independently, showed anti-angiogenic and anti-inflammatory effects (84, 85) and inhibited cell motility (90).

1.2.4 Aim of the study

A tissue microarray (TMA) from 204 patient samples with various types and stages of breast cancer was analyzed in collaboration with Prof. Dr. Doris Mayr and Dr. Elisa Schmoeckel (Institute of Pathology, LMU, Munich). Immunohistochemical staining of the TMA indicated an involvement of Cdk5 in breast cancer. As shown in Figure 1.4, breast cancer cells showed markedly higher expression of Cdk5 comparing to normal breast tissue.

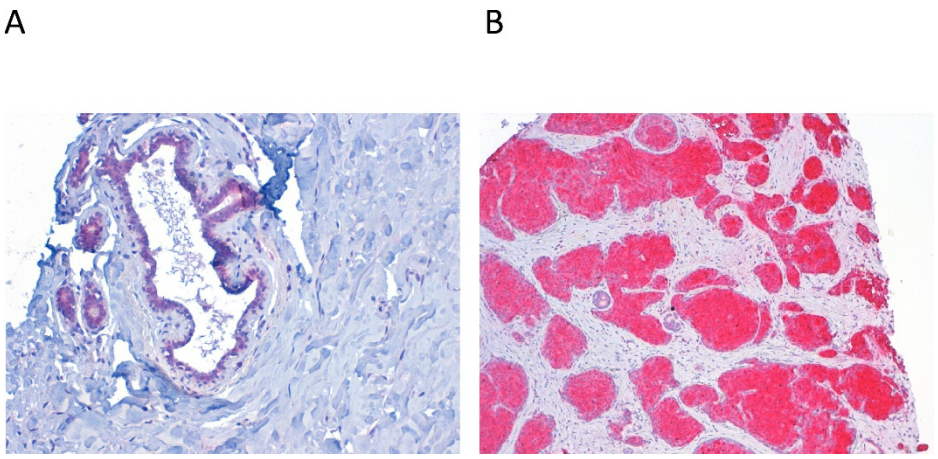

Figure 1.4 Immunostainings for Cdk5 in healthy and breast cancer samples are shown. (A) Staining of Cdk5 in healthy mamma tissue is shown. (B) Breast cancer tissues shown an increased Cdk5 staining.

Therefore, the aim of this study was to elucidate the function of Cdk5 in breast cancer progression, focusing on tumor cell growth, motility as well as effects on breast cancer stem cells.

2 Materials and Methods

2.1 Materials

2.1.1 Compounds

(*R*)-Roscovitine was obtained from Sigma-Aldrich.

Archazolid A was purified, isolated as described previously (47) and provided by the group of Rolf Müller.

The γ-secretase inhibitor Dibenzazepine (DBZ) was purchased from Merck (Darmstadt, Germany).

The compounds were dissolved in dimethyl sulfoxide (DMSO) and stored at -20℃. For experiments, compounds were freshly diluted in culture medium. The final concentration of DMSO didn't exceed 0.1%.

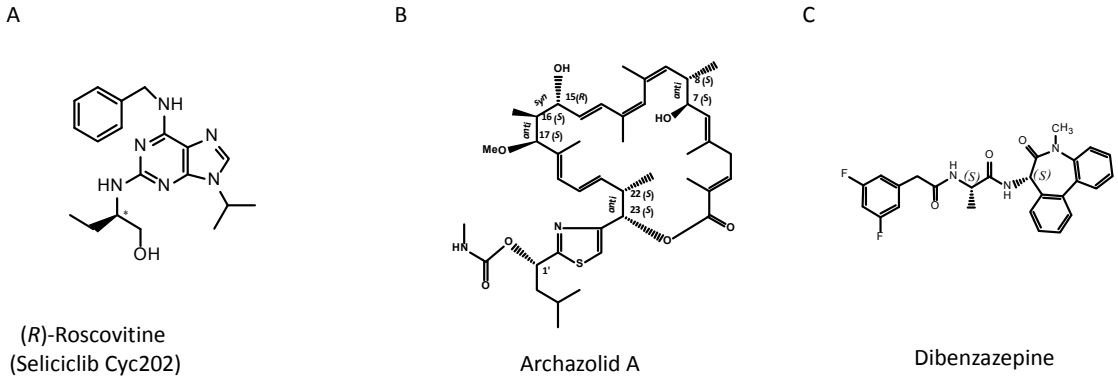

Figure 2.1 Chemical structures of (R)-Roscovitine, Archazolid A and DBZ are shown.

2.1.2 Biochemicals, inhibitors, dyes and cell culture reagents

Table 2.1: Biochemicals, inhibitors, dyes and cell culture reagents.

Reagent	Producer
Accustain® paraformaldehyde (PFA)	Sigma-Aldrich, Taufkirchen, Germany
B27® Supplement (50×)	Life technologies, Carlsbad, USA
Bovine serum albumin (BSA)	Sigma-Aldrich, Taufkirchen, Germany
Bradford reagent, Roti-Quant®	Carl-Roth, Karlsruhe, Germany
CellTiter-Blue®	Promega, Manheim, Germany
CellTracker™ Green CMFDA	Life technologies, Carlsbad, USA
Chromium(III) potassium sulfate dodecahydrate	Merck, Darmstadt, Germany

Collagen G	Biochrom AG, Berlin, Germany
Complete™ mini EDTA free	Roche diagnostics, Penzberg, Germany
Crystal violet	Carl Roth, Karlsruhe, Germany
Cyclohexylamino-1-propane sulfonic acid(CAPS)	Merck, Darmstadt, Germany
Dimethyl sulfoxide (DMSO)	Sigma-Aldrich, Taufkirchen, Germany
Dithiothreithol (DTT)	AppliChem, Darmstadt, Germany
DMEM (high glucose)	PAA Laboratories, Pasching, Austria
Dulbecco's Modified Eagle Medium (DMEM)	PAA Laboratories, Pasching, Austria
EDTA	Carl Roth, Karlsruhe, Germany
Epidermal growth factor, human (hEGF)	Peprotech, Rocky Hill, USA
Fetal calf serum gold (FCS gold)	PAA Laboratories, Pasching, Austria
Fibroblast growth factor-basic, human (bFGF)	Peprotech, Rocky Hill, USA
FluorSave™ Reagent mounting medium	Merck, Darmstadt, Germany
Gelatin (Type A) From Porcine Skin	Sigma-Aldrich, Steinheim, Germany
Glutamine	Sigma-Aldrich, Taufkirchen, Germany
Glycine	Sigma-Aldrich, Taufkirchen, Germany
Hoechst (bisBenzimide H33342)	Sigma-Aldrich, Taufkirchen, Germany
LysoTracker® dye	Molecular Probes, Darmstadt, Germany
MEGM™ Bullet Kit	Lonza, Basel, Switzerland
Methylcellulose	Sigma-Aldrich, Taufkirchen, Germany
Na_3VO_4	ICN Biomedicals, Aurora, Ohio, USA
NaF	Merck, Darmstadt, Germany
Non-fat dry milk powder (Blotto)	Carl Roth, Karlsruhe, Germany
Page Ruler™ Prestained Protein Ladder	Fermentas, St. Leon-Rot, Germany
Penicillin/Streptomycin 100×	PAA Laboratories, Pasching, Austria
Phenylmethylsulfonyl fluoride (PMSF)	Sigma-Aldrich, Munich, Germany
Poly(2-hydroxyethyl methacrylate) (Poly-HEMA)	Sigma-Aldrich, Taufkirchen, Germany
Polyacrylamid (Rotiphorese® Gel A 30%)	Carl Roth, Karlsruhe, Germany
Propidium iodide (PI)	Sigma-Aldrich, Taufkirchen, Germany
Puromycin Dihydrochloride, ready made solution	Sigma-Aldrich, Taufkirchen, Germany
Pyronin Y	Sigma-Aldrich, Taufkirchen, Germany
Pyruvate	PAA Laboratories, Pasching, Austria

RPMI 1640	PAN Biotech, Aidenbach, Germany
Tris-Base	Sigma-Aldrich, Taufkirchen, Germany
Tris-HCl	Sigma-Aldrich, Taufkirchen, Germany
Trisodium citrate	Carl Roth, Karlsruhe, Germany
Triton X-100	Merck, Darmstadt, Germany
Trypsin	PAN Biotech, Aidenbach, Germany
Tween®20	AppliChem, Darmstadt, Germany
β-Mercaptoethanol	Sigma-Aldrich, Taufkirchen, Germany

Table 2.2: Commonly used buffers

PBS+ Ca^{2+}/Mg^{2+} (pH 7.4)	
NaCl	137 mM
KCl	2.68 mM
Na_2HPO_4	8.10 mM
KH_2PO_4	1.47 mM
$MgCl_2$	0.25 mM
H_2O	

PBS (pH 7.4)	
NaCl	132.2 mM
Na_2HPO_4	10.4 mM
KH_2PO_4	3.2 mM
H_2O	

Trypsin/EDTA (T/E)	
Trypsin	0.05%
EDTA	0.20%
PBS	

Collagen G	
Collagen G	0.001%
PBS	

2.1.3 Technical equipment

Table 2.3 Technical equipment

Name	Device	Producer
ABI 7300 RT-PCR	Real-time PCR system	Applied Biosystems, Foster City, USA
Axiovert 25 / 200	Inverted microscope	Zeiss, Jena, Germany
Canon EOS 450D	Digital camera	Canon, Tokio, Japan
Culture flasks, plates, dishes	Disposable cell culture material	TPP, Trasadingen, Switzerland
FACSCalibur	Flow cytometer	Becton Dickinson, Heidelberg, Germany
Hera Cell	Incubator	Heraeus, Hanau, Germany
IBIDI™ µ-slide	Microscope slide	Ibidi GmbH, Munich, Germany
Leica TCS SP8	Confocal laser scanning microscope	Leica, Wetzlar, Germany
LSM 510 Meta	Confocal laser scanning microscope	Zeiss, Jena, Germany
Megafuge 1.0s	Centrifuge	Heraeus, Hanau, Germany
Mikro 22R	Table centrifuge	Hettich, Tuttlingen, Germany
Nanodrop® ND-1000	Spectrophotometer	Peqlab,Wilmington, USA
Olympus DP25 Microscope	Biological microscope	Olympus, Hamburg, Germany
Primus 25 advanced	Thermocycler	Peqlab, Wilmington, USA
SpectraFluor Plus™	Microplate multifunction reader	Tecan, Männedorf, Switzerland
TB1	Thermoblock	Biometra, Göttingen, Germany
Vi-Cell™ XR	Cell viability analyzer	Beckman Coulter, Fullerton, CA, USA

2.2 Methods

2.2.1 Cell culture

The human breast cancer cell line MDA-MB-231 was purchased from CLS cell lines service GmbH (Eppelheim, Germany) and maintained in DMEM supplemented with 10% fetal calf serum (FCS) (PAA Laboratories, Cölbe, Germany).

Human leukemia Jurkat T cells (J16) (S-Jurkat) were kindly provided by P.H. Krammer and H. Walczak (Heidelberg, Germany). S-Jurkat cells were cultured in RPMI 1640 medium (PAN Biotech, Aidenbach, Germany) supplemented with 10% FCS and 1% sodium pyruvate (PAA Laboratories, Pasching, Austria). CEM (CCRF-CEM) cells were kindly provided by Dr. Joachim Arend (Mainz, Germany). CEM cells were cultured in RPMI 1640 medium supplemented with10% FCS.

All cell lines were cultivated at 37°C with 5% CO_2 in a humidified incubator.

MDA-MB-231 cells were passaged (1:10) every 3-4 days. Therefore, the growth medium was removed and the cells were washed with pre-warmed PBS. Cells were detached by incubating with 2ml Trypsin/EDTA for 5 min at 37℃. To terminate trypsin reaction, 7ml stopping-medium containing FCS was added. Subsequently, cells were centrifuged and supplied with fresh medium.

Leukemia cell lines were passaged every 2-3 days. S-Jurkat cells were maintained at a density below 1×10^6 cells/ml. CEM cells were maintained at a density below 2×10^6 cells/ml.

The cell lines were used up to passage 25.

Table 2.4 Growth medium for different cell lines

MDA-MB-231 growth medium		**CEM growth medium**	
DMEM	500 ml	RPMI 1640	500 ml
FCS gold	50 ml	FCS gold	50 ml
Pen / Strep*	5 ml	Pen / Strep*	5 ml
MDA-MB-231 shRNA-clones medium		**S-Jurkat growth medium**	

DMEM	500 ml	RPMI 1640	500 ml
FCS gold	50 ml	FCS gold	50 ml
Pen / Strep*	5 ml	Pen / Strep*	5 ml
Puromycin (10 mg/ml)	55 µl	Sodium pyruvate	1%

* Pen / Strep: Penicillin 10 000 Units/ml, Streptomycin 10 mg/ml

2.2.2 Seeding for experiments

MDA-MB-231 cells were seeded (1:3-1:5) in multiwell plates for experiments up to 48 h. Leukemia cell lines were seeded at 5×10^5 cells/ml (for experiments up to 24 h) or at 1×10^5 cells/ml (for experiments up to 48 h).

2.2.3 Freezing and thawing

Nitrogen stocks were prepared for each cell line. For MDA-MB-231 cells, cells were detached by Trypsin/EDTA and collected by centrifugation. Suspension cells were collected by centrifugation. Cells were resuspended in freezing medium (70% normal medium for each cell line, 10% DMSO and 20% additional FCS), transferred to cryovials (2-4×10^6 cells in 1.5 ml per vial) and kept at -80°C and transferred to liquid nitrogen (-196°C) after two days for long-term storage.

2.3 Proliferation Assay

2.3.1 Proliferation assay for breast cancer cells using crystal violet staining

MDA-MB-231 cells were seeded in 96-well plates (1,500 cells per well). After overnight incubation, cells in a reference plate were stained with crystal violet and served as initial control. The cells in a treatment plate were either left untreated or treated with indicated concentrations of Roscovitine for 72 h. After treatment, the medium was removed and cells were stained with crystal violet for 10 min, RT. Afterwards, the plate was rinsed with water to remove free crystal violet and was dried overnight. Cell-bound crystal violet was dissolved with sodium citrate buffer and the absorbance which correlates with cell number was measured at 550nm using a SpectraFluor Plus™ (Tecan, Männedorf, Switzerland) plate reader. For statistical analysis, cells treated with vehicle control were set to 100%.

Table 2.5 Crystal violet and sodium citrate buffer.

Crystal violet staining solution		Sodium citrate buffer	
Crystal violet	0.5%	$Na_3C_6H_5O_7$	0.05 M
Methanol	20%	Ethanol	50%
H_2O		H_2O	

2.3.2 Proliferation assay for leukemia cells by CellTiter-Blue® Assay

S-Jurkat and CEM cells were collected by centrifugation and subsequently resuspended in culture medium at 3×10^4 cells/ml. 100 µl of the cell suspension was seeded into a 96-wells. The next day, Archazolid A and DBZ were added. After 70 h of incubation, 20µl CTB solution was added and incubated at 37℃ for further 2h. Fluorescence ($550_{Ex}/590_{Em}$) was measured using a SpectraFluor Plus™ (Tecan, Männedorf, Switzerland) plate reader. For statistical evaluation, cells with vehicle control were set to 100% viable cells.

2.4 Flow cytometry

Flow cytometry (FCM) was used for the analysis of cell death, apoptosis and cell cycle. Measurements were performed using a FACS Calibur (Becton Dickinson, Heidelberg, Germany).

Table 2.6 FACS buffer for FACSCalibur

Sheath fluid (pH 7.37)	
NaCl	8.12 g
KH_2PO_4	0.26 g
Na_2HPO_4	2.35 g
KCl	0.28 g
Na_2EDTA	0.36 g
LiCl	0.43 g
NaN_3	10 mM
H_2O	ad 1,000 ml

2.4.1 Quantification of cell death

Quantification of cell death was either performed according to Nicoletti *et al* (91) or by propidium iodide (PI) exclusion.

2.4.1.1 Quantification of apoptotic cell death and cell cycle analysis using the Nicoletti assay.

Cells (1×10^5 cells/ml was used for 24 h and 48 h experiments; 5×10^4 cells/ml was used for 72 h experiments) were seeded in 24-well-plates and stimulated with the respective substances for indicated times. After stimulation, cells were collected by centrifugation (600 xg, 10 min, 4℃). Supernatants were discarded and pellets were washed with PBS twice. For PI staining, cell pellets were resuspended in HFS-solution containing PI (50µg/ml) and incubated at 4℃ overnight followed by analysis via flow cytometry the next day.

Table 2.7 HFS solution

HFS solution	
Sodium citrate	0.1%
Triton X-100	0.1%
PBS	Add 1 ml

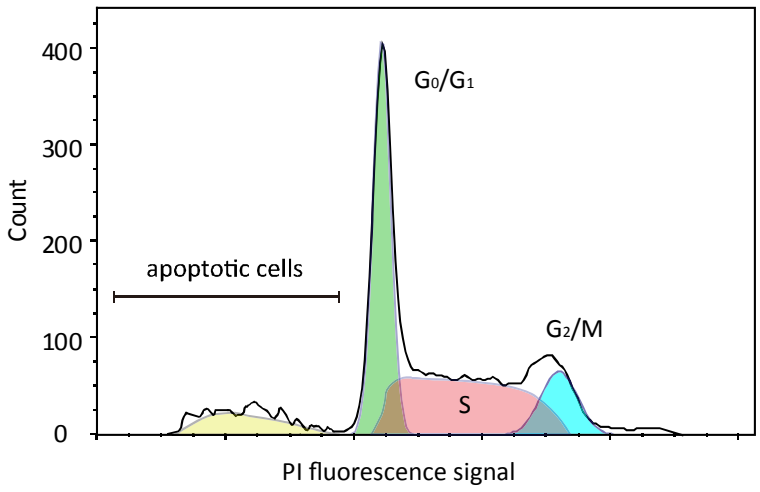

Figure 2.2: Analysis of apoptotic cells and cell cycle.

Since PI quantitatively stains DNA, the fluorescence intensity depends on the respective DNA content of the cell. As the DNA content changes during duplicating, the different stages (G_0/G_1-phase, S-phase, G_2/M-phase) during cell cycle can be distinguished, i.e. the fluorescence intensity of the cells in G_2/M-phase would be twice as high as that of cells in the G_0/G_1-phase. In the S-phase, fluorescence intensity is between the G_0/G_1 and G_2/M. When cells undergo apoptosis, DNA gets condensed and fragmented, resulting in the sub-G_0/G_1 peak left of the G_0/G_1 peak. The relative amount of cells in different cell cycle phases was quantified using the FlowJo 7.6 analysis software (Tree Star Unc., Ashland, USA).

2.4.1.2 PI exclusion assay for leukemia patient samples

Leukemia patient samples were obtained from Helmholtz Center Munich.

Cells were collected by centrifugation and resuspended in RPMI 1640 medium supplemented with 20% FCS, 1% Glutamine and Penicillin/Streptomycin. Cell number was adjusted to 1×10^6 cells/ml and 100µl of cell suspension per wellwere seeded into 96-well-plates. Tested substances were diluted to 2-fold end concentration in culture medium, and 100 µl were added to the cells. Medium with the same amount of DMSO was used as control. After treatment for 48 h, cells were stained with 300 µl PI-PBS solution (end concentration 5 µg/ml) before incubation for 5 min in the dark on ice followed by analysis via flow cytometer. Cells with high PI intensity were considered dead.

2.5 Colony formation assay

2.5.1 Colony formation assay for adherent breast cancer cells

MDA-MB-231 cells were seeded and stimulated with Roscovitine (10 µM, 20 µM, 30 µM) for 24 h. For Cdk5 silencing, nt or Cdk5 siRNA transfected cells were seeded 24 h after transfection. Nt or Cdk5 shRNA cells were directly seeded.

After treatment, cells were trypsinized and 5,000 cells per well were seeded in a 6-well plate. The cells were allowed to grow for 7 days. Cells were stained with crystal violet for 10 min. The plate was rinsed with water to remove free crystal violet and dried overnight. Representative pictures from each treatment were taken. Cell-bound crystal violet was dissolved with sodium citrate buffer and the absorbance which correlates with cell number was measured at 550nm at the SpectraFluor Plus™ (Tecan, Maennedorf, Switzerland) plate reader. For statistical analysis, cells treated with vehicle control were set to 100%.

2.5.2 Colony formation assay for leukemia cell lines

Leukemia cells were adjusted to 5×10^5 cells/ml, and 1ml of the cell suspension was added to a 6-well and stimulated with Archazolid A and DBZ for 24 h. Cells were washed once with PBS and resuspended in 1.5 ml culture medium. After counting and adjusting the cell number to 5×10^5 cells/ml, 100 µl of the suspension were mixed with 900µl colony formation assay medium, vortexed and seeded (100 µl) into 96-well-plates (3 wells per treatment). Then the plates were incubated for 11days in the incubator. After treatment, images from each well were taken with a Zeiss 510 Meta Confocal Microscope. Colonies formed with more than four cells were counted with Image J (NIH, USA) using the cell counter plugin.

Table 2.8 Colony formation assay medium for leukemia cell lines

RPMI 1640 Medium	
FCS gold	40%
Methylcellulose	(0.52%)
Sodium pyruvate	1%
(included only for S-Jurkat Cells)	

2.6 Cell motility assays

Transwell® permeable supports (8 µm pore size, 6.5 mm inserts) were used according to the manufacturer's instructions. The transwell inserts were coated with collagen G for transwell migration assay or with Matrigel® for invasion assay. Transwell inserts were placed into 24-well plates containing 700µl DMEM with 0.1% BSA (negative control, -Co), or 700 µl DMEM containing 10% FCS and 0.1% BSA (positive control, +Co). 1×10^5-3×10^5 cells labeled with CellTracker™ Green CMFDA were added to the inserts, and allowed to migrate for 16 h. In the experiment with Roscovitine, MDA-MB-231 cells were pretreated with Roscovitine for 24 h and allowed to migrate in the presence of Roscovitine in both upper and lower chamber. After 16 h of migration, the non-migrated cells in the upper chamber were removed with cotton swab. Then the inserts were put in the wells 24-well plate containing PBS^+(Ca^{2+}/Mg^{2+}). Pictures of each inserts were taken using a Axiovert 25/200 microscope (Zeiss, Jena, Germany). Four pictures from each group were taken and cell numbers were counted with Image J using the cell counter plugin.

2.7 Mammosphere assay

Mammosphere assays were performed according to Dontu G *et al* (92).
MDA-MB-231 cells were freshly seeded and stimulated with Roscovitine at indicated concentrations for 24 h. The cells were washed with PBS and detached by trypsin/EDTA and collected by centrifugation. Cell pellets were resuspended in mammosphere culture medium at 40,000 cells/ml. 1 ml of cell suspension was added to a poly-HEMA coated 12-well plate and cells were allowed to form mammospheres for 10 days. In the case of Roscovitine repeated treatment, Roscovitine was added every second day. In the case of nt/Cdk5 shRNA clones, the cells were freshly seeded in the same density in mammosphere medium containing puromycin. After treatment, mammospheres larger than 50μm were counted. Untreated cells (Co) or nt shRNA were set as 100%.

Table 2.9 Mammosphere culture medium

Content	Amount
MEGM™ Bullet Kit (Lonza)	500 ml
EGF	20 ng/ml
bFGF (human)	10 ng/ml
Gibco® B-27® Supplements	50 ml
Methylcellulose	1%
Puromycin (for nt/Cdk5 shRNA clones)	1 μg/ml

2.8 Western blotting

2.8.1 Whole cell lysate preparation

For Western blot analysis, cells were treated with desired substances as indicated.
Cells were detached by trypsin/EDTA (for adherent cells) or directly collected by centrifugation and washed twice with ice-cold PBS, centrifuged, then appropriate amounts of lysis buffer were added. Samples were incubated on ice for 30 min and vortexed every 10 min. Lysates were centrifuged at 14,000 rpm for 10 min. Supernatants were collected and transferred to a new tube. Protein concentrations were determined according to Bradford (93). Samples were diluted with 5x SDS sample buffer (4 parts lysate, 1 part buffer) and boiled for 5 min at 96℃. Samples were stored at -20℃ until further analysis.

Table 2.10 Buffers for the preparation of total cell lysates

Lysis buffer	
Tris-HCl, pH 7.5	30 mM
NaCl	150 mM
EDTA	2 mM
Triton X-100	1%
H_2O	Add 1,000 µl
Complete™	1:25

Lysis buffer for phospho-proteins	
Tris-Base	20 mM
NaCl	137 mM
EDTA	2 mM
Triton X-100	1%
$C_3H_7Na_2O_6P$	20 mM
NaF	10 mM
Na_3VO_7	2 mM
$Na_4P_2O_7$	2 mM
PMSF	1 mM
Glycerol	10%
Complete™	1:25

5x SDS sample buffer	
Tris-HCl, pH6.8	3.125 M, 100 µl
Glycerol	500 µl
SDS 20%	250 µl
DTT 16%	125µl
Pyronin Y 5%	5 µl
H_2O	Add 1,000 µl

2.8.2 Protein quantification

To employ equal amounts of protein for Western blot analysis, protein concentration was determined by Bradford assay (93). 10 µl protein samples were 1 : 10 diluted in water and mixed with 190 µl Bradford solution for 5 min. Afterwards, absorbance was measured at 592 nm using Tecan Sunrise™ Microplate reader. Serial diluted BSA samples were used as protein standards. Linear regression was used to calculate protein concentration from each sample.

2.8.3 Sample preparation

After protein quantification, each sample was mixed with 5x SDS sample buffer as predescribed, and protein concentration was adjusted to the lowest concentration by adding 1x SDS sample buffer. Afterwards, the samples were boiled at 95℃ for 5 min. At this stage, the samples were kept at -20℃ or directly subjected to SDS-PAGE analysis.

2.8.4 SDS-PAGE

The SDS-PAGE gels were prepared in a discontinuous manner, with a stacking gel (Tris, pH 6.8) on top of the separation gel (Tris, pH 8.8). The concentrations of acrylamide in the separation gels were adjusted to optimize the separation of proteins according to their molecular weights.

The Mini-PROTEAN 3 electrophoresis module (Bio-Rad, Munich, Germany) was used. Prior to sample loading, the apparatus was assembled according to manufacturer's protocol and the chamber was filled with pre-cooled electrophoresis buffer.

Before loading, samples were boiled at 95°C for 5 min. Equal amounts of protein (volume) from each sample were loaded on to the stacking gel.

An equal volume of 1x SDS sample buffer containing 2 µl of prestained protein ladder PageRuler™ was loaded on each gel to estimate the molecular weights of the separated proteins. Electrophoresis was carried out at 100 V for 21 min for protein stacking and 200 V for 35-45 min for protein separation.

Table 2.11 Acrylamide gels

Stacking gel		Separation gel 12 %	
Rotiphorese™ Gel 30	1.7 ml	Rotiphorese™ Gel 30	6 ml
Tris-HCl 1.25M, (pH 6.8)	1 ml	Tris-HCl 1.25M, (pH 6.8)	3.75 ml
SDS 10%	100 µl	SDS 10%	150 µl
TEMED	20 µl	TEMED	15 µl
APS 10%	100 µl	APS 10%	75 µl
H_2O	7.0 ml	H_2O	5.1 ml

Table 2.12 Electrophoresis buffer

Electrophoresis buffer	
Tris	4.9 mM
Glycine	38 mM
SDS	0.1%
H_2O	6.1 ml

2.8.5 Semi-dry blotting

After protein separation, proteins on the gel were transferred onto a nitrocellulose membrane (Hybond ECL™, Amersham Bioscience, Freiburg, Germany) by semi-dry blotting.

The membrane was equilibrated with anode buffer 30 minutes before use. Blotting papers soaked in 4℃ pre-cooled buffers were used to build the blotting sandwich in the Trans-Blot® SD Semi-Dry Electrophoretic Transfer Cell (Bio-Rad). Transfers were carried out at room temperature at 133 mA (for two gels) for 60 minutes.

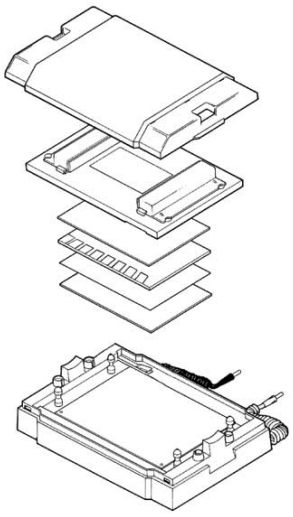

Figure 2.3 Assembly of semi-dry blot sandwich. Image was adapted from Bio-Rad, Trans-Blot® SD Semi-Dry Assembly Guide.

Table 2.13 Semi-dry blotting buffers

5x Tris-CAPS:	
Tris-Base	36.24 g
CAPS (Amersham)	44.26 g
H_2O	To 1000 ml

Anode buffer		**Cathode buffer**	
5x Tris-CAPS	20 ml	5x Tris-CAPS	20 ml
Methanol	15 ml	10% SDS	1 ml
H_2O	to 100 ml	H_2O	to 100 ml

2.8.6 Protein detection

After transferring proteins to the membrane, the gels were stained with comassie blue. Unspecific epitopes were blocked for 1 h (RT) with either 5% blotto or 5% BSA in PBS according to the requirements of different antibodies. Membranes were washed with 1x PBS-T and incubated with respective antibodies at 4℃ overnight. The next day, the membranes were washed three times for 10 min with 1x PBS-T and then incubated in secondary antibodies for 2 h at room temperature.

Table 2.14: Primary antibodies used for Western blotting analysis

Antigen	**Source**	**Dilution**	**Provider**
β-actin	Mouse monocl.	1:1000	Millipore
Cdk5 human	Mouse monocl.	1:1000	Invitrogen
Cleaved Notch1 (Val1744) (D3B8)	Rabbit monocl.	1:1000	Cell Signaling Technology, Inc
Notch1 (D1E11) XP®	Rabbit monocl.	1:1000	Cell Signaling Technology, Inc
Survivin	Rabbit polycl.	1:1000	Cell Signaling Technology, Inc
c-Myc (C-19)	Rabbit polycl.	1:500	Santa Cruz Biotechnology
β-tubulin	Rabbit polycl.	1:1000	Cell Signaling Technology, Inc

Antibodies were diluted according to manufacturer's instructions.

Table 2.15 : Secondary antibodies used for Western blotting analysis

Antibody	Dilutions in Blotto 1%	Provider
HRP, Goat-Anti-Mouse IgG1	1:1000	Biozol
HRP, Goat-Anti-Rabbit IgG (H+L)	1:1000	Bio-Rad

2.8.7 Enhanced chemiluminescence (ECL)

Proteins were detected by enhanced chemiluminescence (ECL) using horseradish peroxidase (HRP)-conjugated secondary antibodies. After incubating with the secondary antibodies, the membranes were washed three times with PBS-T. Membranes were incubated with ECL Plus™ Western Blotting detection reagent (Amersham Bioscience) and chemiluminescence was detected by exposing an X-ray film (Super RX, Fuji, Düsseldorf, Germany) for an appropriate period of time in the darkroom. Exposed X-ray films were then developed using Curix 60 developing system (Agfa-Gevaert AG, Cologne, Germany).

2.8.8 Staining of gels and membranes

Gels were stained for 30 minutes in the coomassie staining solution and destained with the Coomassie destaining solution (1h, RT) and with distilled water (ON, RT) to control equal loading of the gel and the performance of the transfer.

Table 2.16 Gel staining solution

Coomassi staining solution	
Coomassie blue	3.0 g
Glacial acetic acid	100 ml
Ethanol	450 ml
H_2O	to 1,000 ml

Coomassi destaining solution	
Glacial acetic acid	100 ml
Ethanol	333 ml
H_2O	ad 1,000 ml

2.8.9 Gene expression profiling

2.8.9.1 Preparation of cells

Leukemia cells were suspended at 5×10^5 cells/ml, and 2 ml of the cell suspension was added into a 6-well-plate. Archazolid A (10 nM) and DBZ (50 μM) were added to the cells. After 24 h of treatment,

the cells were collected and resuspended in 100 µl PBS, then 350 µl of RLT Buffer (with β-mercapto ethanol, QIAGEN, Hilden, Germany) were added. The samples were stored at -80℃ until further experiments were performed

2.8.9.2 RNA isolation

Total RNA was isolated using RNeasy kit (QIAGEN, Hilden, Germany) according to the manufacturer's protocol. RNA was eluted in RNA-free water. RNA concentrations were measured with the NanoDrop® spectrophotometer (NanoDrop Technologies, Wilmington, Germany).

2.8.9.3 Reverse transcription

For the reverse transcription of RNA into cDNA, 3µg RNA from each sample were used and the reverse transcription reaction was performed using the High Capacity cDNA Revers Transcription Kit (Applied Biosystems, Foster City, CA, USA), which includes random primers. The reactions were taken out for 2 h at 37℃. cDNA was stored at 4℃ until qRT-PCR was performed.

2.8.9.4 Semi-quantitive real-time PCR analysis

For the quantitative real-time PCR the ABI 7300 Real-Time PCR system with the TaqMan Universal PCR Mastermix (Life Technologies Corporations, Carlsbad, CA, USA) was used. Probes and primers for the respective targets were supplied as mixture (Life Technologies Corporations, Carlsbad, CA, USA).

Human primer of Notch downstream target HES1 (Life Technologies Corporation, Carlsbad, CA, USA) was used.

As housekeeping gene, GAPDH was used (forward/reverse primer, probe sequence, biomers, Ulm, Germany). Fluorescence development was analyzed using the ABI 7300 system software.

Calculation of relative mRNA was done according to Pfaffel (94).

2.9 Transfection of cells

2.9.1 Transfection of siRNA with Dharma FECT I

250,000 MDA-MB-231 cells were seeded in 6 well-plates. After cell attachment, cells were transfected with the non-targeting (nt) siRNA or Cdk5 siRNA. To achieve optimal silencing effect,

two different ON-TARGET plus Cdk5 siRNA were equally used in a mixture (J-003239-09 and J-003239-10; Thermo Scientific). A transfection mix per sample was prepared by mixing 5µM of siRNA in 10µl of sterile water with 190µl medium in tube A. Then 5µl of Dharma FECT I solution were diluted with 195µl medium in tube B. Five minutes later, the solution was mixed and left at RT for another 15min. Silencing of Cdk5 was achieved after 24 h.

2.9.2 Cdk5 shRNA stable transduction in MDA-MB-231 cells

Lentiviral transduction of MDA-MB-231 cells with Cdk5 shRNA and nt shRNA was performed by Bianca Hager (Ludwig-Maximilians-University, Munich, Germany) by means of MISSION® shRNA Lentiviral Transduction Particles (Sigma-Aldrich, Taufkirchen, Germany) according to the manufacturer´s protocol. Knockdown of Cdk5 was examined by Western blot analysis.

2.10 Confocal microscopy

2.10.1 Coating of coverslips for suspension cell staining

2.10.1.1 Preparation of Chrome alum-gelatin coating solution

Gelatin was dissolved in deionized H_2O at 45℃. After the gelatin has dissolved, 0.5 g chromium potassium sulfate dodecahydrate (dissolved in 20 ml dH_2O) was added. The solution was kept at 4℃ until use.

Table 2.17 Chrome alum-gelatin coating solution

Chrome alum-gelatin coating solution	
Gelatin (sigma)	4 g
$CrK(SO_4)_2 \cdot 12H_2O$	0.5 g
H_2O	to 1000 ml

2.10.1.2 Coating of coverslips

Gelatin solution was heated to 45℃ before use. Coverslips were submerged completely into the coating solution and then left drying for 2 days at room temperature.

2.10.2 Immunostaining

S-Jurkat cells were treated with Archazolid A (10 nM) and DBZ (50 μM) for 24 h, were then collected by centrifugation, resuspended in PBS, and seeded on chrome alum-gelatin coated coverslips and let adhere for 30 min at 37℃. Then the coverslips were individually put in each well of a 6-well plate. The samples were fixed in 4% PFA in PBS at room temperature for 10 min, washed with PBS for three times, permablized in PBS containing 0.2% Triton X-100 for 5 min, blocked with PBS containing 0.2% BSA for 1 h. Cells were then incubated with primary antibody in blocking solution for 1 h, RT. Before the secondary antibody was added, cells were washed three times with PBS before adding the secondary antibody for 1 h at RT. Cells were washed three times in PBS before mounting on a glass slide (Superfrost® Plus Micro Slide, VWR, Germany).
For the LysoTracker® experiment, cells were collected after centrifugation, resuspended in PBS containing LysoTracker®. Cell suspension was then transferred to a ibidi μ-slide (8 well) and incubated at 37℃ for a further 45 min. Hoechst 33342 was added and incubated at room temperature for 5 min in the dark. Then the samples were subjected to confocal microscopy.

Table 2.18 Primary antibodies for immunostaining

Antigen	Source	Dilution	Provider
Cleaved Notch1 (Val1744) (D3B8)	Rabbit monocl.	1:100	Cell Signaling Technology, Inc
Notch1 (D1E11) XP®	Rabbit monocl.	1:100	Cell Signaling Technology, Inc
EEA1 (N-19)	Goat polycl.	1:100	Santa Cruz Biotechnology
LAMP1(H4A3)	Mouse monocl.	1:200	Developmental Studies Hybridoma Bank

Table 2.19 Secondary antibodies for immunostaining

Antibody	Dilution	Provider
Alexa Fluor® 488 goat anti-rabbit IgG (H+L)	1:400	Molecular Probes®
Alexa Fluor® 546 goat anti-mouse IgG (H+L)	1:400	Molecular Probes®
Alexa Fluor® 546 donkey anti-goat IgG (H+L)	1:400	Molecular Probes®
Alexa Fluor® 647 chicken anti-rabbit IgG (H+L)	1:400	Molecular Probes®

2.11 Statistic evaluation

All experiments were conducted at least three times in duplicates/triplicates. Results are expressed as mean value ± SEM. One-way ANOVA/Turkey and individual students t tests were conducted using Graph Pad Prism (version 5.04, GraphPad Software, Inc.). P values less than 0.05 were considered as significant.

3 Results - Part 1:

Evaluation of the V-ATPase inhibitor Archazolid for treatment of T-cell acute lymphoblastic leukemia

3.1 Archazolid A inhibits V-ATPase activity in leukemia cells

To confirm that Archazolid A inhibits V-ATPase activity in leukemia cells, we monitored endo-lysosomal pH by LysoTracker® staining (Figure 3.1).

In non-stimulated cells (Figure 3.1 Co), the pH sensitive Lysotracker accumulated in acidic organelles (such as endosomes and lysosomes), indicating intraorganellar acidification by active V-ATPase. After Archaolizd A (10 nM, 24 h) treatment, endo-lysosomal acidification was reduced, as indicated by marked reduction in Lysotracker fluorescence intensity. As expected, treatment with the γ-secretase inhibitor Dibenzazepine (DBZ 50 µM, 24 h) did not alter V-ATPase activity. These results indicate that Archazolid A inhibits V-ATPase activity in leukemia cells.

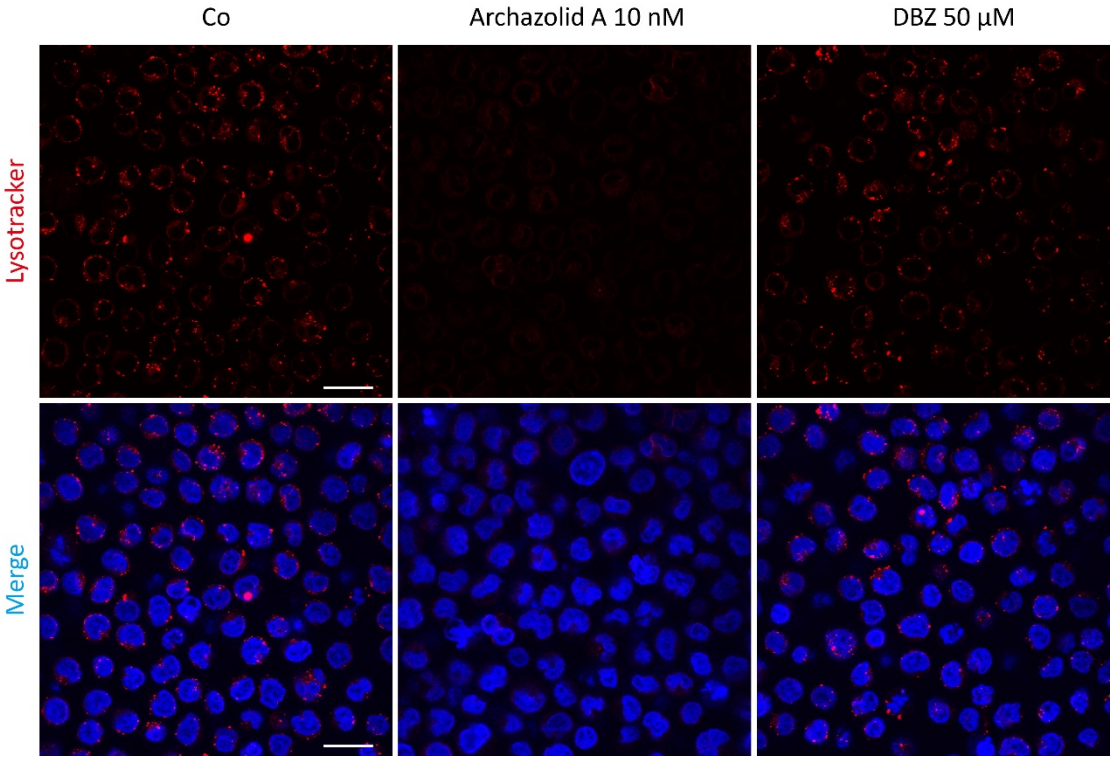

Figure 3.1: Archazolid A inhibits V-ATPase activity in S-Jurkat cells.

S-Jurkat cells were either left untreated or treated with Archazolid A (10 nM) or DBZ (50 µM) for 24 h. V-ATPase activity is monitored by pH sensitive dye LysoTracker® (red) staining. Nuclei are stained with Hoechst 33342 (blue). Scale bar 20 µm.

3.2 Functional effects of Archazolid A and DBZ on leukemia cells

To compare the effects of Archazolid A and γ-secretase inhibitor Dibenzazepine (DBZ) on two leukemia cell lines that were previously described to resist GSI treatment, we applied various functional assays.

3.2.1 Archazolid A and DBZ inhibit leukemia cell proliferation

Initially, to test the sensitivity of leukemia cells to Archazolid A and DBZ, a proliferation assay was performed, in which the cells were treated with various concentrations of these two substances for 72 h. As shown in Figure 3.2 upper panel, Archazolid A inhibited proliferation of S-Jurkat and CEM cells at nanomolar concentrations (EC_{50} Jurkat 0.56 nM and EC_{50} CEM 0.51 nM), whereas DBZ showed anti-proliferative effects with lower potency at micromolar concentrations (EC_{50} Jurkat 15.5 µM and EC_{50} CEM 12.7µM) (Figure 3.2 lower panel).

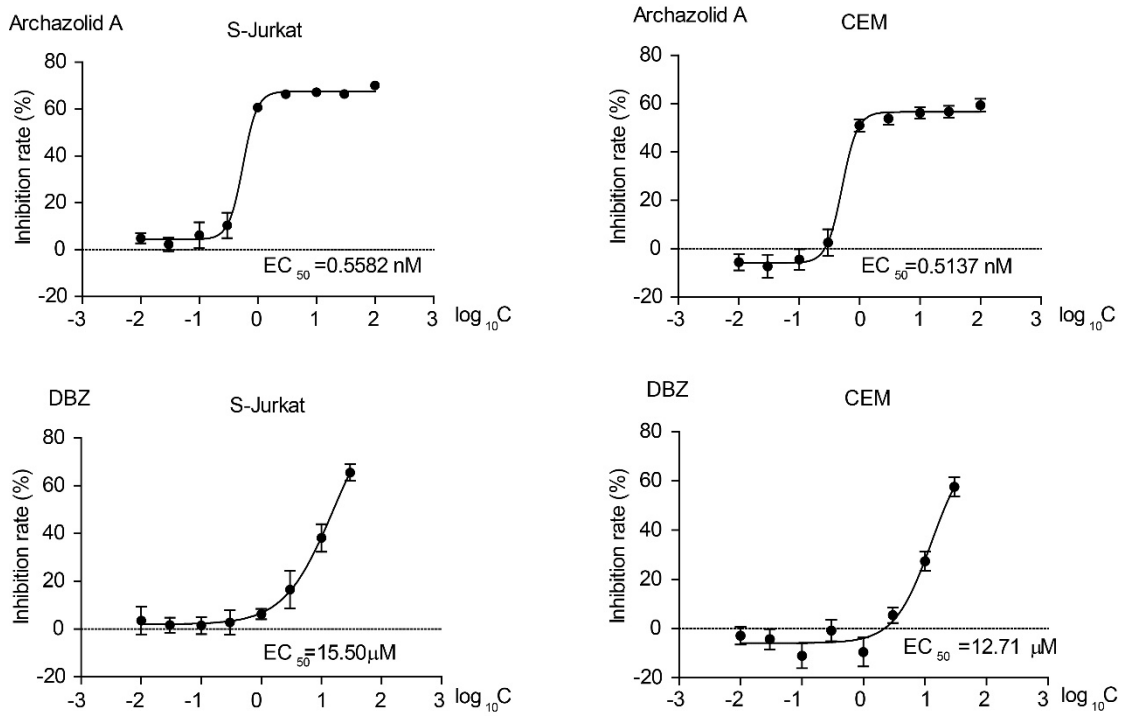

Figure 3.2: Archazolid A and DBZ inhibit leukemia cells proliferation in a dose-dependent manner. Leukemia cell proliferation with Archazolid A and DBZ at indicated concentrations are shown (n=3, mean ± SEM). EC50 values were calculated with Graph Pad Prism.

3.2.2 Archazolid A and DBZ inhibit leukemia cell colony formation

Various cancers including leukemia can acquire therapy resistance, meaning that some cells are able to recover upon short-time treatment. To analyze whether the leukemia cells were able to recover from treatment with Archazolid A and DBZ, a colony formation assay was performed. As shown in Figure 3.3 short-time treatment with Archazolid A for 24 h was able to dose-dependently decrease long-term colony formation in both leukemia cell lines. DBZ reduced colony formation as well, but with lower potency.

A

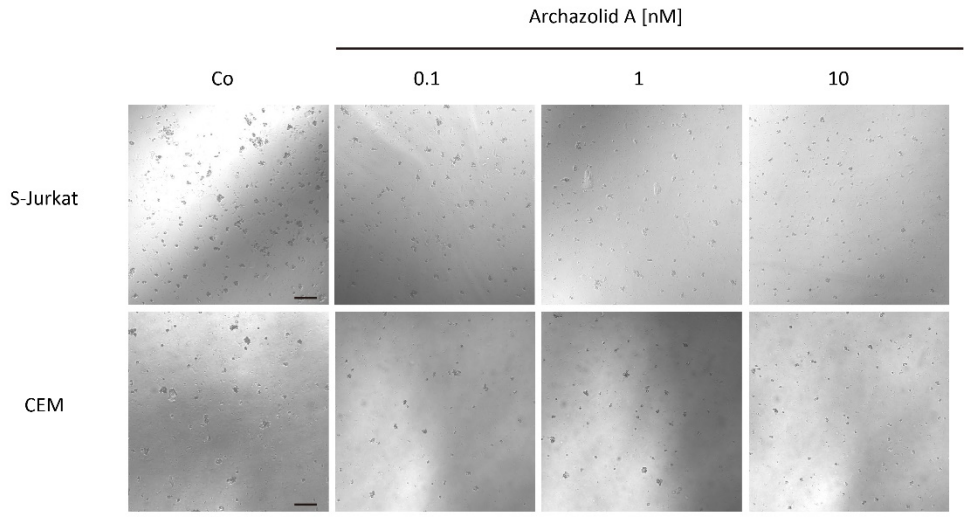

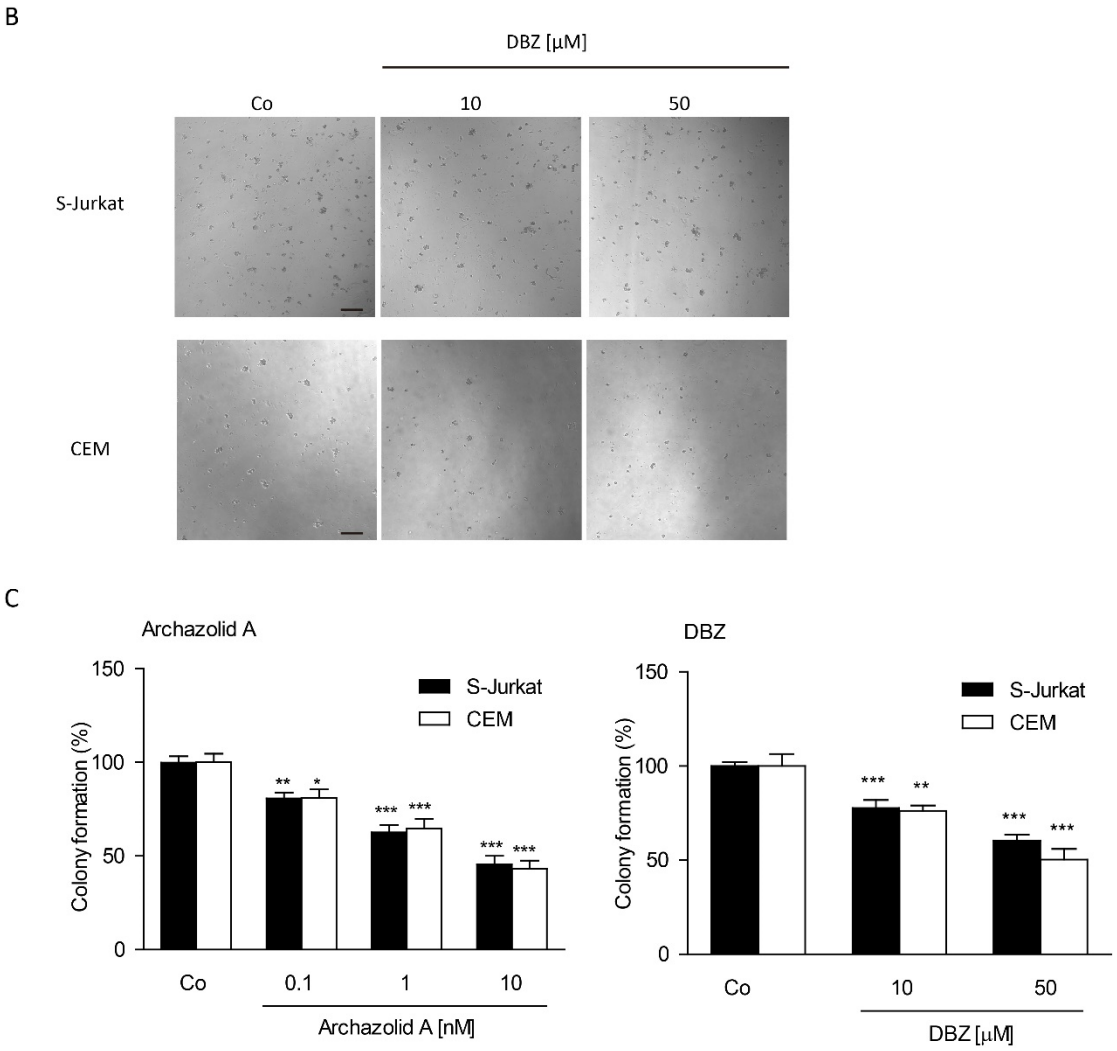

Figure 3.3: Archazolid A and DBZ inhibit leukemia cells colony formation.

(A,B) Colony formation of leukemia cells treated with Archazolid A and DBZ for 24 h and freshly seeded for 11 days are shown. Scale bar 100 µm. (C) Evaluation of colony formation in leukemia cells with indicated substances and concentrations is displayed. (n=3, mean ± SEM. One-way ANOVA, Tukey's post-test, comparing to respective control *p<0.05,**p<0.01, ***p<0.001).

3.2.3 The effects of Archazolid A and DBZ on apoptosis and cell cycle in leukemia cells

In order to clarify the mechanism by which Archazolid A and DBZ inhibit leukemia cell growth, we stained cell with PI and performed apoptosis assay and cell cycle analysis.

The apoptosis rate of leukemia cell lines treated with Archazolid A and DBZ at indicated time and doses are shown in Figure 3.3. Archazolid A treatment induced apoptosis time- and dose-dependently in both tested leukemia cell lines, whereas DBZ treatment showed no effect.

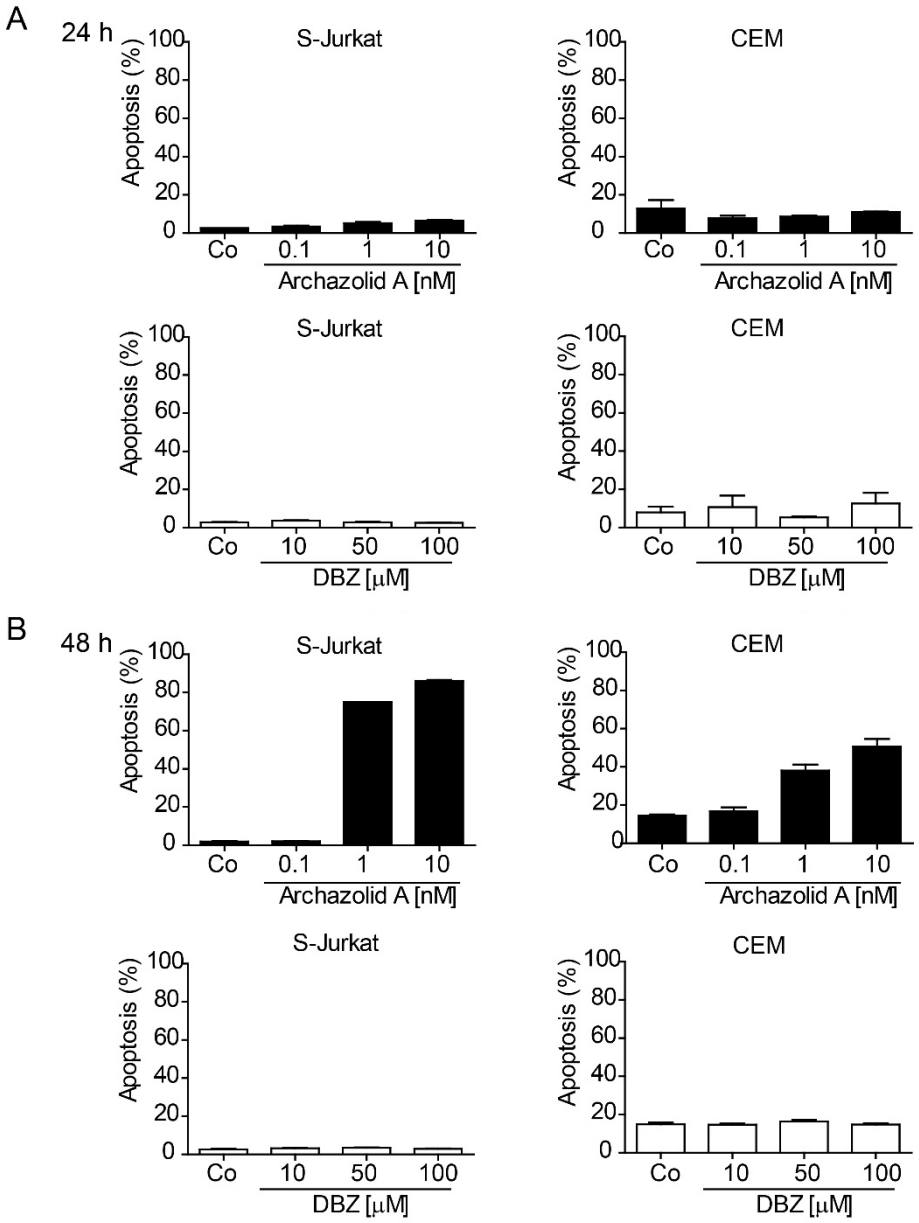
A
24 h
S-Jurkat
CEM
Apoptosis (%)
0
20
40
60
80
100
Co
0.1
1
10
Archazolid A [nM]
S-Jurkat
CEM
Co
10
50
100
DBZ [µM]
B
48 h
S-Jurkat
CEM
Archazolid A [nM]
DBZ [µM]

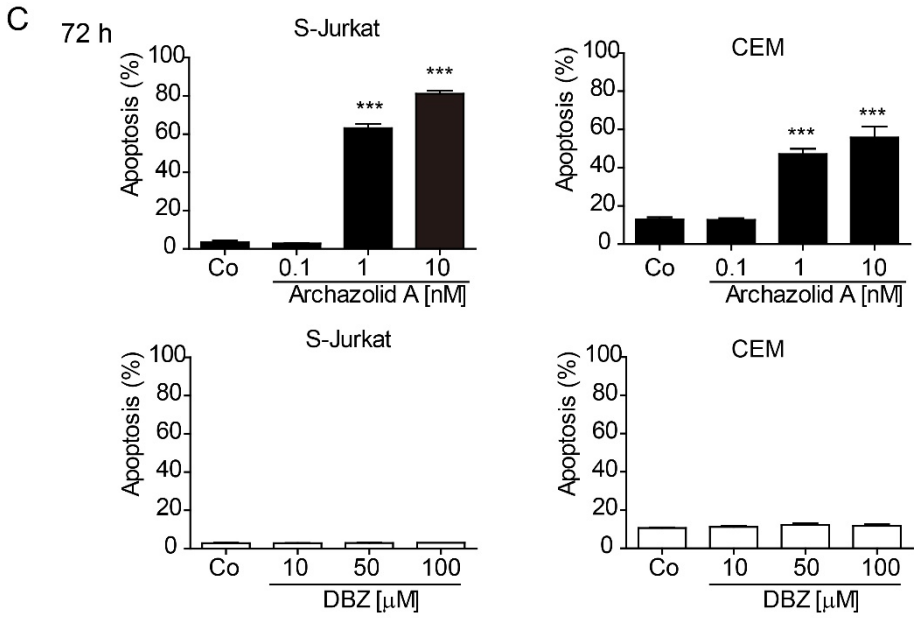

Figure 3.4: Archazolid A dose- and time- dependently induced apoptosis in leukemia cells.

(A-C) Apoptosis rate of S-Jurkat and CEM cells at indicated times and after treatment with indicated concentrations of Archazolid A and DBZ are shown. Bars represent mean ± SEM. (C) n=3, one-way ANOVA, Tukey's post-test, ***p<0.001.

The inhibition of V-ATPase has been shown to induce apoptosis as well as cell cycle arrest in tumor cells (50, 95-97). Thus, we investigated the effects of Archazolid A and DBZ on cell cycle in leukemic cells. As shown in Figure 3.5, Archazolid A treatment induced G2-phase arrest in S-Jurkat cells (Figure 3.5 A), but had no influence on cell cycle in CEM cells (Figure 3.5 C). DBZ had no effect on both cell lines (Figure 3.5 B, D).

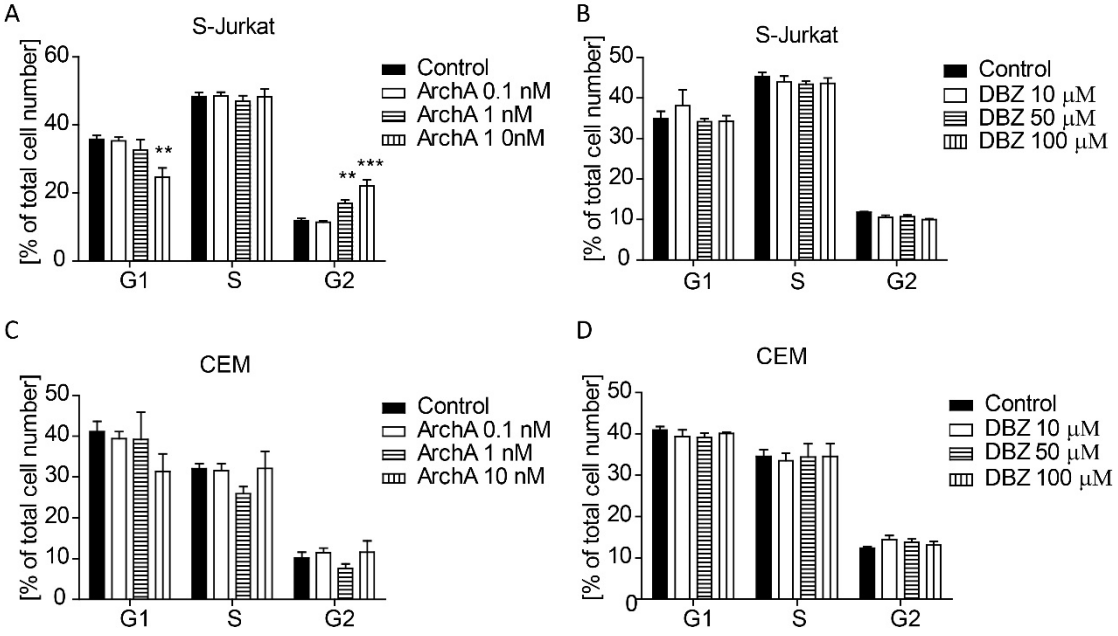

Figure 3.5: Archazolid A induces G2-phase arrest in S-Jurkat cells.

(A-D) Cell cycle analysis for S-Jurkat and CEM cells after 72 h of treatment with Archazolid A and DBZ at indicated concentrations is shown (n=3). (A) Archazolid A induced G2-phase arrest in S-Jurkat cells (n=3, student t-test, comparing to control **p<0.01,***p<0.001), but had no influence on CEM cells (C). (B,D) DBZ had no effects on cell cycle in both tested cell lines.

3.3 Effects of Archazolid A and DBZ on Notch signaling in leukemia cells

To investigate the effect of Archazolid A and DBZ on Notch signaling, we first tested the expression of Notch downstream target HES1 after treatment with Archazolid A and DBZ. As shown in Figure 3.6, HES1 expression was reduced by both Archazolid A and DBZ.

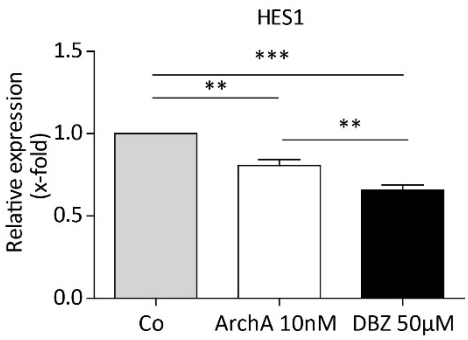

Figure 3.6 Archazolid A and DBZ reduce Notch downstream target HES1.
Relative expression level of HES1 in S-Jurkat cells after Archazolid A (10 nM) and DBZ (50 µM) treatment are shown. n=3, one-way ANOVA, Tukey's post-test, **p<0.01, ***p<0.001.

Furthermore, we analyzed whether Archazolid A affects Notch intracellular domain (NICD), which represents the active cleaved form of Notch receptor and is an indicator for Notch signaling activity. As it is revealed in Figure 3.7, Archazolid A treatment decreased NICD and, as expected, DBZ reduced NICD level as well. Furthermore, the Notch downstream target c-Myc was reduced by V-ATPase inhibition with Archazolid A. DBZ also reduced c-Myc, but to a less extent, as it was previously described to contribute to GSI resistance of leukemic cells. Interestingly, in contrast to DBZ, V-ATPase inhibition by Archazolid A increased the level of Notch1 full-length receptor. Because Archazolid A induced apoptosis in leukemia cells, whereas DBZ had no effect. We further investigated whether the anti-apoptotic protein survivin was affected. In consistence with apoptosis induction, survivin level was decreased upon Archazolid A treatment, while it was unaffected by DBZ.

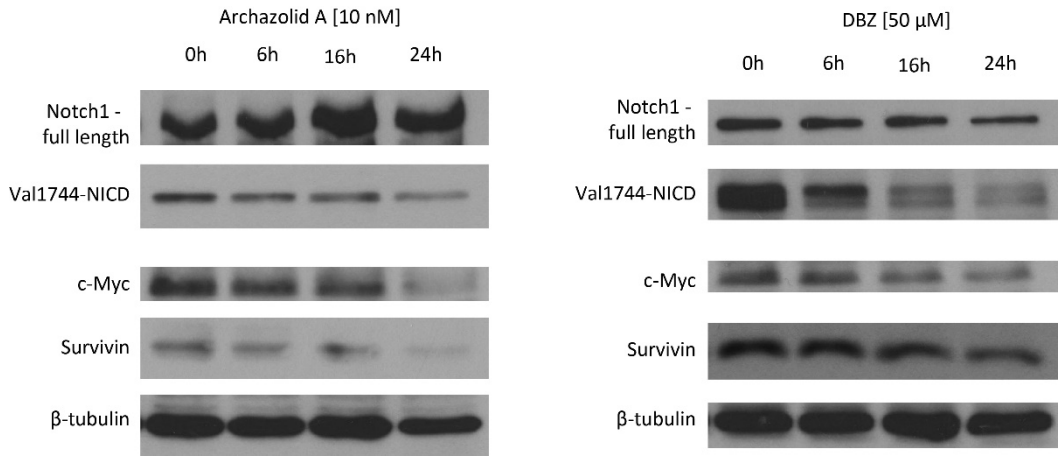

Figure 3.7: Archazolid A and DBZ inhibits Notch signaling.
Immunoblots from S-Jurkat cells treated with Archazolid A (left panel) or DBZ (right panel) and blotted with antibody against Notch1 (full length), NICD (Val1714),c-Myc and survivin are presented. Immunoblots for β-tubulin are shown as loading control. n=3

To further investigate the mechanism by which Archazolid A and DBZ impaired Notch signaling, we performed immunostainings. In line with the results from immunoblots, NICD was decreased upon treatment with Archazolid A as well as DBZ (Figure 3.8, upper panel).

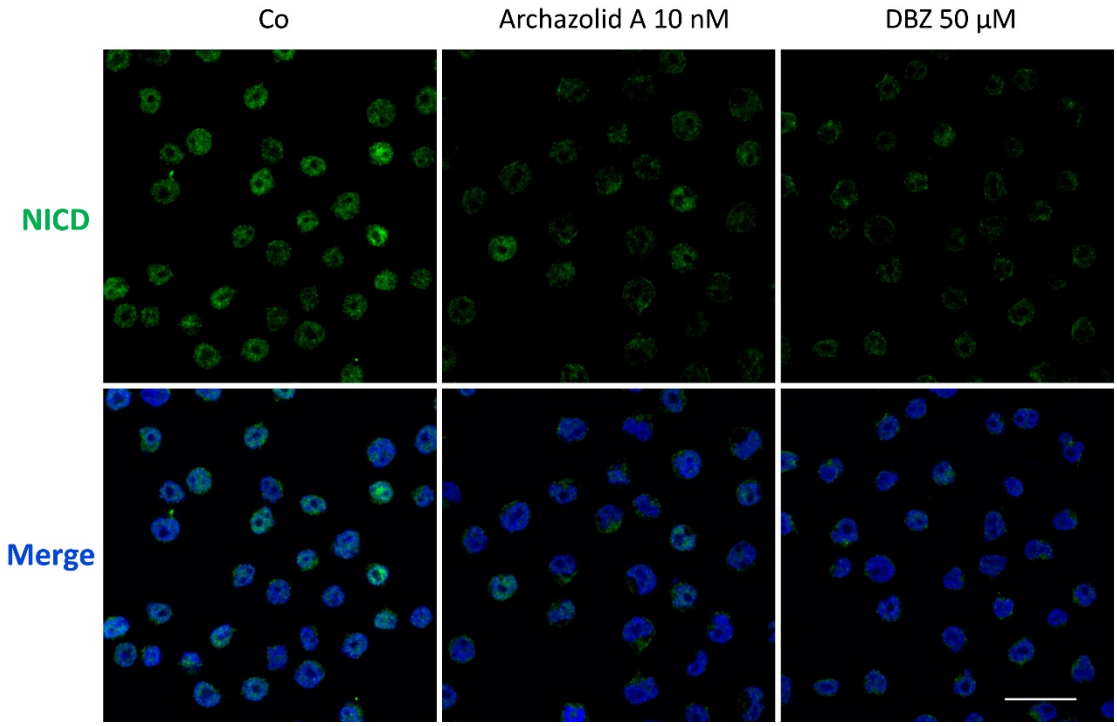

Figure 3.8: Archazolid A and DBZ reduce NICD level.

Immunostaining for NICD (green, upper panel) from S-Jurkat cells treated with Archazolid A and DBZ are shown. Nuclei are stained with Hoechest 33342 and displayed (blue, merged with NICD, lower panel). Scale bar 20 µm.

Since impaired acidification of the endo-lysosomal compartment by V-ATPase inhibition might influence the activity of γ-secretase, and therefore reduce Notch receptor cleavage and leading to reduced NICD, we analyzed Notch1 receptor expression together with endosomal and lysosomal marker EEA1 and LAMP1. As shown in Figure 3.9, Archazolid A treated cells showed accumulation of Notch1 receptors in the endo-lysosomal compartments (Figure 3.9, green channel). These results showed that Notch1 receptors are trapped in the endo-lysosomal compartment. This indicates that Archazolid A treatment inhibited Notch1 cleavage at endo-lysosomal membranes.

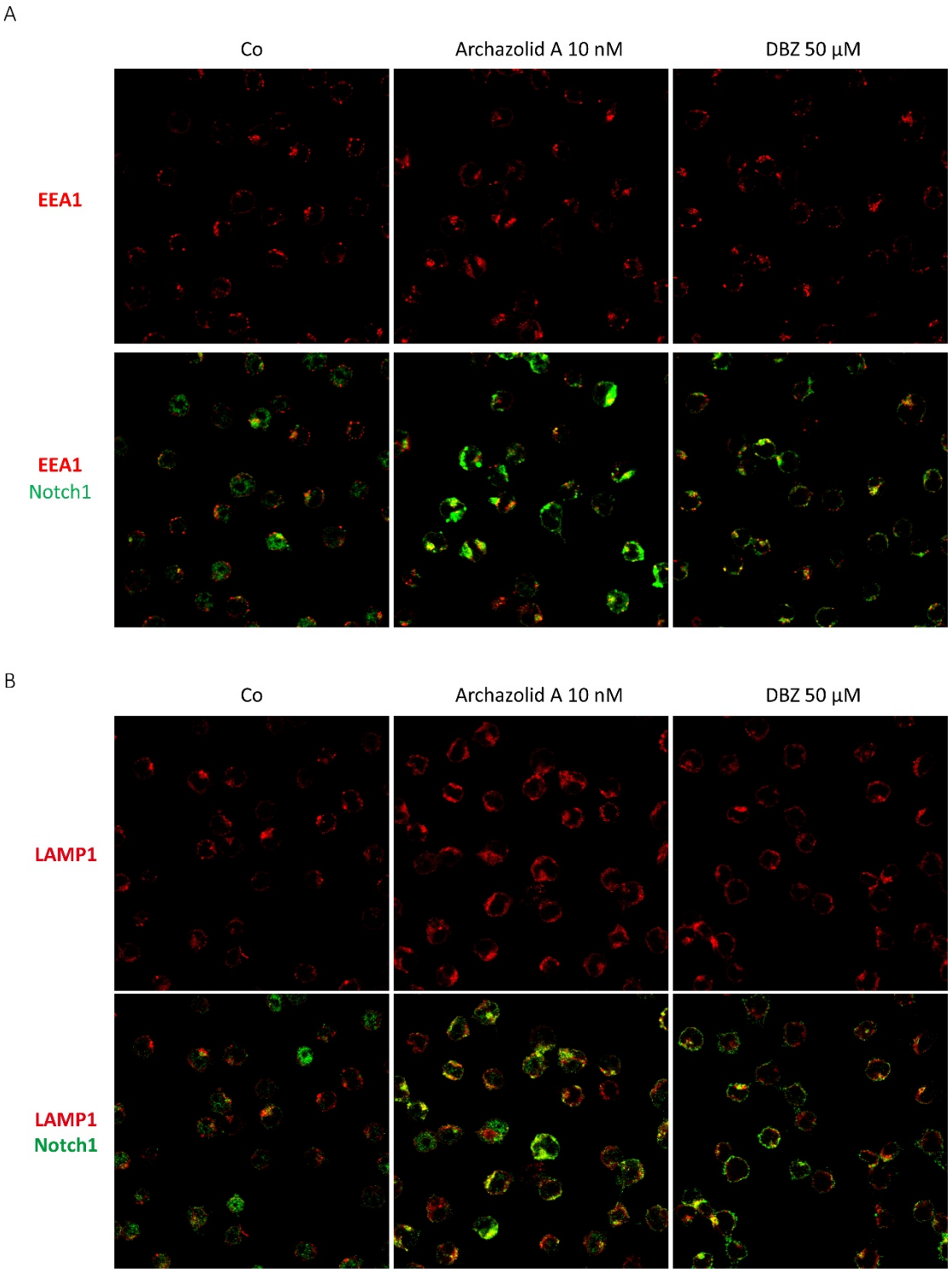

Figure 3.9: Archazolid A induces accumulation of Notch1 receptor in the endo-lysosomal compartments. DBZ trapped Notch1 receptor on the cell surface. S-Jurkat cells were either treated with Archazolid A (10 nM) or DBZ (50 µM) for 24 h, and cells were immonostained with endosomal marker EEA1 (A, red) or lysosomal marker LAMP1 (B, red) together with Notch1 (green). Hoechest 33342 staining was used to visualize nuclei. n=3, Scale bar 20 µm.

3.4 Archazolid A induced death of patient leukemic cells

Finally, in collaboration with Prof. Dr. Jeremias and Dr. Grunert (Helmholtz Center of Munich) we studied the effect of Archazolid A on human primary leukemic cells. As in vitro cultivation of these cells is limited, cells were passaged in vivo by using immunocompromised mice (98). Upon isolation, primary ALL samples from five patients were stimulated with either Archazolid A or DBZ for 48 h. In consistance with cell culture experiments, whereas DBZ showed no effect, Archazolid A induced cell death in all tested patient samples (Figure 3.10). This indicated a therapeutic relevance of V-ATPase inhibition by Archazolid A.

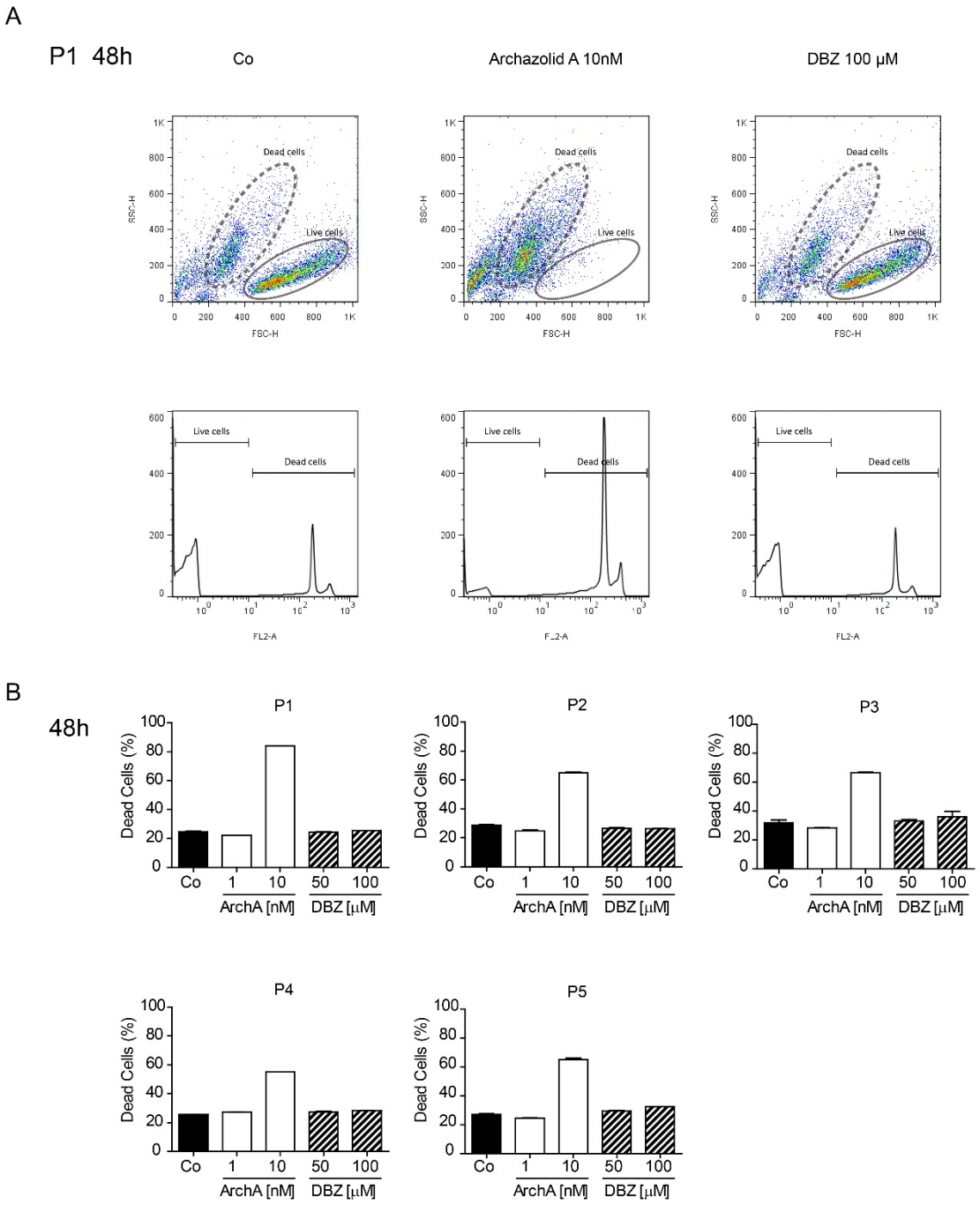

Figure 3.10: Archazolid A strongly induced cell death in primary human leukemic cells.

(A) Dot plots (upper panel) and histograms (lower panel) from patient cells (Patient No.1) treated as indicated (48 h) are shown as example. In dot plots (upper panel), dashed ellipses show dead cells, solid ellipses show live cells. In histograms (lower panel), cells on the right side show high PI-signal and represent dead cells; while cells on the left side show low PI-signal and represent live cells. (B) Evaluations of cell death (%) from each patient samples treated with either Archazolid A or DBZ at indicated concentrations for 48 h are shown, bars represent mean ± SEM. of each sample in duplicates.

4 Results - Part 2:

Evaluation of Cdk5 as target for breast cancer treatment

4.1 Cdk5 inhibition exerts anti-tumor and anti-metastatic effects in metastatic breast cancer cells

To analyze potential effects of Cdk5 inhibition by Roscovitine on breast cancer, we applied various functional assays by using MDA-MB-231 cells, highly metastatic and proliferating mesenchymal breast cancer cells.

4.1.1 Roscovitine inhibits breast cancer cell proliferation

Initially, we examined the effect of Cdk5 inhibition by Roscovitine on proliferation of MDA-MB-231 cells. Roscovitine inhibited proliferation of MDA-MB-231 cells at micromolar concentrations with EC_{50} value of 13.7 µM (Figure 4.1).

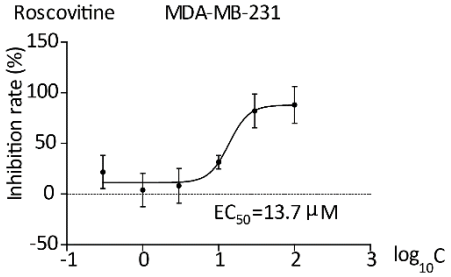

Figure 4.1: Roscovitine inhibits proliferation of MDA-MB-231 cells at micromolar concentrations. The bar graph displays inhibition of proliferation of MDA-MB-231 by Roscovitine. EC_{50}=13.7 µM. (n=3).

4.1.2 Effects of Cdk5 inhibition by Roscovitine on apoptosis and cell cycle

In order to clarify the mechanism by which Roscovitine inhibits cell growth, we analyzed apoptosis and cell cycle transitions by Nicoletti assays. Treatment of proliferating MDA-MB-231 cells with increasing concentrations of Roscovitine induced apoptosis. Roscovitine caused a significant increase of apoptosis at 30 µM (Figure 4.2 A). Moreover, Roscovitine induced G2-phase arrest in MDA-MB-231 cells.

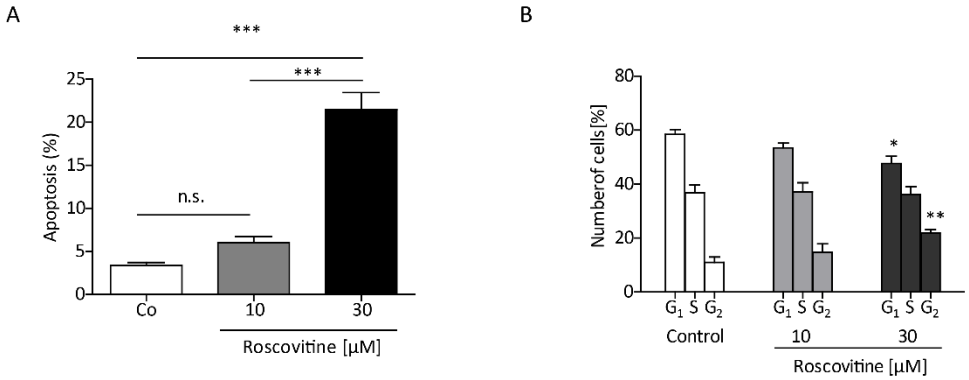

Figure 4.2: Roscovitine induced apoptosis and G2 cell cycle arrest in MDA-MB-231 cells. Proliferating MDA-MB-231 cells were either left untreated or treated with increasing concentrations of Roscovitine for 48 h. (A) Apoptosis was determined according to the Nicoletti method. (One-way ANOVA, Tukey's post-test,***p<0.001). (B) Cell cycle analysis of proliferating MDA-MB-231 cells treated with Roscovitine at indicated concentrations is displayed. (n=3, student t-test, *p<0.05,**p<0.001).

4.1.3 Roscovitine inhibits colony formation of breast cancer cells.

Chemoresistant and metastatic tumor cells characteristically don't get apoptotic upon short pulse of treatment and some cells are able to recover. To elucidate the effect of Roscovitine on long term survival and ability of cells to clonogenically expand, a colony formation assay was performed. As shown in Figure 4.3, Roscovitine reduced colony formation in a dose-dependent manner.

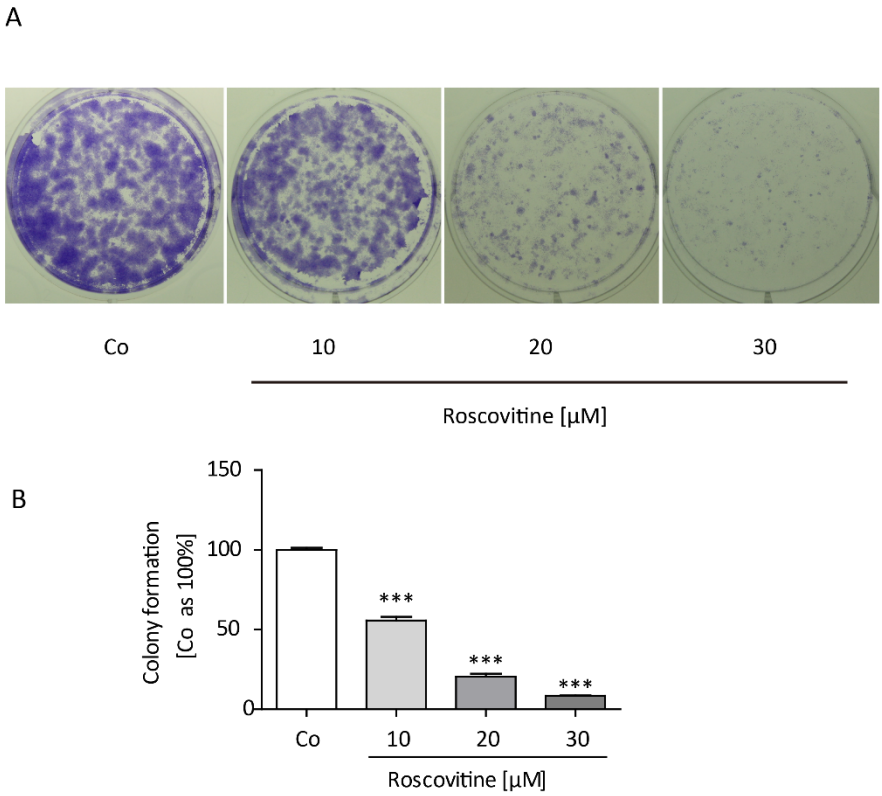

Figure 4.3: Roscovitine reduces colony formation in MDA-MB-231 cells.

(A) Colonies formed from MDA-MB-231 cells treated with Roscovitine at indicated concentrations for 24 h and subsequently freshly seeded at low density and cultivated for further 7 days before staining with crystal violet are displayed. (B) Quantification of colony formation by absorbance measurement is shown. Bars represent mean ± SEM of three independent experiments performed in triplicates. (One-way ANOVA, Tukey's post-test, ***$p<0.001$)

4.1.4 Roscovitine inhibits migration of breast cancer cells

To elucidate the effect of Roscovitine on the migration of metastatic breast cancer cells, transwell migration assays were performed, where cells have to migrate through a porous membrane.

As shown in Figure 4.4, Roscovitine reduced transwell migration of MDA-MB-231 cells.

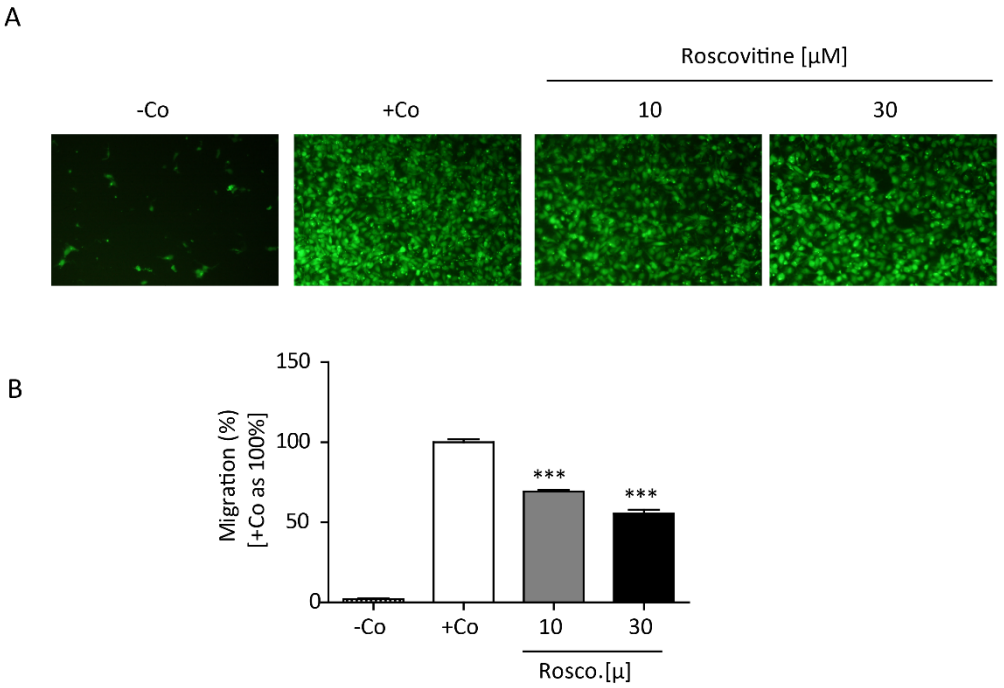

Figure 4.4: Roscovitine inhibits transwell migration of MDA-MB-231 cells.
(A) Migrated MDA-MB-231 cells after pre-treatment before migration for 16 h are shown. Negative control (-Co) and positive control (+Co) refers to absence or presence of FCS in the lower compartment. (B) Quantitative evaluation of transwell migration assays is shown. Bars represent mean± S.E.M. (n=3, One-way ANOVA, Tukey's post-test, ***p<0.001).

4.1.5 Cdk5 inhibition by Roscovitine reduced mammosphere formation.

Cancer stem cells (CSCs) are able give rise to the whole cancer population, show high metastatic potential and can be responsible for treatment resistance. Potential effects of Cdk5 inhibition on CSCs were analyzed by mammosphere formation assays. In mammosphere assays, mammary epithelial cells are cultivated in non-adherent (anchorage-independent), low-nutrient (no-serum) environment, where only CSCs are able to clonally expand and form discrete spheroid-like structures called mammopsheres.

As shown in Figure 4.5, Roscovitine inhibited mammopshere formation when applied at repeated doses as well as at a single dose.

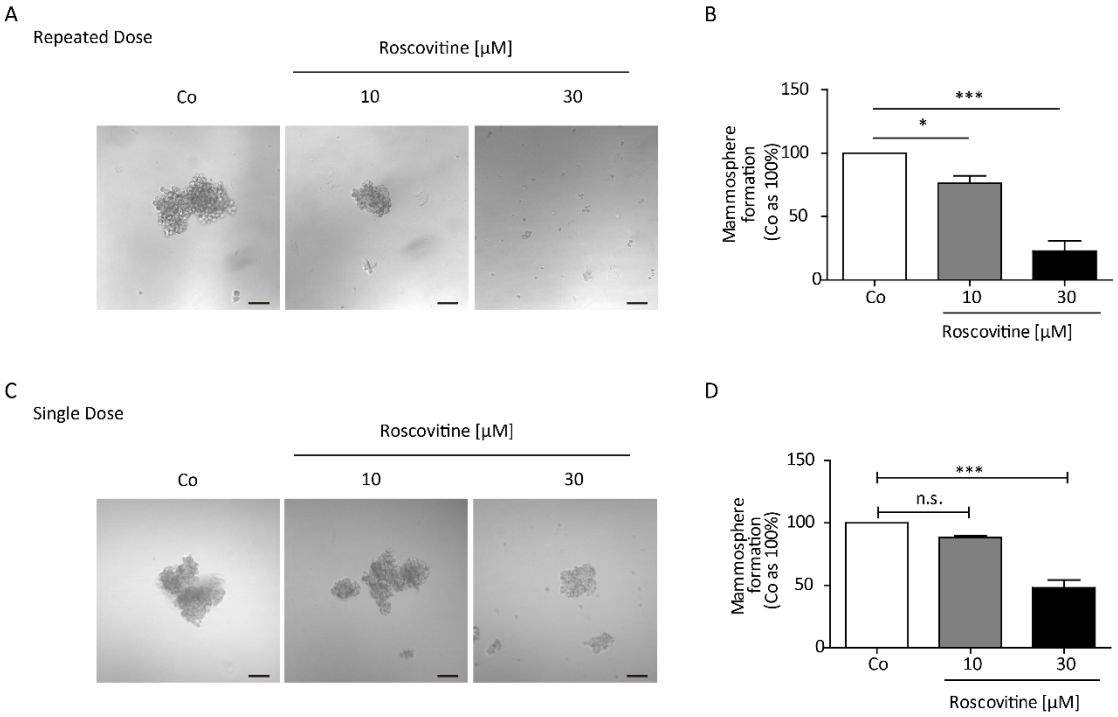

Figure 4.5: Roscovitine reduced mammosphere formation.

(A,C) Mammosphere formation after pretreatment of MDA-MB-231 cells with Roscovitine for 24 h before resuspension in fresh mammosphere medium and cultivation for further 10 days in the absence of Roscovitine (single dose) or continuous presence of Roscovitine (repeated dose) is shown. Scale bar: 100 µm. (B, D) Quantitative evaluation of numbers of mammospheres are shown. Bars represent mean ± SEM. (n=3, One-way ANOVA, Tukey's post-test,*$p<0.05$, ***$p<0.001$).

4.1.6 Silencing of Cdk5 inhibits breast cancer cells proliferation

Roscovitine does not selectively inhibit Cdk5, but also Cdk1, Cdk2, Cdk7, and Cdk9 (88, 99). Therefore, we aimed to proof that Cdk5 is the relevant target of Roscovitine in breast cancer. Cdk5 was genetically downregulated by RNA interference, using siRNA for transient silencing and lentiviral transduction of shRNA for stable knockdown. First, we analyzed the impact of Cdk5 knockdown on proliferation of MDA-MB-231 cells.

MDA-MB-231 cells were stably transduced with lentiviral vector expressing Cdk5 short hairpin RNA (shRNA). Cells that express non-targeting shRNA were used as control. Cdk5 shRNA breast cancer cells showed reduced proliferation (Figure 4.6 A), as compared to the non-targeting control (nt shRNA).

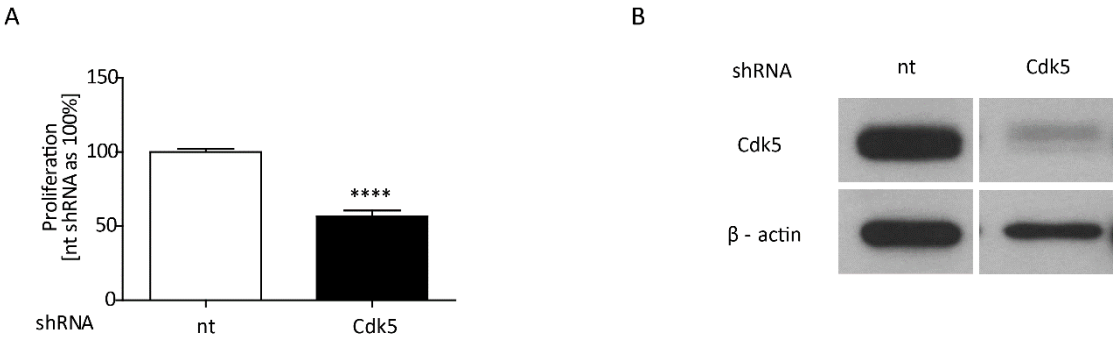

Figure 4.6: Cdk5 silencing inhibits breast cancer cell proliferation.

(A) Proliferation of MDA-MB-231 cells transduced with non-targeting (nt) or Cdk5 shRNA is shown. (n=3, unpaired t-test, ****p<0.0001.). (B) Immunoblot for Cdk5 shows Cdk5 downregulation. β-actin was used as loading control.

4.1.7 Cdk5 downregulation does not affect apoptosis or cell cycle transitions

To test whether cdk5 is involved in the induction of apoptosis and cell cycle regulation in MDA-MB-231 cells, we transiently silenced Cdk5 by siRNA and analyzed apoptosis and cell cycle transitions by Nicoletti assay. As shown in Figure 4.7, Cdk5 silencing did not affect apoptosis or cell cycle.

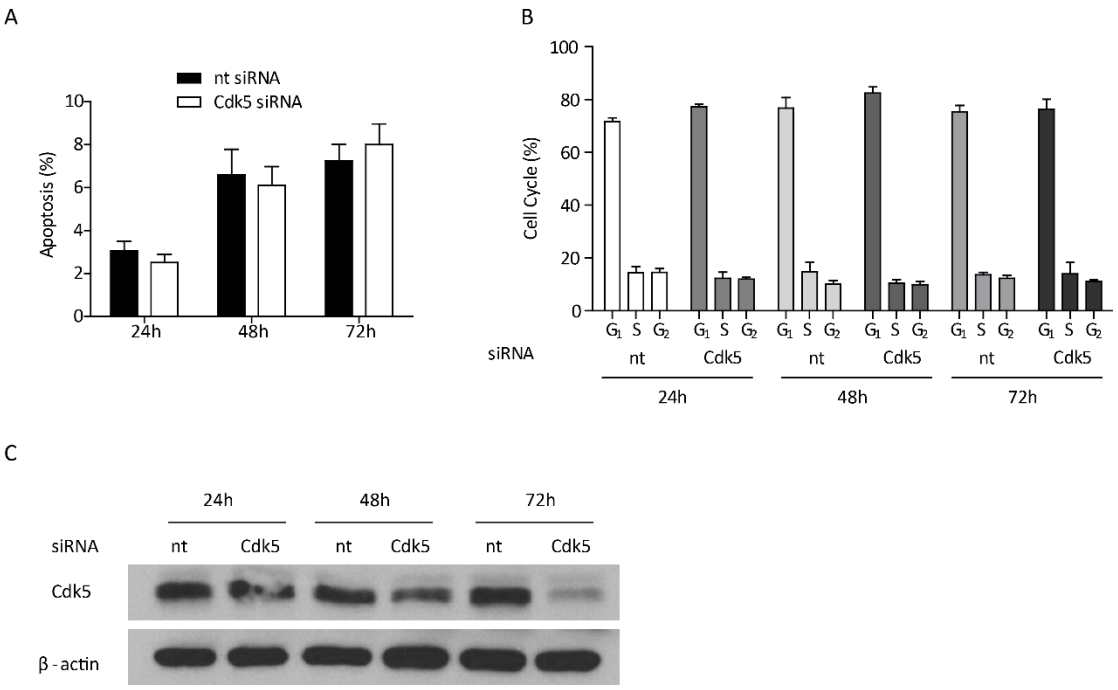

Figure 4.7: Silencing of Cdk5 has no effect on apoptosis induction and cell cycle.
(A) Apoptosis assay and (B) cell cycle analysis in MDA-MB-231 cells transiently transfected with non-targeting (nt) or Cdk5 siRNA. Bars represent mean ± SEM. (n=3) (C) Immunoblot shows Cdk5 silencing.

4.1.8 Silencing of Cdk5 inhibits breast cancer cell colony formation

Moreover, we analyzed colony formation of nt and Cdk5 shRNA MDA-MB-231 cells. Indeed, downregulation of Cdk5 reduced colony formation (Figure 4.8).

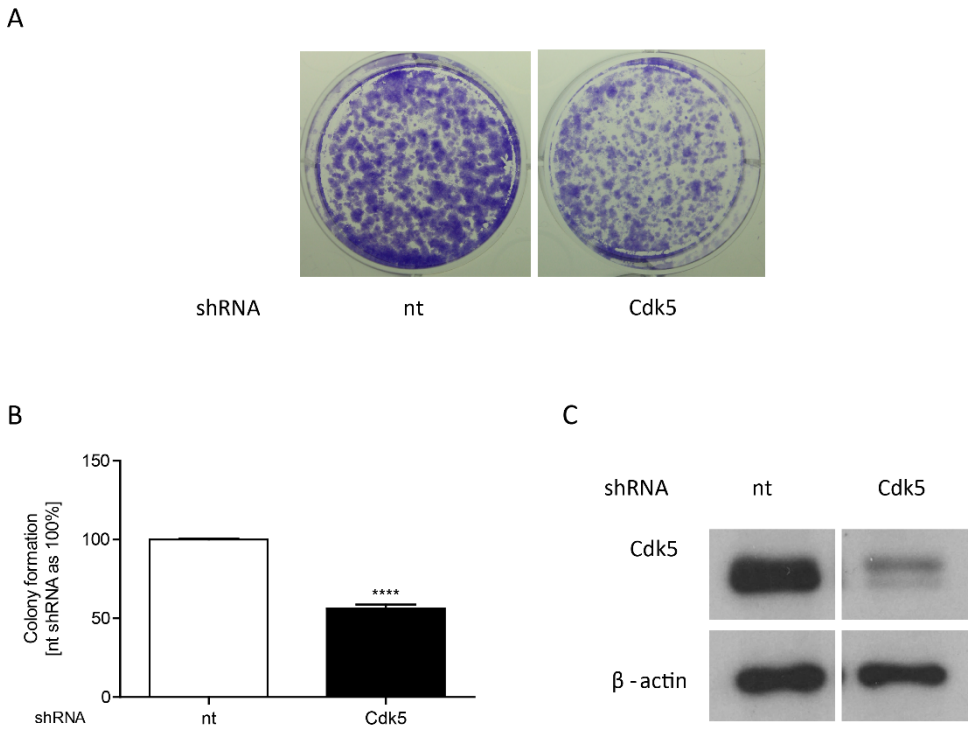

Figure 4.8: Knockdown of Cdk5 inhibits colony formation in MDA-MB-231 cells. (A) Colony formation of nt and Cdk5 shRNA MDA-MB-231 cells is shown. One representative experiment out of three independent experiments is shown. (B) Quantitative evaluation of colony formation assays is shown. Bars represent mean± S.E.M (n=3, paired t-test, ****p<0.0001). (C) Immunoblot shows Cdk5 downregulation. Actin indicates equal loading.

4.1.9 Silencing of Cdk5 inhibits breast cancer cells transwell migration and invasion

In addition, we evaluated the effect of Cdk5 silencing in transwell migration assays. As shown in Figure 4.9, the migration of cells towards FCS was markedly decreased by Cdk5 siRNA.

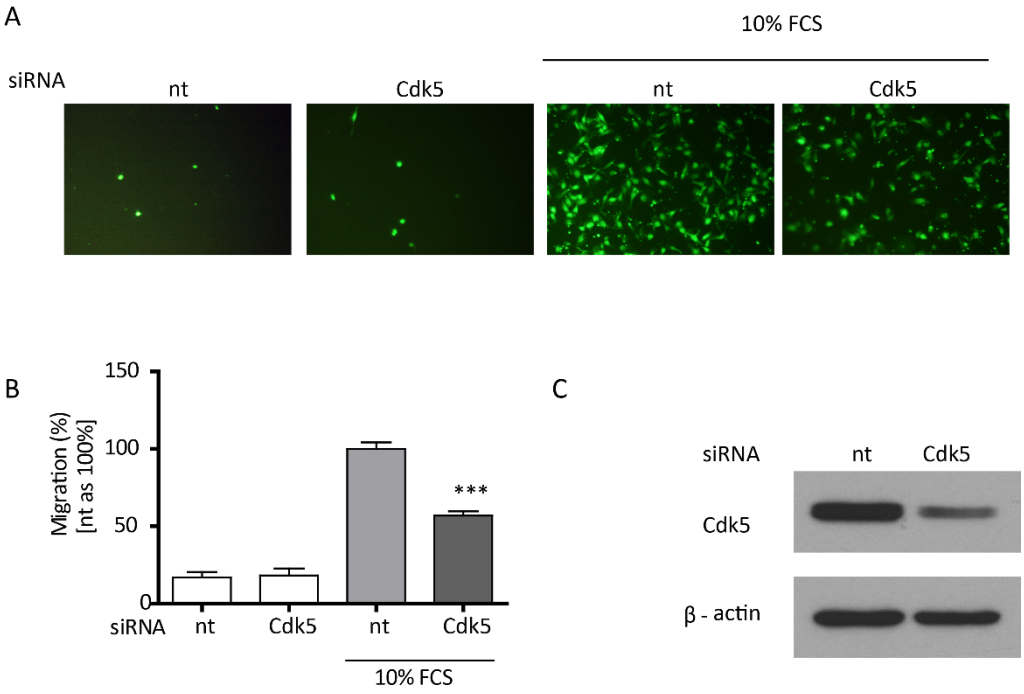

Figure 4.9: Cdk5 silencing reduces MDA-MB-231 cells transwell migration.

(A) FCS-induced migration of nt or Cdk5 siRNA treated MDA-MB-231 cells is shown. One representative experiment out of three independent experiments is shown. (B) Quantitative evaluation of transwell migration assays is shown. Bars represent mean± S.E.M (one-way ANOVA, Tukey's post test,***$p<0.001$). C) Immunoblot shows Cdk5 silencing. Actin was used as loading control.

In addition to migration, during metastasis cancer cells need to interact with the extracellular matrix. In order to analyze whether Cdk5 influences cancer cell invasion, we used a modified transwell migration model and coated the porous membrane with Matrigel®, an artificial extracellular matrix. As shown in Figure 4.10, both transient and stable knockdown of Cdk5 reduced MDA-MB-231 invasion. Thus, Cdk5 was important for migration and invasion of MDA-MB-231 cells.

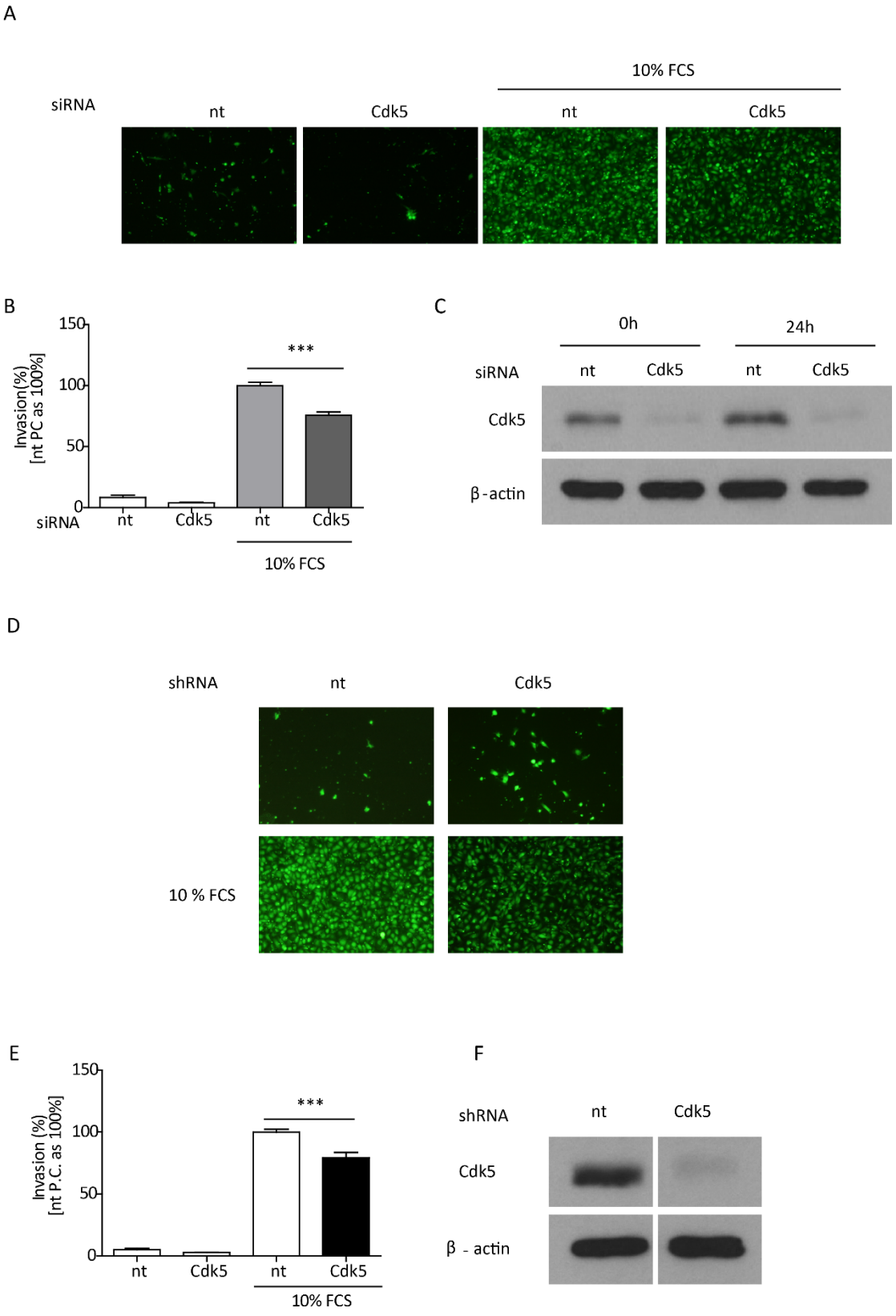

Figure 4.10: Cdk5 knockdown reduced MDA-MB-231 cells invasion.

(A) FCS-induced invasion of MDA-MB-231 cells treated with nt or Cdk5 siRNA is shown. (B) Quantitative evaluation of nt or Cdk5 siRNA treated cells migrated through Matrigel®-coated membranes is shown. (n=3,

one-way ANOVA, Tukey's post-test, ***p<0.001) (C) Immunoblot shows Cdk5 silencing. Actin indicates equal loading. (D) FCS-induced invasion of nt and Cdk5 shRNA MDA-MB-231 cells is shown. (E) Quantitative evaluation of nt or Cdk5 shRNA MDA-MB-231 cells migrated through Matrigel®-coated membranes is shown. Bars represents mean ± SEM. (n=3, one-way ANOVA, ***p<0.001, Tukey's post-test). (C,F) Immunoblot shows Cdk5 knockdown. Actin indicates equal loading.

4.1.10 Silencing of Cdk5 inhibits mammosphere formation

Next, we aimed to determine whether the impaired mammopshere formation by Roscovitine was due to Cdk5 inhibition. As shown in Figure 4.11, Cdk5 downregulation led to reduced mammosphere formation down to approximately 60%. This suggests that Cdk5 was important for mammosphere formation in MDA-MB-231 cells.

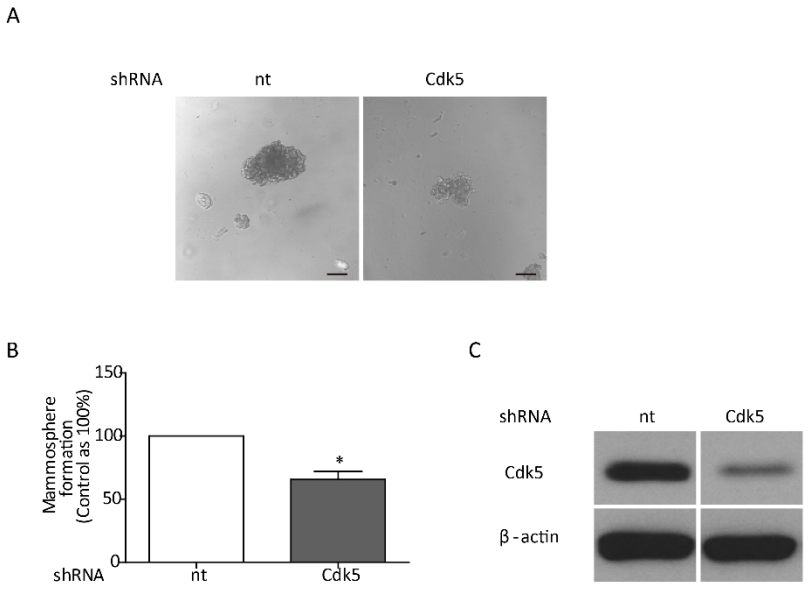

Figure 4.11: Cdk5 downregulation reduced breast cancer cell mammosphere formation.
(A) Mammosphere formation of nt and Cdk5 shRNA MDA-MB-231 cells is shown. Scale bar : 100 µm. (B) Quantitative evaluation of mammosphere formation assays. n=3, paired t-test, *p<0.05. (C) Immunoblot shows Cdk5 downregulation. Actin indicates equal loading.

5 Discussion

5.1 Evaluation of the V-ATPase inhibitor Archazolid for treatment of T-cell acute lymphoblastic leukemia

This study demonstrates that V-ATPase inhibition by Archazolid A induces apoptosis of leukemic cells that are resistant to γ-secretase inhibitor treatment. Archazolid A inhibits Notch signaling in a different mode of action than GSIs, i.e. by blocking endosomal Notch processing due to V-ATPase inhibition, and abrogates the pro-survival protein survivin. Thus, we suggest V-ATPase as a potential drug target for T-ALL and V-ATPase inhibition by Archazolid A as an alternative therapeutic option for T-ALL.

5.1.1 GSI treatment in T-ALL

Studies showing that more than 50% of T-ALL cases have Notch activating mutations have broaden our understanding for T-ALL origin and have highlighted Notch inhibition as a therapeutic strategy (2). Given the strict requirement of γ-secretase for Notch signaling activation, Notch inhibition via GSI seems to be a promising approach to treat T-ALL. Therefore, GSIs have been evaluated in clinical trials for T-ALL therapy. However, in clinical trials, GSI treatment was unsuccessful in T-ALL treatment. GSI treatment exerted only moderate cytostatic effects and failed to induce apoptosis in various leukemic cell lines (2, 5), resulting in only weak anti-leukemic effects and poor clinical response (1). In fact, GSI treatment is only effective when the cells express membrane-bound Notch receptors that require γ-secretase processing. In Notch activation mutant T-ALL cells, such as those lack PEST domain (required for ubiquitination, followed by proteosomal degradation), GSI will not have beneficial effects. In some T-ALL cell lines, GSIs failed to induce Notch down-regulations, because proteasomal Notch degradation was inhibited due to mutations of the Notch receptor that impaired Notch ubiquitination or the ubiquitin ligase FBW7 that is essential for Notch proteasomal degradation (100). In T-ALL cell lines that carry FBW7 mutations, such as Jurkat and CEM, the mutated FBW7 either cannot bind NICD or cannot target its downstream target c-Myc for degradation and therefore contributes to GSI resistance (100).

Moreover, gastrointestinal toxicity was also observed in T-ALL patients with systemic GSI treatment. Nowadays, no drugs that block Notch activation have entered the clinic and the treatment of T-ALL remains a problem due to high rate of relapse and resistance.

5.1.2 Archazolid A inhibits Notch signaling in a mode of action different from GSIs

We suggest V-ATPase inhibition as alternative strategy to block Notch signaling in leukemic cells. We show that V-ATPase inhibition by Archazolid A induces apoptosis in leukemic cell lines that do not get apoptotic by GSI treatment and suggest an alternative mode of action: blocking of Notch activation by inhibition of its endosomal processing. Notch receptor internalization/endocytosis after ligand binding is important for Notch signaling activation (101). Low pH is a prerequisite for γ-secretase mediated Notch signaling activation in the endo-/lysosomal compartment (102). V-ATPase is required for activation of the Notch receptor by regulating its endosomal cleavage via γ-secretase (53, 54). In Drosophila, mutations of V-ATPase lead to defects in processing of the internalized Notch receptor. By V-ATPase inhibition, the Notch receptor is trapped in the endo-lysosomal compartment but cannot get cleaved and activated (53, 54). Kobia *et al* showed V-ATPase inhibition by Bafilomycin A1 (BafA1) reduced Notch signaling during drosophila and zebrafish development and in human cells. BafA1 treatment led to Notch accumulation in the endo-lysosomal system and inhibited growth of Notch-dependent breast cancer cells. In contrast, BafA1 treatment reduced leukemia cell growth without affecting Notch signaling activation. Our results demonstrate that V-ATPase inhibition by Archazolid A induced apoptosis of leukemic cells in contrast to GSI. Although both Archazolid A and DBZ reduced Notch signaling activity, our results demonstrate that V-ATPase inhibition exerted an alternative mode of action. Like DBZ, Archazolid A reduced Notch receptor cleavage at S3-site (Val1744). However, in contrast to GSI treatment, by Archazolid A treatment, the Notch receptor accumulated in the endo-lysosomal compartment but not at the cell surface. Moreover, Archazolid A reduced levels of c-Myc, a crucial transcriptional target of Notch1 (6, 103-105), more efficiently than DBZ. In addition, the anti-apoptotic protein survivin was reduced by Archazolid A but not by DBZ. Thus, reduction of c-Myc and survivin by Archaozlid A could be another and/or an additional mechanism that triggers cell death in leukemia cells (100, 106).

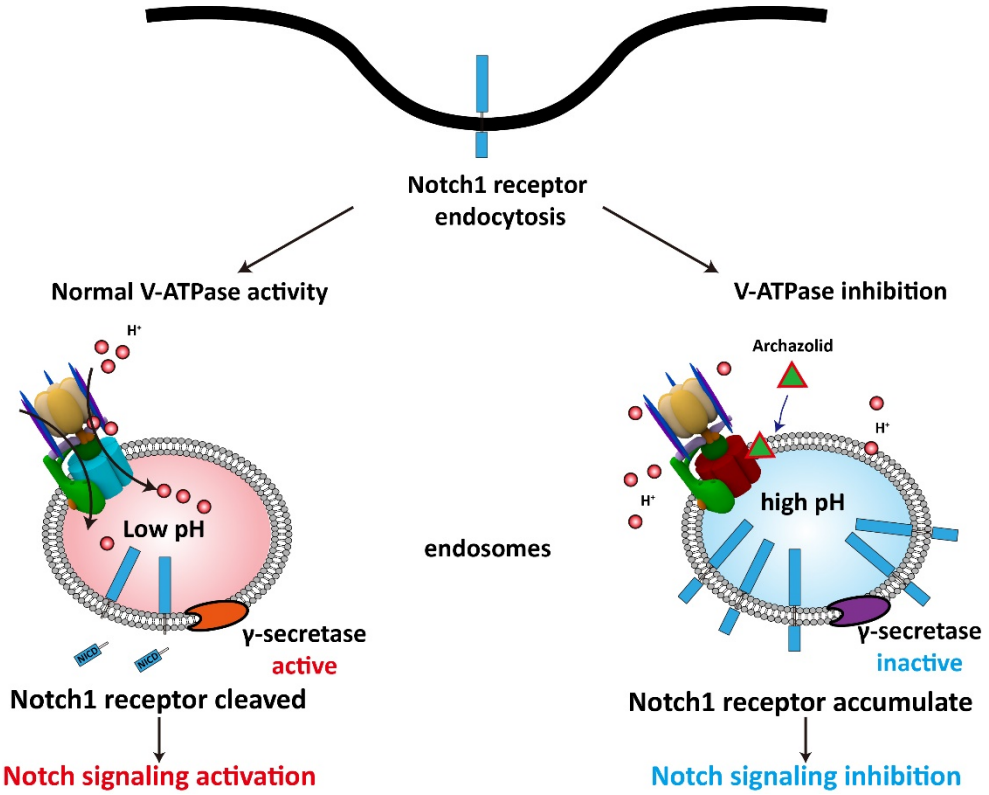

Figure 5.1 Functional V-ATPase is required for Notch signaling activation

Under normal conditions, V-ATPase pumps protons into the endo-lysosomal lumen in an ATP-dependent manner. Acidic environment is essential for optimal Notch1 receptor cleavage by γ-secretase, releasing NICD from plasma membrane, which then translocates to the nucleus and subsequently activates Notch signaling. V-ATPase inhibition by Archazolid A impaired endo-lysosomal acidification, and therefore inhibited endo-lysosomal Notch1 receptor cleavage by γ-secretase, leading to reduced Notch signaling.

Survivin is a member of the inhibitor of apoptosis protein (IAP) family, that is involved in many pathways regulating cellular homeostasis (107). Survivin negatively regulates apoptosis by inhibiting caspase activation. Survivin is shown to be overexpressed in more than 90% of adult T-cell leukemia and in T-ALL cell lines. Increased survivin level is linked to poor clinical outcomes (108, 109) and mediates drug resistance. Targeting survivin using antisense oligonucleotides in combination with chemotherapy was indicated to eliminate relapsed T-ALL in a xenograft model (110). A link between Notch1 and survivin has already been indicated, i.e. Notch1 regulates the expression of survivin through NF-κB. In breast cancer Notch1 triggered NF-κB signaling pathway activation and upregulated the expression of survivin (111). Moreover, downregulation of Notch1 reduced NF-κB activity and pharmacological inhibition NF-κB could suppress the expression of survivin (112, 113). Our results show that V-ATPase inhibiton via Archazolid A decreased survivin whereas DBZ had no effect. This might indicate that the effect of Archazolid A on apoptosis induction does not exclusively depend on inhibition of Notch1, but is mediated at least in part by decreased survivin. A

previous study in cadiomyocytes showed V-ATPase inhibition via Bafilomycin A1 enhanced expression of p53 (114). Because survivin is negatively regulated by p53 and participates in p53-dependent apoptotic pathway (115), V-ATPase inhibition might up-regulate p53, suppressing survivin and inducing apoptosis in leukemic cells.

5.1.3 Conclusions

In summary, our results demonstrate that V-ATPase inhibition by Archazolid A exerts anti-leukemic properties. Archazolid A induces leukemic cell death by inhibition of Notch signaling activation in a way different from γ-secretase inhibitors (GSIs), and by decreasing the anti-apoptotic protein survivin. Therefore, we suggest V-ATPase is an attractive target for T-ALL therapy and V-ATPase inhibition by Archazolid A as an alternative strategy for treating leukemic cells that are resistant to γ-secretase inhibitor treatment.

5.2 Evaluation of Cdk5 as target for breast cancer treatment

Our study indicates an important role of Cdk5 in breast cancer growth and motility and indicates a function of Cdk5 in breast cancer stem cells (CSCs). Therefore, Cdk5 might represent a novel drugable target for breast cancer treatment.

5.2.1 Cdk5 is crucial for breast cancer progression

Cdk5 is a serine/threonine kinase that exerts important functions in the central nervous system (83). In contrast, only recently, the awareness of non-neuronal functions of Cdk5 has grown and its role in cancer is not well investigated. Recently, few reports indicated functions of Cdk5 in cancer (116-119). In pancreatic cancer, Cdk5 expression was amplified and increased metastasis via Ras-Ral signaling and mutant K-Ras (116, 117). In prostate cancer, Cdk5 regulates cell motility and metastatic potential (118). In non-small cell lung cancer (NSCLC) a correlation of Cdk5/p35 expression with poor prognosis of patients has been indicated (119). Furthermore, dysregulated high activity of Cdk5 in C cells of the thyroid gland was reported to initiate the formation of medullary thyroid carcinoma via phosphorylation of retinoblastoma protein (120). Recently, Cdk5 was linked to epithelial-mesenchymal transition (EMT) of breast epithelial cells (121). The authors demonstrated that Cdk5 is essential for TGF-β1 induced EMT in normal breast epithelial cells (121). EMT is a process that can lead to CSC formation. During EMT, epithelial cells lose their polarity, cell-cell-adhesion and gain migratory and invasive properties to become mesenchymal (stem) cells (122). The relatively high rate of relapse of aggressive breast cancer is attributed to breast cancer stem cells (CSCs) (122). Breast CSCs are resistant to standard therapy, show high tumor-initiating potential and cause establishment of metastases (122). Therapeutic strategies that target breast CSCs therefore may substantially improve breast cancer treatment and patient prognosis.
Our present work indicates a function of Cdk5 in breast CSCs. In line with a recent study we elucidated essential functions of Cdk5 in breast cancer cell proliferation and metastasis (121). Above that, our results suggest an implication of Cdk5 in breast CSC formation. Because genetic knockdown as well as pharmacologic inhibition of Cdk5 reduced mammosphere formation, we suggest Cdk5 as druggable target for inhibiting breast CSC formation.

To pharmacologically inhibit Cdk5, we used Roscovitine, a well-established Cdk5 inhibitor. Roscovitine is one of the earliest found and well established Cdk inhibitors and it has already been tested in clinical trials (123). Roscovitine has been shown to induce apoptosis and cell cycle arrest in

many types of cancer (88, 124-127). Although Roscovitine is the most widely used Cdk5 inhibitor, its activity is not restricted to Cdk5. Besides Cdk5, other Cdks are inhibited by Roscovitine, including Cdk1, Cdk2, Cdk7, and Cdk9 (88, 99). Our results point to a potential function of other Cdks besides Cdk5 in breast cancer because, unlike Cdk5 silencing, Roscovitine inhibited cell cycle progression and induced apoptosis of breast cancer cells. Nevertheless, some studies indicated the involvement of Cdk5 in cell death of cervical and prostate cancer (124, 128, 129).

Along this line, it would be interesting to analyze the effects of more specific Cdk5 inhibitors in breast cancer. Recent work aimed to develop new Cdk5 inhibitors with higher specificity and potency. Some of these inhibitors have been developed by using Roscovitine as mother substance and share the core structure of Roscovitine (130-133). Consequently these substances interact with the same ATP-binding pocket, possibly limiting their selectivity. Targeting the interaction of Cdk5 and its activators has been described as new approach to bypass the selectivity problem (134-136). Along this line, inhibiting the interaction of Cdk5 with its activator could represent a promising strategy for breast cancer therapy. However, it is not clear, how Cdk5 gets activated in breast cancer. Thus, further studies are required to better understand Cdk5 regulation in cancer.

To elucidate downstream targets of Cdk5 in breast CSCs remains another interesting question.
The forkhead box protein C2 (FoxC2), also called forkhead-related protein (FKHL14), has been associated with aggressive basal-like breast cancers and is implicated in breast cancer metastasis, EMT and CSC formation (137). Our recent study established a link between Cdk5 and FoxC2. Ivanov *et al.* showed that phosphorylation of FoxC2 regulates its transcriptional activity (138). Extending the knowledge about FoxC2 regulation, we showed that Cdk5 is the kinase responsible for FoxC2 phosphorylation which is essential for lymphatic vessel development and valve formation (Nat. Commun., in revision). Along this line, FoxC2 might be regulated by Cdk5 in breast cancer cells as well, contributing to the effects of Cdk5 on CSC formation. First experiments (performed by Melanie Mandl) point to a link between Cdk5 and FoxC2 in breast CSCs: overexpression of Cdk5/p35 together with FoxC2 increased mammosphere formation at higher extent than single overexpression of Cdk5/p35 respectively FoxC2. To elucidate whether Cdk5-mediated FoxC2 phosphorylation is implicated in breast CSCs, analysis of mammospheres after overexpression of a FoxC2 phosphorylation mutant together with Cdk5 is needed.
The Notch pathway represents another potential Cdk5 downstream target. The Notch pathway is critically involved in breast CSC formation and inhibition of Notch signaling can reduce mammosphere formation (139). We could recently show that Cdk5 controls tumor angiogenesis by

regulating the Notch pathway in the endothelium (manuscript in preparation). Therefore, the Notch pathway might be a possible downstream target of Cdk5 regulating CSCs.

5.2.2 Conclusions

In summary, our study established a crucial role of Cdk5 in breast cancer progression and breast CSC formation. Our study therefore suggests Cdk5 as a potential drugable target for breast cancer treatment.

6 Summary

6.1 Part 1: Evaluation of the V-ATPase inhibitor Archazolid for treatment of T-cell acute lymphoblastic leukemia

T-cell acute lymphoblastic leukemia (T-ALL) is an aggressive hematopoietic malignancy that is characterized by the infiltration of bone marrow with immature T-cells (1). T-ALL patients suffer from huge tumor burden, mediastinal enlargement and also have high a risk of CNS involvement (1). Nowadays, treatment intensification has improved T-ALL treatment. However, the treatment of T-ALL remains a problem in the clinic due to resistance and relapse (1). Notch activating mutations contribute to T-ALL initiation and progression (2). γ-secretase inhibitors (GSIs) are used as therapeutics to inhibit Notch signaling in T-ALL. However, resistance to GSI emerged as major problem and GSIs failed in clinical trials due to moderate cytostatic and poor anti-leukemic property (1). In this study, we demonstrate that V-ATPase inhibition by Archazolid A exerts anti-proliferative effects, induces apoptosis, and inhibits clonogenic survial of T-ALL cell lines that a resistant to GSI treatment. Moreover, Archazolid A inhibits Notch signaling in a different mode of action than GSIs, i.e. by blocking endosomal Notch processing and by abrogating the pro-survival protein survivin. In summary, our results demonstrate that V-ATPase inhibition by Archazolid A exerts anti-leukemic properties. Therefore, we suggest V-ATPase is an attractive target for T-ALL therapy and V-ATPase inhibition by Archazolid A as an alternative strategy for treating leukemic cells that are resistant to γ-secretase inhibitor treatment.

6.2 Part 2: Evaluation of Cdk5 as target for breast cancer treatment

For many years, Cdk5 was thought to function exclusively in the central nervous system. However, there is an increasing number of studies that show its function in the periphery and some reports indicated functions of Cdk5 in cancer progression. Our present study elucidates an important role of Cdk5 in breast cancer, pointing to a function of Cdk5 in breast cancer stem cells (CSCs) and suggesting Cdk5 as a novel drugable target for breast cancer treatment. Tissue micro assay analysis from human patient samples showed elevated Cdk5 expression in breast cancer tissue. Genetic knockdown and pharmacologic inhibition of Cdk5 inhibited breast cancer cell proliferation and colony formation, and reduced cell motility and invasion. Recently, Cdk5 was linked to epithelial-mesenchymal transition (EMT) of breast epithelial cells (121). EMT can induce formation breast CSCs that are resistant to common therapies, have high tumor initiating potential and cause tumor recurrence (64). In fact, genetic and pharmacologic inhibition of Cdk5 decreased mammosphere formation, indicating a function of Cdk5 in breast CSCs. In summary, our study elucidated a crucial

role of Cdk5 in breast cancer progression and breast CSC formation. Our study therefore suggests Cdk5 as a potential drugable target for breast cancer treatment.

7 References

1. Ferrando AA. The role of NOTCH1 signaling in T-ALL. Hematology / the Education Program of the American Society of Hematology American Society of Hematology Education Program. 2009:353-61.

2. Weng AP, Ferrando AA, Lee W, Morris JPt, Silverman LB, Sanchez-Irizarry C, et al. Activating mutations of NOTCH1 in human T cell acute lymphoblastic leukemia. Science (New York, NY). 2004;306(5694):269-71.

3. van Tetering G, van Diest P, Verlaan I, van der Wall E, Kopan R, Vooijs M. Metalloprotease ADAM10 is required for Notch1 site 2 cleavage. The Journal of biological chemistry. 2009;284(45):31018-27.

4. Aster JC, Pear WS, Blacklow SC. Notch signaling in leukemia. Annual review of pathology. 2008;3:587-613.

5. Palomero T, Barnes KC, Real PJ, Glade Bender JL, Sulis ML, Murty VV, et al. CUTLL1, a novel human T-cell lymphoma cell line with t(7;9) rearrangement, aberrant NOTCH1 activation and high sensitivity to gamma-secretase inhibitors. Leukemia. 2006;20(7):1279-87.

6. Palomero T, Lim WK, Odom DT, Sulis ML, Real PJ, Margolin A, et al. NOTCH1 directly regulates c-MYC and activates a feed-forward-loop transcriptional network promoting leukemic cell growth. Proceedings of the National Academy of Sciences of the United States of America. 2006;103(48):18261-6.

7. Palomero T, Sulis ML, Cortina M, Real PJ, Barnes K, Ciofani M, et al. Mutational loss of PTEN induces resistance to NOTCH1 inhibition in T-cell leukemia. Nature medicine. 2007;13(10):1203-10.

8. Hinton A, Bond S, Forgac M. V-ATPase functions in normal and disease processes. Pflugers Archiv : European journal of physiology. 2009;457(3):589-98.

9. Marshansky V, Futai M. The V-type H+-ATPase in vesicular trafficking: targeting, regulation and function. Current opinion in cell biology. 2008;20(4):415-26.

10. Nishi T, Forgac M. The vacuolar (H+)-ATPases--nature's most versatile proton pumps. Nature reviews Molecular cell biology. 2002;3(2):94-103.

11. Forgac M. Vacuolar ATPases: rotary proton pumps in physiology and pathophysiology. Nature reviews Molecular cell biology. 2007;8(11):917-29.

12. Brown D, Breton S. H(+)V-ATPase-dependent luminal acidification in the kidney collecting duct and the epididymis/vas deferens: vesicle recycling and transcytotic pathways. The Journal of experimental biology. 2000;203(Pt 1):137-45.

13. Frattini A, Orchard PJ, Sobacchi C, Giliani S, Abinun M, Mattsson JP, et al. Defects in TCIRG1 subunit of the vacuolar proton pump are responsible for a subset of human autosomal recessive osteopetrosis. Nature genetics. 2000;25(3):343-6.

14. Nanda A, Brumell JH, Nordstrom T, Kjeldsen L, Sengelov H, Borregaard N, et al. Activation of proton pumping in human neutrophils occurs by exocytosis of vesicles bearing vacuolar-type H+-ATPases. The Journal of biological chemistry. 1996;271(27):15963-70.

15. Lafourcade C, Sobo K, Kieffer-Jaquinod S, Garin J, van der Goot FG. Regulation of the V-ATPase along the Endocytic Pathway Occurs through Reversible Subunit Association and Membrane Localization. PLoS ONE. 2008;3(7):e2758.

16. Kane PM. The where, when, and how of organelle acidification by the yeast vacuolar H+-ATPase. Microbiology and molecular biology reviews : MMBR. 2006;70(1):177-91.

17. Powell B, Graham LA, Stevens TH. Molecular characterization of the yeast vacuolar H+-ATPase proton pore. The Journal of biological chemistry. 2000;275(31):23654-60.

18. Beyenbach KW, Wieczorek H. The V-type H+ ATPase: molecular structure and function, physiological roles and regulation. The Journal of experimental biology. 2006;209(Pt 4):577-89.

19. Sennoune SR, Bakunts K, Martinez GM, Chua-Tuan JL, Kebir Y, Attaya MN, et al. Vacuolar H+-ATPase in human breast cancer cells with distinct metastatic potential: distribution and functional activity. American journal of physiology Cell physiology. 2004;286(6):C1443-52.

20. Lu Q, Lu S, Huang L, Wang T, Wan Y, Zhou CX, et al. The expression of V-ATPase is associated with drug resistance and pathology of non-small-cell lung cancer. Diagnostic pathology. 2013;8:145.

21. Fogarty FM, O'Keeffe J, Zhadanov A, Papkovsky D, Ayllon V, O'Connor R. HRG-1 enhances cancer cell invasive potential and couples glucose metabolism to cytosolic/extracellular pH gradient regulation by the vacuolar-H ATPase. Oncogene. 2013.

22. Hinton A, Sennoune SR, Bond S, Fang M, Reuveni M, Sahagian GG, et al. Function of a subunit isoforms of the V-ATPase in pH homeostasis and in vitro invasion of MDA-MB231 human breast cancer cells. The Journal of biological chemistry. 2009;284(24):16400-8.

23. Lu X, Qin W, Li J, Tan N, Pan D, Zhang H, et al. The growth and metastasis of human hepatocellular carcinoma xenografts are inhibited by small interfering RNA targeting to the subunit ATP6L of proton pump. Cancer research. 2005;65(15):6843-9.

24. Huss M, Wieczorek H. Inhibitors of V-ATPases: old and new players. The Journal of experimental biology. 2009;212(Pt 3):341-6.

25. Werner G, Hagenmaier H, Drautz H, Baumgartner A, Zahner H. Metabolic products of microorganisms. 224. Bafilomycins, a new group of macrolide antibiotics. Production, isolation, chemical structure and biological activity. The Journal of antibiotics. 1984;37(2):110-7.

26. Kinashi H, Someno K, Sakaguchi K. Isolation and characterization of concanamycins A, B and C. The Journal of antibiotics. 1984;37(11):1333-43.

27. Kinashi H, Sakaguchi K, Higashijima T, Miyazawa T. Structures of concanamycins B and C. The Journal of antibiotics. 1982;35(11):1618-20.

28. Bowman EJ, Siebers A, Altendorf K. Bafilomycins: a class of inhibitors of membrane ATPases from microorganisms, animal cells, and plant cells. Proceedings of the National Academy of Sciences of the United States of America. 1988;85(21):7972-6.

29. Drose S, Altendorf K. Bafilomycins and concanamycins as inhibitors of V-ATPases and P-ATPases. The Journal of experimental biology. 1997;200(Pt 1):1-8.

30. Drose S, Bindseil KU, Bowman EJ, Siebers A, Zeeck A, Altendorf K. Inhibitory effect of modified bafilomycins and concanamycins on P- and V-type adenosinetriphosphatases. Biochemistry. 1993;32(15):3902-6.

31. Drose S, Boddien C, Gassel M, Ingenhorst G, Zeeck A, Altendorf K. Semisynthetic derivatives of concanamycin A and C, as inhibitors of V- and P-type ATPases: structure-activity investigations and developments of photoaffinity probes. Biochemistry. 2001;40(9):2816-25.

32. Gagliardi S, Gatti PA, Belfiore P, Zocchetti A, Clarke GD, Farina C. Synthesis and structure-activity relationships of bafilomycin A1 derivatives as inhibitors of vacuolar H+-ATPase. Journal of medicinal chemistry. 1998a;41(11):1883-93.

33. Gagliardi S, Rees M, Farina C. Chemistry and structure activity relationships of bafilomycin A1, a potent and selective inhibitor of the vacuolar H+-ATPase. Current medicinal chemistry. 1999;6(12):1197-212.

34. Hanada H, Moriyama Y, Maeda M, Futai M. Kinetic studies of chromaffin granule H+-ATPase and effects of bafilomycin A1. Biochemical and biophysical research communications. 1990;170(2):873-8.

35. Bowman BJ, Bowman EJ. Mutations in subunit C of the vacuolar ATPase confer resistance to bafilomycin and identify a conserved antibiotic binding site. The Journal of biological chemistry. 2002;277(6):3965-72.

36. Huss M, Ingenhorst G, Konig S, Gassel M, Drose S, Zeeck A, et al. Concanamycin A, the specific inhibitor of V-ATPases, binds to the V(o) subunit c. The Journal of biological chemistry. 2002;277(43):40544-8.

37. Erickson KL, Beutler JA, Cardellina IJ, Boyd MR. Salicylihalamides A and B, Novel Cytotoxic Macrolides from the Marine Sponge Haliclona sp. The Journal of organic chemistry. 1997;62(23):8188-92.

38. Galinis DL, McKee TC, Pannell LK, Cardellina JH, Boyd MR. Lobatamides A and B, Novel Cytotoxic Macrolides from the Tunicate Aplidium lobatum†. The Journal of organic chemistry. 1997;62(26):8968-9.

39. Kim JW, Shin-Ya K, Furihata K, Hayakawa Y, Seto H. Oximidines I and II: Novel Antitumor Macrolides from Pseudomonas sp. The Journal of organic chemistry. 1999;64(1):153-5.

40. Kunze B, Jansen R, Sasse F, Hofle G, Reichenbach H. Apicularens A and B, new cytostatic macrolides from Chondromyces species (myxobacteria): production, physico-chemical and biological properties. The Journal of antibiotics. 1998;51(12):1075-80.

41. Boyd MR, Farina C, Belfiore P, Gagliardi S, Kim JW, Hayakawa Y, et al. Discovery of a novel antitumor benzolactone enamide class that selectively inhibits mammalian vacuolar-type (H+)-atpases. The Journal of pharmacology and experimental therapeutics. 2001;297(1):114-20.

42. Gagliardi S, Nadler G, Consolandi E, Parini C, Morvan M, Legave MN, et al. 5-(5,6-Dichloro-2-indolyl)-2-methoxy-2,4-pentadienamides: novel and selective inhibitors of the vacuolar H+-ATPase of osteoclasts with bone antiresorptive activity. Journal of medicinal chemistry. 1998b;41(10):1568-73.

43. Nadler G, Morvan M, Delimoge I, Belfiore P, Zocchetti A, James I, et al. (2Z,4E)-5-(5,6-dichloro-2-indolyl)-2-methoxy-N-(1,2,2,6,6- pentamethylpiperidin-4-yl)-2,4-pentadienamide, a novel, potent and selective inhibitor of the osteoclast V-ATPase. Bioorganic & medicinal chemistry letters. 1998;8(24):3621-6.

44. Dixon N, Pali T, Kee TP, Ball S, Harrison MA, Findlay JB, et al. Interaction of spin-labeled inhibitors of the vacuolar H+-ATPase with the transmembrane Vo-sector. Biophysical journal. 2008;94(2):506-14.

45. Pali T, Whyteside G, Dixon N, Kee TP, Ball S, Harrison MA, et al. Interaction of inhibitors of the vacuolar H(+)-ATPase with the transmembrane Vo-sector. Biochemistry. 2004;43(38):12297-305.

46. Reichenbach H, Hofle G. Biologically active secondary metabolites from myxobacteria. Biotechnology advances. 1993;11(2):219-77.

47. Sasse F, Steinmetz H, Hofle G, Reichenbach H. Archazolids, new cytotoxic macrolactones from Archangium gephyra (Myxobacteria). Production, isolation, physico-chemical and biological properties. The Journal of antibiotics. 2003;56(6):520-5.

48. Huss M, Sasse F, Kunze B, Jansen R, Steinmetz H, Ingenhorst G, et al. Archazolid and apicularen: novel specific V-ATPase inhibitors. BMC biochemistry. 2005;6:13.

49. Wiedmann RM, von Schwarzenberg K, Palamidessi A, Schreiner L, Kubisch R, Liebl J, et al. The V-ATPase-inhibitor archazolid abrogates tumor metastasis via inhibition of endocytic activation of the Rho-GTPase Rac1. Cancer research. 2012;72(22):5976-87.

50. von Schwarzenberg K, Wiedmann RM, Oak P, Schulz S, Zischka H, Wanner G, et al. Mode of cell death induction by pharmacological vacuolar H+-ATPase (V-ATPase) inhibition. J Biol Chem. 2013;288(2):1385-96.

51. von Schwarzenberg K, Lajtos T, Simon L, Muller R, Vereb G, Vollmar AM. V-ATPase inhibition overcomes trastuzumab resistance in breast cancer. Molecular oncology. 2014;8(1):9-19.

52. Hassfeld J, Fares C, Steinmetz H, Carlomagno T, Menche D. Stereochemical determination of Archazolid A and B, highly potent vacuolar-type ATPase inhibitors from the Myxobacterium Archangium gephyra. Organic letters. 2006;8(21):4751-4.

53. Yan Y, Denef N, Schupbach T. The vacuolar proton pump, V-ATPase, is required for notch signaling and endosomal trafficking in Drosophila. Developmental cell. 2009;17(3):387-402.

54. Vaccari T, Duchi S, Cortese K, Tacchetti C, Bilder D. The vacuolar ATPase is required for physiological as well as pathological activation of the Notch receptor. Development (Cambridge, England). 2010;137(11):1825-32.

55. Kobia F, Duchi S, Deflorian G, Vaccari T. Pharmacologic inhibition of vacuolar H+ ATPase reduces physiologic and oncogenic Notch signaling. Molecular oncology. 2014;8(2):207-20.

56. Sukhai MA, Prabha S, Hurren R, Rutledge AC, Lee AY, Sriskanthadevan S, et al. Lysosomal disruption preferentially targets acute myeloid leukemia cells and progenitors. The Journal of clinical investigation. 2013;123(1):315-28.

57. Tinoco G, Warsch S, Gluck S, Avancha K, Montero AJ. Treating breast cancer in the 21st century: emerging biological therapies. J Cancer. 2013;4(2):117-32.

58. Siegel R, Ward E, Brawley O, Jemal A. Cancer statistics, 2011: the impact of eliminating socioeconomic and racial disparities on premature cancer deaths. CA: a cancer journal for clinicians. 2011;61(4):212-36.

59. Rakha EA, El-Sayed ME, Green AR, Lee AH, Robertson JF, Ellis IO. Prognostic markers in triple-negative breast cancer. Cancer. 2007;109(1):25-32.

60. Yagi H, Tan W, Dillenburg-Pilla P, Armando S, Amornphimoltham P, Simaan M, et al. A synthetic biology approach reveals a CXCR4-G13-Rho signaling axis driving transendothelial migration of metastatic breast cancer cells. Science signaling. 2011;4(191):ra60.

61. Vogel CL, Cobleigh MA, Tripathy D, Gutheil JC, Harris LN, Fehrenbacher L, et al. Efficacy and safety of trastuzumab as a single agent in first-line treatment of HER2-overexpressing metastatic

breast cancer. Journal of clinical oncology : official journal of the American Society of Clinical Oncology. 2002;20(3):719-26.

62. Burstein HJ, Kuter I, Campos SM, Gelman RS, Tribou L, Parker LM, et al. Clinical activity of trastuzumab and vinorelbine in women with HER2-overexpressing metastatic breast cancer. Journal of clinical oncology : official journal of the American Society of Clinical Oncology. 2001;19(10):2722-30.

63. Montemurro F, Choa G, Faggiuolo R, Donadio M, Minischetti M, Durando A, et al. A phase II study of three-weekly docetaxel and weekly trastuzumab in HER2-overexpressing advanced breast cancer. Oncology. 2004;66(1):38-45.

64. Dave B, Mittal V, Tan NM, Chang JC. Epithelial-mesenchymal transition, cancer stem cells and treatment resistance. Breast cancer research : BCR. 2012;14(1):202.

65. Ouyang. G. Epithelial-Mesenchymal Transition and Cancer Stem Cells. In: Stanley Shostak eds. Cancer Stem Cells - The Cutting Edge. InTech. 2011.

66. Thiery JP, Acloque H, Huang RY, Nieto MA. Epithelial-mesenchymal transitions in development and disease. Cell. 2009;139(5):871-90.

67. Yang J, Mani SA, Donaher JL, Ramaswamy S, Itzykson RA, Come C, et al. Twist, a master regulator of morphogenesis, plays an essential role in tumor metastasis. Cell. 2004;117(7):927-39.

68. Yang J, Weinberg RA. Epithelial-mesenchymal transition: at the crossroads of development and tumor metastasis. Developmental cell. 2008;14(6):818-29.

69. Mani SA, Guo W, Liao MJ, Eaton EN, Ayyanan A, Zhou AY, et al. The epithelial-mesenchymal transition generates cells with properties of stem cells. Cell. 2008;133(4):704-15.

70. Brabletz T, Jung A, Spaderna S, Hlubek F, Kirchner T. Opinion: migrating cancer stem cells - an integrated concept of malignant tumour progression. Nat Rev Cancer. 2005;5(9):744-9.

71. Polyak K, Weinberg RA. Transitions between epithelial and mesenchymal states: acquisition of malignant and stem cell traits. Nat Rev Cancer. 2009;9(4):265-73.

72. Chang JC, Wooten EC, Tsimelzon A, Hilsenbeck SG, Gutierrez MC, Tham YL, et al. Patterns of resistance and incomplete response to docetaxel by gene expression profiling in breast cancer patients. Journal of clinical oncology : official journal of the American Society of Clinical Oncology. 2005;23(6):1169-77.

73. Li X, Lewis MT, Huang J, Gutierrez C, Osborne CK, Wu MF, et al. Intrinsic resistance of tumorigenic breast cancer cells to chemotherapy. Journal of the National Cancer Institute. 2008;100(9):672-9.

74. Hellmich MR, Pant HC, Wada E, Battey JF. Neuronal cdc2-like kinase: a cdc2-related protein kinase with predominantly neuronal expression. Proceedings of the National Academy of Sciences of the United States of America. 1992;89(22):10867-71.

75. Meyerson M, Enders GH, Wu CL, Su LK, Gorka C, Nelson C, et al. A family of human cdc2-related protein kinases. The EMBO journal. 1992;11(8):2909-17.

76. Lew J, Winkfein RJ, Paudel HK, Wang JH. Brain proline-directed protein kinase is a neurofilament kinase which displays high sequence homology to p34cdc2. The Journal of biological chemistry. 1992;267(36):25922-6.

77. Xiong Y, Zhang H, Beach D. D type cyclins associate with multiple protein kinases and the DNA replication and repair factor PCNA. Cell. 1992;71(3):505-14.

78. Ohshima T, Ward JM, Huh CG, Longenecker G, Veeranna, Pant HC, et al. Targeted disruption of the cyclin-dependent kinase 5 gene results in abnormal corticogenesis, neuronal pathology and perinatal death. Proceedings of the National Academy of Sciences of the United States of America. 1996;93(20):11173-8.

79. Smith DS, Tsai LH. Cdk5 behind the wheel: a role in trafficking and transport? Trends in cell biology. 2002;12(1):28-36.

80. Su SC, Tsai LH. Cyclin-dependent kinases in brain development and disease. Annual review of cell and developmental biology. 2011;27:465-91.

81. Patrick GN, Zukerberg L, Nikolic M, de la Monte S, Dikkes P, Tsai LH. Conversion of p35 to p25 deregulates Cdk5 activity and promotes neurodegeneration. Nature. 1999;402(6762):615-22.

82. Cruz JC, Tsai LH. Cdk5 deregulation in the pathogenesis of Alzheimer's disease. Trends in molecular medicine. 2004;10(9):452-8.

83. Liebl J, Furst R, Vollmar AM, Zahler S. Twice switched at birth: cell cycle-independent roles of the "neuron-specific" cyclin-dependent kinase 5 (Cdk5) in non-neuronal cells. Cellular signalling. 2011;23(11):1698-707.

84. Berberich N, Uhl B, Joore J, Schmerwitz UK, Mayer BA, Reichel CA, et al. Roscovitine blocks leukocyte extravasation by inhibition of cyclin-dependent kinases 5 and 9. British journal of pharmacology. 2011;163(5):1086-98.

85. Liebl J, Weitensteiner SB, Vereb G, Takacs L, Furst R, Vollmar AM, et al. Cyclin-dependent kinase 5 regulates endothelial cell migration and angiogenesis. J Biol Chem. 2010;285(46):35932-43.

86. Vesely J, Havlicek L, Strnad M, Blow JJ, Donella-Deana A, Pinna L, et al. Inhibition of cyclin-dependent kinases by purine analogues. European journal of biochemistry / FEBS. 1994;224(2):771-86.

87. De Azevedo WF, Leclerc S, Meijer L, Havlicek L, Strnad M, Kim SH. Inhibition of cyclin-dependent kinases by purine analogues: crystal structure of human cdk2 complexed with roscovitine. European journal of biochemistry / FEBS. 1997;243(1-2):518-26.

88. Meijer L, Borgne A, Mulner O, Chong JP, Blow JJ, Inagaki N, et al. Biochemical and cellular effects of roscovitine, a potent and selective inhibitor of the cyclin-dependent kinases cdc2, cdk2 and cdk5. European journal of biochemistry / FEBS. 1997;243(1-2):527-36.

89. Meijer L BK, Galons H. (R)-Roscovitine (CYC202, Seliciclib). In: Smith PJ, Yue EW, eds. Inhibitors of cyclin dependent kinases as anti-tumor agents. CRC Press Taylor & Francis Group. 2006.

90. Tanaka T, Serneo FF, Tseng HC, Kulkarni AB, Tsai LH, Gleeson JG. Cdk5 phosphorylation of doublecortin ser297 regulates its effect on neuronal migration. Neuron. 2004;41(2):215-27.

91. Nicoletti I, Migliorati G, Pagliacci MC, Grignani F, Riccardi C. A rapid and simple method for measuring thymocyte apoptosis by propidium iodide staining and flow cytometry. Journal of immunological methods. 1991;139(2):271-9.

92. Dontu G, Abdallah WM, Foley JM, Jackson KW, Clarke MF, Kawamura MJ, et al. In vitro propagation and transcriptional profiling of human mammary stem/progenitor cells. Genes & development. 2003;17(10):1253-70.

93. Bradford MM. A rapid and sensitive method for the quantitation of microgram quantities of protein utilizing the principle of protein-dye binding. Analytical biochemistry. 1976;72:248-54.

94. Pfaffl MW. A new mathematical model for relative quantification in real-time RT-PCR. Nucleic acids research. 2001;29(9):e45.

95. Okahashi N, Nakamura I, Jimi E, Koide M, Suda T, Nishihara T. Specific inhibitors of vacuolar H(+)-ATPase trigger apoptotic cell death of osteoclasts. Journal of bone and mineral research : the official journal of the American Society for Bone and Mineral Research. 1997;12(7):1116-23.

96. Schempp CM, von Schwarzenberg K, Schreiner L, Kubisch R, Müller R, Wagner E, et al. V-ATPase inhibition regulates anoikis resistance and metastasis of cancer cells. Molecular Cancer Therapeutics. 2014.

97. De Milito A, Iessi E, Logozzi M, Lozupone F, Spada M, Marino ML, et al. Proton Pump Inhibitors Induce Apoptosis of Human B-Cell Tumors through a Caspase-Independent Mechanism Involving Reactive Oxygen Species. Cancer research. 2007;67(11):5408-17.

98. Fakler M, Loeder S, Vogler M, Schneider K, Jeremias I, Debatin KM, et al. Small molecule XIAP inhibitors cooperate with TRAIL to induce apoptosis in childhood acute leukemia cells and overcome Bcl-2-mediated resistance. Blood. 2009;113(8):1710-22.

99. Bach S, Knockaert M, Reinhardt J, Lozach O, Schmitt S, Baratte B, et al. Roscovitine targets, protein kinases and pyridoxal kinase. The Journal of biological chemistry. 2005;280(35):31208-19.

100. O'Neil J, Grim J, Strack P, Rao S, Tibbitts D, Winter C, et al. FBW7 mutations in leukemic cells mediate NOTCH pathway activation and resistance to gamma-secretase inhibitors. The Journal of experimental medicine. 2007;204(8):1813-24.

101. Fortini ME, Bilder D. Endocytic regulation of Notch signaling. Current opinion in genetics & development. 2009;19(4):323-8.

102. Pasternak SH, Bagshaw RD, Guiral M, Zhang S, Ackerley CA, Pak BJ, et al. Presenilin-1, nicastrin, amyloid precursor protein, and gamma-secretase activity are co-localized in the lysosomal membrane. The Journal of biological chemistry. 2003;278(29):26687-94.

103. Weng AP, Millholland JM, Yashiro-Ohtani Y, Arcangeli ML, Lau A, Wai C, et al. c-Myc is an important direct target of Notch1 in T-cell acute lymphoblastic leukemia/lymphoma. Genes & development. 2006;20(15):2096-109.

104. Chan SM, Weng AP, Tibshirani R, Aster JC, Utz PJ. Notch signals positively regulate activity of the mTOR pathway in T-cell acute lymphoblastic leukemia. Blood. 2007;110(1):278-86.

105. Sharma VM, Calvo JA, Draheim KM, Cunningham LA, Hermance N, Beverly L, et al. Notch1 contributes to mouse T-cell leukemia by directly inducing the expression of c-myc. Molecular and cellular biology. 2006;26(21):8022-31.

106. King B, Trimarchi T, Reavie L, Xu L, Mullenders J, Ntziachristos P, et al. The ubiquitin ligase FBXW7 modulates leukemia-initiating cell activity by regulating MYC stability. Cell. 2013;153(7):1552-66.

107. Altieri DC. Survivin, cancer networks and pathway-directed drug discovery. Nat Rev Cancer. 2008;8(1):61-70.

108. Nakayama K, Kamihira S. Survivin an important determinant for prognosis in adult T-cell leukemia: a novel biomarker in practical hemato-oncology. Leukemia & lymphoma. 2002;43(12):2249-55.

109. Sugahara K, Uemura A, Harasawa H, Nagai H, Hirakata Y, Tomonaga M, et al. Clinical relevance of survivin as a biomarker in neoplasms, especially in adult T-cell leukemias and acute leukemias. International journal of hematology. 2004;80(1):52-8.

110. Park E, Gang EJ, Hsieh YT, Schaefer P, Chae S, Klemm L, et al. Targeting survivin overcomes drug resistance in acute lymphoblastic leukemia. Blood. 2011;118(8):2191-9.

111. Li L, Zhao F, Lu J, Li T, Yang H, Wu C, et al. Notch-1 Signaling Promotes the Malignant Features of Human Breast Cancer through NF-κB Activation. PLoS ONE. 2014;9(4):e95912.

112. Wang Z, Zhang Y, Li Y, Banerjee S, Liao J, Sarkar FH. Down-regulation of Notch-1 contributes to cell growth inhibition and apoptosis in pancreatic cancer cells. Molecular Cancer Therapeutics. 2006;5(3):483-93.

113. Kawakami H, Tomita M, Matsuda T, Ohta T, Tanaka Y, Fujii M, et al. Transcriptional activation of survivin through the NF-kappaB pathway by human T-cell leukemia virus type I tax. International journal of cancer Journal international du cancer. 2005;115(6):967-74.

114. Long X, Crow MT, Sollott SJ, O'Neill L, Menees DS, de Lourdes Hipolito M, et al. Enhanced expression of p53 and apoptosis induced by blockade of the vacuolar proton ATPase in cardiomyocytes. The Journal of clinical investigation. 1998;101(6):1453-61.

115. Mirza A, McGuirk M, Hockenberry TN, Wu Q, Ashar H, Black S, et al. Human survivin is negatively regulated by wild-type p53 and participates in p53-dependent apoptotic pathway. Oncogene. 2002;21(17):2613-22.

116. Feldmann G, Mishra A, Hong SM, Bisht S, Strock CJ, Ball DW, et al. Inhibiting the cyclin-dependent kinase CDK5 blocks pancreatic cancer formation and progression through the suppression of Ras-Ral signaling. Cancer research. 2010;70(11):4460-9.

117. Eggers JP, Grandgenett PM, Collisson EC, Lewallen ME, Tremayne J, Singh PK, et al. Cyclin-dependent kinase 5 is amplified and overexpressed in pancreatic cancer and activated by mutant K-Ras. Clinical cancer research : an official journal of the American Association for Cancer Research. 2011;17(19):6140-50.

118. Strock CJ, Park JI, Nakakura EK, Bova GS, Isaacs JT, Ball DW, et al. Cyclin-dependent kinase 5 activity controls cell motility and metastatic potential of prostate cancer cells. Cancer research. 2006;66(15):7509-15.

119. Liu JL, Wang XY, Huang BX, Zhu F, Zhang RG, Wu G. Expression of CDK5/p35 in resected patients with non-small cell lung cancer: relation to prognosis. Medical oncology (Northwood, London, England). 2011;28(3):673-8.

120. Pozo K, Castro-Rivera E, Tan C, Plattner F, Schwach G, Siegl V, et al. The role of Cdk5 in neuroendocrine thyroid cancer. Cancer cell. 2013;24(4):499-511.

121. Liang Q, Li L, Zhang J, Lei Y, Wang L, Liu DX, et al. CDK5 is essential for TGF-beta1-induced epithelial-mesenchymal transition and breast cancer progression. Scientific reports. 2013;3:2932.

122. Singh A, Settleman J. EMT, cancer stem cells and drug resistance: an emerging axis of evil in the war on cancer. Oncogene. 2010;29(34):4741-51.

123. Benson C, White J, De Bono J, O'Donnell A, Raynaud F, Cruickshank C, et al. A phase I trial of the selective oral cyclin-dependent kinase inhibitor seliciclib (CYC202; R-Roscovitine), administered twice daily for 7 days every 21 days. British journal of cancer. 2007;96(1):29-37.

124. Goodyear S, Sharma MC. Roscovitine regulates invasive breast cancer cell (MDA-MB231) proliferation and survival through cell cycle regulatory protein cdk5. Experimental and molecular pathology. 2007;82(1):25-32.

125. Hahntow IN, Schneller F, Oelsner M, Weick K, Ringshausen I, Fend F, et al. Cyclin-dependent kinase inhibitor Roscovitine induces apoptosis in chronic lymphocytic leukemia cells. Leukemia. 2004;18(4):747-55.

126. Lacrima K, Rinaldi A, Vignati S, Martin V, Tibiletti MG, Gaidano G, et al. Cyclin-dependent kinase inhibitor seliciclib shows in vitro activity in diffuse large B-cell lymphomas. Leukemia & lymphoma. 2007;48(1):158-67.

127. Wesierska-Gadek J, Gueorguieva M, Horky M. Dual action of cyclin-dependent kinase inhibitors: induction of cell cycle arrest and apoptosis. A comparison of the effects exerted by roscovitine and cisplatin. Polish journal of pharmacology. 2003;55(5):895-902.

128. Lin H, Juang JL, Wang PS. Involvement of Cdk5/p25 in digoxin-triggered prostate cancer cell apoptosis. The Journal of biological chemistry. 2004;279(28):29302-7.

129. Kuo HS, Hsu FN, Chiang MC, You SC, Chen MC, Lo MJ, et al. The role of Cdk5 in retinoic acid-induced apoptosis of cervical cancer cell line. The Chinese journal of physiology. 2009;52(1):23-30.

130. Demange L, Abdellah FN, Lozach O, Ferandin Y, Gresh N, Meijer L, et al. Potent inhibitors of CDK5 derived from roscovitine: synthesis, biological evaluation and molecular modelling. Bioorganic & medicinal chemistry letters. 2013;23(1):125-31.

131. Weitensteiner SB, Liebl J, Krystof V, Havlíček L, Gucký T, Strnad M, et al. Trisubstituted Pyrazolopyrimidines as Novel Angiogenesis Inhibitors. PLoS ONE. 2013;8(1):e54607.

132. Liebl J, Krystof V, Vereb G, Takacs L, Strnad M, Pechan P, et al. Anti-angiogenic effects of purine inhibitors of cyclin dependent kinases. Angiogenesis. 2011;14(3):281-91.

133. Putey A, Fournet G, Lozach O, Perrin L, Meijer L, Joseph B. Synthesis and biological evaluation of tetrahydro[1,4]diazepino[1,2-a]indol-1-ones as cyclin-dependent kinase inhibitors. European journal of medicinal chemistry. 2014;83c:617-29.

134. Corbel C, Wang Q, Bousserouel H, Hamdi A, Zhang B, Lozach O, et al. First BRET-based screening assay performed in budding yeast leads to the discovery of CDK5/p25 interaction inhibitors. Biotechnology journal. 2011;6(7):860-70.

135. Zhang B, Corbel C, Gueritte F, Couturier C, Bach S, Tan VB. An in silico approach for the discovery of CDK5/p25 interaction inhibitors. Biotechnology journal. 2011;6(7):871-81.

136. Zheng YL, Li BS, Amin ND, Albers W, Pant HC. A peptide derived from cyclin-dependent kinase activator (p35) specifically inhibits Cdk5 activity and phosphorylation of tau protein in transfected cells. European journal of biochemistry / FEBS. 2002;269(18):4427-34.

137. Mani SA, Yang J, Brooks M, Schwaninger G, Zhou A, Miura N, et al. Mesenchyme Forkhead 1 (FOXC2) plays a key role in metastasis and is associated with aggressive basal-like breast cancers. Proceedings of the National Academy of Sciences of the United States of America. 2007;104(24):10069-74.

138. Ivanov KI, Agalarov Y, Valmu L, Samuilova O, Liebl J, Houhou N, et al. Phosphorylation regulates FOXC2-mediated transcription in lymphatic endothelial cells. Molecular and cellular biology. 2013;33(19):3749-61.

139. Dontu G, Jackson K, McNicholas E, Kawamura M, Abdallah W, Wicha M. Role of Notch signaling in cell-fate determination of human mammary stem/progenitor cells. Breast cancer research : BCR. 2004;6(6):R605 - R15.

8 Appendix

8.1 Abbreviations

Table 8.1 List of Abbrevations

ANOVA	Analysis of variance between groups
APS	Ammoniumpersulfate
Arg	Arginine
ATP	Adenosine triphosphate
bFGF	human basic fibroblast growth factor
BSA	Bovine serum albumin
CAPS	Cyclohexylamino-1-propane sulfonic acid
Cdk	Cyclin dependent kinase
cDNA	Complementary desoxyribonucleic acid
CIP	Cdk5 inhibitory peptide
CNS	Central Nervous System
DBZ	Dibenzazepine
DMEM	Dulbecco's Modified Eagle Medium
DMSO	Dimethyl sulfoxide
DNA	Deoxyribonucleic acid
DTT	Dithiothreitol
EC_{50}	Half maximal effective concentration
ECL	Enhanced chemiluminescence
EDTA	Ethylenediaminetetraacetic acid
FACS	Fluorescence activated cell sorter
FCS	Fetal calf serum
FL2-A	Fluorescent channel 2 area
FL2-H	Fluorescent channel 2 height
FS	Fluorochrome solution
FSC	Forward scatter
Glu	Glutamic acid

h	Hour
hEGF	Human epidermal growth factor
HFS	Hypotonic fluorescent solution
HRP	Horseradish peroxidase
LSM	Laser scanning microscope
mg, ml, mM	Milligram, milliliter, millimolar
min	Minute(s)
mRNA	Messenger ribonucleic acid
nM	Nanomolar
nm	Nanometer
nt siRNA	Non targeting small interfering ribonucleic acid
PBS	Phosphate buffered saline
PFA	Paraformaldehyde
PI	Propidium iodide
PMSF	Phenylmethylsulfonyl fluoride
Poly-HEMA	Poly(2-hydroxyethyl methacrylate)
RNA	Ribonucleic acid
rpm	Revolutions per minute
RT	Room temperature
RT PCR	Reverse transcriptase polymerase chain reaction
SEM	Standard error of the mean value
SDS	Sodium dodecyl sulfate
SDS-PAGE	Sodium dodecyl sulfate polyacrylamide gel electrophoresis
shRNA	Short hairpin ribonucleic acid
siRNA	Small interfering ribonucleic acid
T/E	Trypsin/EDTA
TACE	TNF-α converting enzyme
TEMED	*N, N, N', N'* tetramethylethylene diamine
TMA	Tissue microarray

Tris	Trishydroxymethylaminomethane
µg, µl, µM	Microgram, microliter, micromolar
ANOVA	Analysis of variance between groups

8.2 Publications

8.2.1 Original publication

Johanna Liebl *, Markus Moser, Yan Agalarov, **Siwei Zhang**, Bianca Hager, James A. Bibb, Ralf H. Adams, Friedemann Kiefer, Naoyuki Miura, Tatiana V. Petrova, Angelika M. Vollmar, Stefan Zahler. **Cdk5 controls lymphatic vessel development and function by phosphorylation of FoxC2**. (Nat. Commun., in revision)

8.2.2 Presentations

Johanna Liebl, **Siwei Zhang**, Melanie Mandl, Elisa Schmoeckel, Doris Mayr, Stefan Zahler, Angelika M. Vollmar

Cdk5 is implicated in breast cancer stem cell formation.

DGPT Annual Meeting 2014, Hannover, Germany

Johanna Liebl, Markus Moser, Bianca Hager, **Siwei Zhang**, Robert Fürst, James A Bibb, Ralf H. Adams, Angelika M. Vollmar, Stefan Zahler

Novel function of Cdk5 in lymphatic vessel development

DGPT Annual Meeting 2013, Halle, Germany

Johanna Liebl, Markus Moser, Bianca Hager, **Siwei Zhang**, Robert Fürst, James A Bibb, Ralf H. Adams, Angelika M. Vollmar, Stefan Zahler

A Vascular function of Cyclin dependent kinase 5 (Cdk5)

DPhG Annual Meeting 2012, Greifswald, Germany

Johanna Liebl, Markus Moser, James A Bibb, **Siwei Zhang**, Robert Fürst, Angelika M. Vollmar, Stefan Zahler

A novel role of Cyclin dependent kinase 5 in angiogenesis and lymphangiogenesis
DGPT Annual Meeting 2011, Frankfurt, Germany

Johanna Liebl, Markus Moser, James A Bibb, **Siwei Zhang**, Robert Fürst, Angelika M. Vollmar, Stefan Zahler
Conditional knockout of Cyclin dependent kinase 5 in endothelial cells reveals its role in angiogenesis and lymphangiogenesis
EC8 2011, Zurich, Switzerland

Johanna Liebl, Markus Moser, James A Bibb, **Siwei Zhang**, Robert Fürst, Angelika M. Vollmar, Stefan Zahler
Cyclin dependent kinase 5 controls angiogenesis and lymphangiogenesis
Gordon Research Conference 2011, Ventura, CA, USA

Johanna Liebl, Markus Moser, Bianca Hager, **Siwei Zhang**, Robert Fürst, James A Bibb, Ralf H. Adams, Angelika M. Vollmar, Stefan Zahler
Cyclin dependent kinase 5 (Cdk5) and its function in the endothelium
Joint Meeting of the ESM and the GfMVB 2011, Munich, Germany

8.3 Acknowledgements

I would like to deeply thank Prof. Dr. Angelika M. Vollmar and Prof. Dr. Stefan Zahler.

Ms. Vollmar, thank you for giving me the opportunity to perform my PhD studies in your laboratories. Your expert and excellent supervision and mentorship throughout the past years always motivated me. It was a true pleasure and honor for me to be part of your research team.

Mr. Zahler, thank you for interviewing me on the phone and give me the opportunity to come to Germany. Thank you as well for being my second examiner and for offering your time and effort to appraise this work. Your effective scientific suggestions and supportive guidance have always inspired me in my works.

Moreover, I am very grateful to my postdoctoral supervisor Dr. Johanna Liebl. Dear Hanna, thank you for great support and for your help in all kind of scientific questions, daily business problems or discussion of results. And thanks to your enthusiastic and profound efforts to finalize the fantastic projects.

I want to sincerely acknowledge the time and interest of the members of my committee: PD Dr. Dietmar E. Martin, Prof. Dr. Franz F. Paintner, PD Dr. Stylianos Michalakis, Prof. Dr. Wolfgang Frieß.

Very special thanks to the cooperation partners, who contributed to this work: Thanks to Prof. Dr. Jeremias and Dr.Michaela Grunert (Helmholtz Center of Munich) for providing leukemia patient samples. Thanks to PD Dr. Doris Mayr and Dr. Elisa Schmoeckel (Institute of Pathology, LMU, Munich) for performing tissue micro array in breast cancer patient samples.

Special thanks to my master supervisor, Prof. Dayuan Sui, who is always pushing me forward, both scientifically and personally.

Thanks to the China scholarship Council and Chinese Government Graduate Student Overseas Study Program for offering me the opportunity to study abroad and for the financial support that allows me to stay in Germany.

I thank all people in the Vollmar lab for creating such a great lab environment.

Many thanks to Lina, for contributing to the leukemia project.

Our secretary, Amélie von Thielmann, thank you for helping me looking for apartments and solving all kinds of troubles for me.

I would like to express my thanks to the wonderful TAs : Jana, Bianca, Kerstin, Rita, Frau Schnegg, all of you helped me at various stages of this work.

Sebastian, my brother, I really miss the days we sit next to each other in the lab. Thank you for being my wonderful friend and neighbor. Also, thank you for inviting me to your home in Berlin during easter holidays and being my guide around the city. You and your mother make Germany like my second home.

Michi, Flo, Sabine, Elisabeth, Sandra, Tini, Lena,Verena, Simone, Julia, Betina, Karin, Romina, thank you all, for the precious years we spent together, and you all appeared to be at my side just in the very right moment. Thanks to Henriette, for being a great friend and neighbor in the last two years.

Special thanks to my dearest girlfriend Nan, for being supportive for my work in the lab, and being good companion and always by my side.

I would like to thank my family for their indescribable support from the other side of the world. Their love and trust have always motivated me. They made what I am today.

Last but not least, I would like to thank my Chinese friends in Munich, for the great time we spent together.

8.4 Manuscript "Cdk5 controls lymphatic vessel development and function by phosphorylation of FoxC2"

Initially we were interested in the function of Cdk5 in the endothelium. We established endothelial cells-specific Cdk5 knockout mice and studied Cdk5 function *in vivo*. I participated in this project and performed a huge variety of experiments that contributed to the characterization of the phenotypes of the EC-Cdk5 knockout mice.

Here, under Dr. Johanna Liebl's permission, I attached the submitted manuscript for the paper "Cdk5 controls lymphatic vessel development and function by phosphorylation of FoxC2" as appendix in my thesis.

Cdk5 controls lymphatic vessel development and function by phosphorylation of Foxc2

Johanna Liebl[1, *], Markus Moser[2], Yan Agalarov[3], Siwei Zhang[1], Bianca Hager[1], James A. Bibb[5], Ralf H. Adams[6, 7], Friedemann Kiefer[8], Naoyuki Miura[9], Tatiana V. Petrova[3, 4], Angelika M. Vollmar[1], Stefan Zahler[1]

[1] Department of Pharmacy, Pharmaceutical Biology, Ludwig-Maximilians-University, 81377 Munich, Germany

[2] Department of Molecular Medicine, Max Planck Institute of Biochemistry, 81377 Martinsried, Germany

[3] Department of Oncology, University Hospital of Lausanne, and Department of Biochemistry, University of Lausanne, 1066 Epalinges, Switzerland

[4] Ecole Polytechnique Federale de Lausanne (EPFL), Swiss Institute for Experimental Cancer Research (ISREC), 1015 Lausanne, Switzerland

[5] Department of Psychiatry and Neurology and Neurotherapeutics, The University of Texas Southwestern Medical Center, Dallas, Texas 75390-9070, USA

[6] Department of Tissue Morphogenesis, Max Planck Institute for Molecular Biomedicine, 48149 Münster, Germany

[7] University of Münster, Faculty of Medicine, 48149 Münster, Germany

[8] Mammalian Cell Signaling Laboratory, Department of Vascular Cell Biology, Max Planck Institute for Molecular Biomedicine, 48149 Münster, Germany

[9] Department of Biochemistry, Hamamatsu University School of Medicine, 431-3192 Hamamatsu, Japan

* corresponding author

Abstract

The lymphatic system maintains tissue fluid balance, and dysfunction of lymphatic vessels and valves causes human lymphedema syndromes. Yet, our knowledge on the molecular mechanisms of lymphatic vessel development is still limited. This study demonstrates Cdk5 as essential regulator of lymphatic vessel development. Endothelial-specific Cdk5 knockdown causes congenital lymphatic dysfunction and lymphedema due to defective lymphatic vessel patterning and valve formation. We identify Foxc2 as responsible Cdk5 substrate in lymphatic vasculature, mechanistically linking Cdk5 to lymphatic development and valve morphogenesis. We present the Cdk5-Foxc2 interaction as critical regulator of lymphatic vessel development and the transcriptional network underlying lymphatic vascular remodeling.

Introduction

The lymphatic system maintains key physiological functions like tissue fluid homeostasis, immune surveillance, and uptake of dietary lipids. In consequence, the lymphatic vasculature plays a key role in various human pathologies. Lymphangiogenesis occurs in chronic inflammation and tumor dissemination, and dysfunction of lymphatic vessels causes human lymphedema syndromes [1]. Yet, our knowledge about the mechanisms regulating lymphatic vessel development and function is still limited.

Lymphatic vessel formation starts after the circulatory system has established. Lymphatic endothelial cells emerge from the cardinal veins and migrate away to form the primary lymphatic vessels, i.e. the lymph sacs, which get separated from the blood vasculature by lymphovenous valves [2-4]. Peripheral lymphatic vessels remodel into lymphatic capillaries that take up interstitial fluid and collecting lymphatic vessels that drain the lymph into the venous system. Lymphatic capillaries are blind-ending and lack mural cells, whereas collecting lymphatic vessels contain smooth muscle cell (SMC) coverage and intraluminal valves [5]. Several regulators of lymphatic vessel remodeling and valve formation have been identified,

including ephrinB2 [6], integrin-α9 [7], semaphorinA3 [8,9], Prox1 [4] and Foxc2 [10]. Yet, their molecular regulation in the lymphatic endothelium is largely unknown.

Cyclin dependent kinase 5 (Cdk5), a proline-directed serine/threonine kinase, does not drive cell cycle transitions though it belongs to the Cdk family. Since it exerts essential functions in the central nervous system (CNS) such as neuronal migration, axonal guidance, and synaptic plasticity, and has been associated with neurodegenerative and neuropsychiatric diseases, Cdk5 was supposed to be neuron-specific for a long time [11].

Recently, the awareness about extra-neuronal functions of Cdk5 has grown. Cdk5 was linked with inflammation, i.e. leukocyte activation, with obesity and insulin-resistance by phosphorylating the transcription factor PPARγ, and some reports indicate functions of Cdk5 in cancer (reviewed in [12]). In contrast, a detailed investigation of a possible function of Cdk5 in the endothelium *in vivo* is still lacking. To address this issue, we generated two endothelial specific Cdk5 knockout models as a basis for mechanistic studies on the role of Cdk5 in the vascular system, including the search for the functionally relevant endothelial substrate of Cdk5.

Results and Discussion

Phenotype of endothelial-specific Cdk5 knockout mice.

Cdk5 and its activator p35 are ubiquitously expressed in the vasculature (Supplementary Fig. S1 and S3). We disrupted the *Cdk5* gene specifically in mouse endothelium by using the Cre/loxP system with a constitutive Tie2Cre and a tamoxifen-inducible VE-Cadherin Cdh5(PAC)-CreERT2 transgene [13] (Supplementary Fig. S2 and S3). Loss of Cdk5 in the mouse endothelium resulted in postnatal lethality with more than 40% of mice dying during the first two days after birth or at the age of 3-4 weeks after weaning (Fig. 1a). Born $Cdk5^{fl/fl}$Tie2Cre mice showed reduced size and body weight (Fig. 1b,c) and we observed frequent bleedings (Fig. 1d, Supplementary Fig. S2e). Instead of expected 25%, only 15% of

progeny had the Cdk5$^{fl/fl}$Tie2Cre genotype (Fig. 1e), suggesting embryonic lethality. Indeed, endothelial-specific Cdk5 knockout embryos died from E16.5 onwards. They showed blood-filled dilated tortuous vessels extending from the jugular region towards the abdominal area, bleedings especially prevalent in jugular regions and edema formation (Fig. 1f-h), indicating severe lymphatic vessel defects. Cdk5 protein levels were attenuated in lymphatic endothelial cells (LECs) and blood vessel endothelial cells (BECs) of Cdk5$^{fl/fl}$Tie2Cre embryos (Fig. 1i). The Tie2 promoter is active both in endothelial cells and some hematopoietic cells such as monocytes or macrophages [14]. In addition, functions of Cdk5 in the hematopoietic system have been reported, including an implication of Cdk5 in T-cell activation and experimental autoimmune encephalomyelitis [15] or an involvement of Cdk5 in hematopoietic cell differentiation [16-18]. To confirm the role of Cdk5 in endothelial cells, we used a VE-Cadherin (VEC) Cre driver line, i.e. the tamoxifen-inducible Cdh5(PAC)-CreERT2 line. Cdk5$^{fl/fl}$Cdh5(PAC)-CreERT2 (Cdk5$^{fl/fl}$VECCre) embryos from tamoxifen-treated mothers show a highly similar phenotype as embryos with Cdk5$^{fl/fl}$Tie2Cre genotype (Fig. 1f,g), demonstrating an endothelial cell autonomous function of Cdk5. To assess the effect of more prevalent loss of Cdk5 in the endothelium, we derived mice in which one Cdk5 allele was constitutively deleted (Δ) and the remaining allele was floxed (fl) (Fig. 1h,j). Indeed, embryos with Cdk5$^{\Delta/fl}$Tie2Cre genotype died at E15.5, with blood-filled dilated tortuous vessels, hemorrhaging and edema formation (Fig. 1h). Thus, more pronounced loss of Cdk5 resulted in more severe lymphatic deficiencies. In summary, the similarity of the phenotypes of endothelial Cdk5 knockdown mice achieved by different Cre driver lines indicates a specific and essential function of endothelial Cdk5 for lymphatic vessel development.

Knockdown of Cdk5 in the endothelium leads to lymphatic vessel dysfunction.

EC-specific Cdk5 knockout embryos exhibited markedly dilated vessels that were of lymphatic origin as they expressed Lyve1, but contained blood cells, demonstrating a persisting connection between lymphatic and blood vessels (Fig. 2a and Supplementary Fig. S5a,b). Also the primary lymph sacs of Cdk5$^{fl/fl}$Tie2Cre embryos were severely dilated and

filled with blood (Fig. 2b-d). Moreover, lymphatic capillaries displayed defective patterning. They were covered with ectopic SMCs, irregularly dilated and showed decreased branching (Fig. 2e-g).

In contrast to the striking lymphatic vessel defects, blood vessel morphology of $Cdk5^{fl/fl}$Tie2Cre embryos was not affected. EphrinB2 and EphB4 were expressed at comparable levels in arteries and veins of control and $Cdk5^{fl/fl}$Tie2Cre embryos and SMC coverage of blood vessels was not changed (Supplementary Fig. S4).

In consequence, our further studies focused on the lymphatic vessel phenotype of EC-specific Cdk5 knockout mice. FITC-lectin or Evans Blue was intravenously injected to study the abnormal connection of blood and lymphatic systems. The dye exclusively stained blood vessels in control, but reached large collecting lymphatic vessels in $Cdk5^{fl/fl}$Tie2Cre mice (Fig. 2h,i and Supplementary Fig. S5c). FITC-lectin or Evans blue dye did not stain subcutaneous tortuous lymphatic microvessels of $Cdk5^{fl/fl}$Tie2Cre embryos (Supplementary Fig. S5d,e) indicating that the abnormal communication was not due to anastomosis between blood and lymphatic capillaries.

The functionality of lymphatic vessels was further tested by subcutaneous injection of Evans blue at E16.5 or postnatally. The significantly impaired dye removal in $Cdk5^{fl/fl}$Tie2Cre mice demonstrated a lymphatic drainage defect (Fig. 2j,k).

Arrested lymphatic valve formation in endothelial-specific Cdk5 knockout mice.

To understand the lymphatic drainage defect, we first analyzed EC apoptosis which was not affected in $Cdk5^{fl/fl}$Tie2Cre embryos (Supplementary Fig. S6a-d). Intraluminal valves are crucial for lymphatic function and expressed Cdk5 (Fig. 3a). Stainings of skin and mesentery revealed reduced numbers of lymphatic valves and impaired lymphatic valve morphogenesis in EC-specific Cdk5 knockout embryos (Fig. 3b-j and Supplementary Fig. S7). The majority of lymphatic valve forming cells failed to reorient and form valve leaflets (Fig. 3g-j), which was especially prevalent in embryos with severe phenotypes. Moreover, quantification of Prox1 positive nuclei of lymphatic endothelial cells indicated hyperplasia of lymphatic vessels

in Cdk5$^{fl/fl}$Tie2Cre embryos (Supplementary Fig. S6e-h). In addition, we analyzed whether the role of Cdk5 in lymphatic valve formation also encompasses lymphovenous valves, which separate the primordial thoracic duct (pTD) and adjacent cardinal vein (CV) [3,4,19,20]. Three dimensional (3D) reconstructions of image stacks obtained by optical sectioning of entire wholemount immunostained E12.5 embryos showed lymphovenous valves, *i.e.* two contact sites of double layer of endothelial cells with high Prox1 expression, in control littermates and demonstrated frequent failure of lymphovenous valve formation in Cdk5$^{fl/fl}$Tie2Cre embryos (Fig. 4). To understand whether Cdk5 is also essential for valve maintenance, we postnatally deleted endothelial Cdk5 in mature valves by using tamoxifen inducible Cdh5(PAC)-CreERT2 mice. Lymphatic vessels and valves appeared normal in tamoxifen-treated Cdk5$^{fl/fl}$VECCre mice (Fig. 5a,b). In sum, our data demonstrate an indispensable endothelial cell autonomous requirement of Cdk5 for lymphatic vessel development and valve formation but not for valve maintenance.

Cdk5 controls Foxc2 transcriptional activity by phosphorylation.

Next, we aimed to understand Cdk5-driven signaling in the lymphatic vasculature. We analyzed expression of crucial LEC specific genes whose inactivation or mutation revealed lymphatic vessel phenotypes reminiscent to endothelial Cdk5 knockout embryos: the forkhead transcription factor Foxc2 [10], the O-glycoprotein podoplanin [21,22], T-synthase (T-Syn), *i.e.* a glycosyltransferase critical for the biosynthesis of O-glycans including podoplanin [23], the homeobox transcription factor Prox1 [4], Ets transcription factors Ets1 and Ets2 [24]. The transcription factors Ets1, Ets2, and Foxc2 are regulated by phosphorylation at serine/threonine residues [24,25] and therefore might be of special interest as potential Cdk5 targets. However, we did not find obvious changes in expression of Foxc2, Prox1, Ets1 and Ets2, podoplanin, or VEGFR3 (Supplementary Fig. S8). Nevertheless, the defects of Cdk5$^{fl/fl}$Tie2Cre mice - defective lymphatic vessel patterning with ectopic SMC coverage, arrested valve formation, lymphatic dysfunction and lymphedema - are in striking similarity to Foxc2 deficient mice [10]. Foxc2 is a forkhead transcription factor crucial for lymphatic vessel

development and valve formation [10,26] and is associated with human lymphedema-distichiasis [27,28]. In addition to lymphatic vessel defects, Foxc2 deficient mice show defects of aortic arch formation and skeletogenesis as well as cardiovascular defects. Foxc2-/- mice die within 10 min after birth due to respiratory defects and cyanosis, showing overall embryonic and perinatal lethality [29,30]. Thus, nevertheless, we hypothesized that Foxc2 could be the target of Cdk5 mediating its effects in the lymphatic endothelium. Foxc2 expression and electrophoretic mobility was not changed in LECs or BECs from EC-specific Cdk5 knockdown embryos (Supplementary Fig. S9a-d,i). Similar expression of Foxc2 in wildtype and global Cdk5 knockout embryos (Supplementary Fig. S9j) excluded that this was due to EC contamination with other cells. In line, Cdk5 silencing in human LECs or HUVECs only slightly reduced Foxc2 (Supplementary Fig. S9e-h,k,l). Furthermore, Cdk5 downregulation did not influence Foxc2 localization (Supplementary Fig. S9m), nor Foxc2 binding to naked DNA (Supplementary Fig. S10a,b). However, Cdk5 overexpression (Supplementary Fig. S10c) significantly increased Foxc2 reporter gene activation (Fig. 6a), suggesting that Cdk5 is required for Foxc2 transcriptional activity.

Next, we wanted to understand how Cdk5 regulates Foxc2 activity. Recently, it has been shown that Foxc2 is phosphorylated at eight conserved serine/threonine residues, essential for Foxc2-dependent transcription but a kinase that mediates Foxc2 phosphorylation *in vivo* has not been identified yet [25]. Coimmunoprecipitation of overexpressed or endogenous Cdk5 and Foxc2 indicated their direct interaction in human LECs (Fig. 6b,c). In fact, we found that recombinant Cdk5/p35 efficiently phosphorylated Foxc2 *in vitro*, which was reduced by the Cdk5 inhibitor roscovitine (Fig. 6d). Arguing that Foxc2 is a direct substrate of Cdk5, Cdk5 overexpression increased ^{32}P-phosphate incorporation into Foxc2 (Fig. 6e) whereas Cdk5 silencing reduced ^{32}P-labeled Foxc2 (Fig. 6f). Importantly, Foxc2 ^{32}P-phosphate incorporation was reduced in Cdk5$^{fl/fl}$Tie2Cre LECs *in vivo* (Fig. 6g). In sum, our data demonstrate that Cdk5 phosphorylates Foxc2.

Interestingly, Cdk5 downregulation failed to induce a change in Foxc2 electrophoretic mobility (Supplemental Fig. S9i-l), characteristic for loss of Foxc2 phosphorylation [25]. This

suggests that Cdk5 does not regulate all but only (a) specific Foxc2 phosphorylation site(s). Moreover, this indicates that Foxc2 most likely gets regulated by additional other kinases besides Cdk5, *i.e.* ERK1/2 and cell cycle Cdks, as it was previously suggested [25]. We checked whether Cdk5 collaborates with these pathways that have been associated with Foxc2 regulation, i.e. ERK1/2 and cell cycle related Cdks [25]. In $Cdk5^{fl/fl}$Tie2Cre LECs neither ERK1/2 activity or expression (Fig. 6h) nor levels of cell cycle related Cdks 1, 2, 7, 8, and 9 (Fig. 6i) were changed. This suggests that Cdk5 does not cooperate with these pathways in regulating Foxc2.

We finally aimed to assess the functional relevance of Cdk5-mediated Foxc2 phosphorylation. Whereas Cdk5 alone did not activate the Foxc2 reporter Cdk5 significantly increased wild type Foxc2-driven reporter activation, *i.e.* the Cdk5-mediated increase of Foxc2 reporter activation significantly differed from the effect of Foxc2-wt alone (Fig. 6a,j). In contrast, if Cdk5 was co-expressed with Foxc2 phosphorylation mutants – pmFoxc2 with all eight serine/threonine residues mutated to alanine and Foxc2-mutΔS219-366 that lacks the complete phosphorylation region (Supplementary Fig. S10d) - Cdk5 was not able to induce Foxc2 reporter activation, *i.e.* there was no significant difference between the Foxc2 mutants with and without Cdk5 in Foxc2 reporter activation (Fig. 6j). In line with these results, Cdk5 did not interact with Foxc2 phosphorylation mutants (Fig. 6k). This demonstrates that Cdk5-mediated phosphorylation is important for Foxc2 transcriptional activity.

Cdk5-dependent Foxc2 phosphorylation is required for Foxc2 downstream target expression.

Disruption in Cdk5-Foxc2 signaling should affect Foxc2 target gene expression. Connexin37 (Cx37) is a downstream target of Foxc2 important for lymphatic valve formation [31,32]. Similar to *Foxc2*$^{-/-}$ mice, $Cdk5^{fl/fl}$Tie2Cre mice demonstrated attenuated Cx37 expression in lymphatic vessels, but not arteries (Fig. 7a). In line, RT-qPCR analysis revealed more than 95% down-regulation of Cx37 mRNA in $Cdk5^{fl/fl}$Tie2Cre LECs but not BECs (Fig. 7b,c). Moreover, Cdk5

223 silencing decreased Cx37 mRNA and protein in hLECs (Fig. 7d,e). Prox1 and VE-cadherin
224 were analyzed as markers and confirm LEC and BEC identity (Supplementary Fig. S10e-h).
225 Foxc2 phosphorylation was shown to selectively recruit Foxc2 to chromatin, differentially
226 regulating expression of specific Foxc2 target genes [25]. Thus, next we aimed to clarify
227 whether Cdk5-mediated activation of Foxc2-dependent transcription is due to
228 phosphorylation. Therefore, we investigated the influence of Cdk5 on the expression of
229 Foxc2 target genes that have been found to be dependent or independent on Foxc2
230 phosphorylation. Corroborating our previous results, Cdk5 silencing in hLECs decreased
231 EPB41L5 and CSNK1G3, Foxc2 downstream target genes that require Foxc2
232 phosphorylation [25] (Fig. 7f,g) but did not regulate BMP4 and MEF2C, Foxc2 target genes that
233 do not depend on its phosphorylation [33] (Fig. 7h,i). Importantly, *in vivo*, EPB41L5 mRNA was
234 reduced in $Cdk5^{fl/fl}$Tie2Cre LECs (Fig. 7j). Thus, Cdk5 specifically influences expression of
235 Foxc2 target genes that depend on Foxc2 phosphorylation, demonstrating that Cdk5 controls
236 Foxc2-dependent transcription by phosphorylation. Foxc2 phosphorylation regulates its
237 chromatin recruitment only in the context on native chromatin, but not in reconstituted in vitro
238 systems [25]. Therefore, although Cdk5 did not influence Foxc2 binding to naked DNA
239 (Supplementary Fig. S10a,b), our results raise questions regarding the role of Cdk5 in the
240 interaction of Foxc2 with DNA and transcription-associated proteins.
241 Taken together, our results demonstrate that Cdk5 is essential for lymphatic vessel
242 development and valve formation. We highlight Cdk5 as important player in the
243 transcriptional control of lymphatic vessel remodeling, suggesting a function of Cdk5 in
244 linking cell signaling and gene expression in the lymphatic endothelium. Our study provides
245 the rationale for investigating CNS-related Cdk5-driven signaling in the context of lymphatic
246 vessel biology with the aim to better understand the mechanism underlying human
247 lymphedema syndromes.
248
249
250 **Materials and Methods**

EC-specific Cdk5 knockout mice

Mouse experiments were performed with approval by the District Government of Upper Bavaria in accordance with the German animal welfare and institutional guidelines. Tie2Cre mice were from Jackson Laboratory (B6.Cg-Tg(Tek-cre)12Flv/J, 004128). Floxed Cdk5 mice [34], Tamoxifen-inducible Cdh5(PAC)-CreERT2 mice [13], and deleterCre mice [35] were described. To obtain $Cdk5^{fl/fl}$Tie2Cre, $Cdk5^{fl/fl}$Cdh5(PAC)-CreERT2 ($Cdk5^{fl/fl}$VECCre), or $Cdk5^{fl/\Delta}$Tie2Cre mice, $Cdk5^{fl/fl}$ or $Cdk5^{wt/\Delta}$ females were crossed to $Cdk5^{wt/fl}$Tie2Cre or $Cdk5^{wt/fl}$VECCre males. To induce Cdk5 downregulation, pregnant mice were injected with tamoxifen (100 µl, 10 mg/ml in peanut oil) on E10.5, E11.5, E12.5 and embryos were collected at E16.5.

Primers for Genotyping: Cdk5 floxed: 5'ctgcatttctcgtccctagc3'; 5'acgcttcagagccacaatct3'. Cdk5 excised: 5'ctgcatttctcgtccctagc3'; 5'ggccctgctttgtatctctg3'. Tie2Cre: 5'gctgccacgaccaagtgacagcaatg3'; 5'gtagttattcggatcatcagctacac3'. Cdh5(PAC)-CreERT2 and deleterCre: 5'gcctgcattaccggtcgatgcaacga3'; 5'gtggcagatggcgcggcaacaccatt3'.

Tracer experiments

Evans blue (1% in PBS, E2129 Sigma) or FITC-lectin (1 mg/ml in PBS, L9381 Sigma) was injected intravenously (LV/BV separation; E16.5 embryos: periorbital sinus, 3 µl; anesthesized adult mice: tail vein, 250 µl) or subcutaneously (LV function; E16.5 embryos 3 µl; anesthesized adult mice: hind paw, 100 µl). Olympus SZX7/SZ-BI30 stereomicroscope, Olympus DP25 camera, CellSens software version 1.3.

Stainings

Immunohistochemistry. For paraffin sections, tissues were fixed with 4% formalin for 24 h, left in 1%formalin, paraffin embedded, and sectioned (5 µm). For cryosections, tissues were frozen into TissueTek. 10 µm sections were prepared and fixed with formalin 4% (10 min, RT). Sections were blocked (1% BSA/PBS), incubated with primary antibodies (2h RT or o/n

4°C), washed, incubated with AlexaFluor-labeled secondary antibodies (45min, RT, Life Technologies) and Hoechst 33342 (5 µg/ml) or detection was performed using Vectastain ABC Kit and ImmPACT AEC Peroxidase Substrate Kit (Biozol), and mounted (Fluorsave Reagent, Calbiochem). For TUNEL staining, ApopTag Plus Fluorescein In Situ Apoptosis Detection Kit (S7110, Millipore) was used. Liver: 4 mice, 60 fields; brain: 4 mice, 30 fields; spinal column: 3 mice, 6 fields per genotype. Proliferating Ki67-positive cells. E16.5: 3 mice, 36 pictures; E13.5: 5 mice, at least 47 pictures per genotype.

Whole mount staining. Tissues were fixed (formalin 4%, 30min, RT or methanol 5min, -20°C), washed, blocked (1h, RT, 0.5% TritonX, 2% BSA/PBS), incubated with primary antibodies (o/n, 4°C), washed, incubated with AlexaFluor-labeled secondary antibodies (2h, RT), and mounted. Valve analysis was done in back skin and intestines of E16.5 and E18.5 embryos [31]. E16.5: 9 embryos; E18.5: 5 embryos per genotype. Numbers of valves at specific stages were calculated in 10 fields (skin) or 4 mesenteric branches per embryo.

Primary antibodies: CD31 (553370, BD Pharmingen), Cdk5 (AHZ0492, Life Technologies), Connexin37 [31], endomucin (sc-65495, Santa Cruz), EphB4 (AF446, R&D Systems), ephrinB2 (AF496, R&D Systems), Ets1 (sc-350, Santa Cruz), Ets2 (sc-351, Santa Cruz), Foxc2 [31], Ki67 (ab15580, abcam), Lyve1 (ab14917, abcam), p35 (sc-820 Santa Cruz), podoplanin (sc-134483, Santa Cruz), Prox1 (AF2727, R&D Systems), α-SMA (C6198, Sigma), VEGFR3 (AF743, R&D Systems).

Pictures were taken with an Olympus BX41 microscope or with a Zeiss LSM 510 META confocal microscope. ImageJ and the particle counter plugin were used for counting.

Lymphovenous valve staining: Wholemount staining of E12.5 embryos was performed as previously described [3]. In brief, embryos were fixed (2h RT), permeabilized (0.5%TX in PBS, 4°C, 48h), blocked (1% BSA, 0.1% Tween20 in PBS, 4°C, 48h), incubated with primary antibodies (anti-Prox1, 102-PA32 Relia Tech; anti-CD31 553370 BD Biosciences; anti-VEGFR3, AF743 R&D Systems) in blocking solution (4°C, 1 week), washed (0.1% Tween in PBS, 2d), incubated with secondary antibodies (Alexa Flour, Life Technologies), and washed

306 (0.1% Tween in PBS, 2d) befor clearing with BABB. Embryos were imaged using a Leica
307 SP8 SMD confocal microscope with appropriate software.
308
309 **Isolation of mouse endothelial cells**
310 Liver sinusoidal endothelial cells (LSECs) were isolated according to manufacturer's
311 instructions (Milteny Biotech miniMACS Separation System). LECs and BECs were isolated
312 from embryo skin as described [31] and cultured with EGM2 (Lonza).
313
314 **Cell culture**
315 HUVECs were cultured as described [36]. Human telomerase-immortalized LECs (hLECs, S.
316 Geleff, University of Vienna, Vienna, Austria) [37,38] were cultivated in EGM2-MV (Lonza) and
317 HepG2 cells (ATCC) in DMEM/10% FCS.
318
319 **Cell transfection**
320 The amaxa system (Lonza) with HUVEC nucleofector kit (VPB-1002, ECs) or cell line kit T
321 (VCA-1002, HepG2) and indicated siRNAs was used [36]. Plasmids: Cdk5 (addgene 1871),
322 p35 (addgene 1347), Foxc2 [33], Foxc2-mutA8 and Foxc2-mut∆219-366 [25]. Adenoviral
323 transduction: Sirion Biotech GmbH (Martinsried, Germany).
324
325 **RT-PCR**
326 mRNA isolation was done with Qiagen RNeasy Mini Kit, reverse transcription with High-
327 Capacity cDNA Reverse Transcription Kit (Applied Biosystems), and RT-PCR with the 7300
328 Real Time PCR System. Taqman gene expression assays: BMP4 Mm00432087_m1,
329 connexin37 Hs00704917_s1 and Mm00433610_s1, Cdk5 Hs00358991_g1 and
330 Mm01134945_g1, CSNK1G3 Mm00666283_m1, EPB41L5 Mm00521096_m1, Foxc2
331 Hs00270951_s1 and Mm00546194_s1, MEF2C Mm01340842_m1, Prox1 Hs00896294_m1
332 and Mm00435969_m1, VE-cadherin Mm00486938_m1 (Applied Biosystems). GAPDH was
333 used as housekeeper.

334

335 **Immunoblotting**

336 Immunoblotting was described [36]. Primary antibodies: actin (MAB 150 1R, Chemicon), Cdk1
337 (9116, Cell Signalling), Cdk2 (sc-163, Santa Cruz), Cdk5 (AHZ0492, Life Technologies),
338 Cdk7 (2916, Cell Signalling), Cdk8 (sc-1521, Santa Cruz), Cdk9 (sc-13130, Santa Cruz),
339 ERK (p44/p42 MAPK, 9202, Cell Signalling), ERK-phspho (p44/p42 MAPK, 9206, Cell
340 Signalling), Ets1 (sc-350, Santa Cruz), Ets2 (sc-351, Santa Cruz), (Foxc2 (AF5044, R&D
341 Systems), Lyve1 (ab14917, R&D Systems), podoplanin (sc-134483, Santa Cruz), Prox1
342 (AF2727, R&D Systems), VEGFR3 (AF743, abcam).

343

344 **Immunoprecipitation**

345 After cell lysis, Cdk5 or Foxc2 antibodies were added. After incubation (o/n, 4°C), ProteinG
346 beads (50 µl per sample, P3296, Sigma) were added. After incubation (3h, 4°C), proteins
347 were extracted and subjected to immunoblotting.

348

349 **Luciferase reporter assay**

350 HepG2 cells were transfected as indicated. Luciferase plasmids were 6xFOXC2-luc-reporter
351 (firefly) [33] pGL4.74[hRluc/TK] (Renilla, Promega). Dual-Luciferase® Reporter Assay System
352 (Promega) and an Orion II Microplate Luminometer (Berthold) were used.

353

354 **Electrophoretic mobility shift assay (EMSA)**

355 EMSA was described [39]. Foxc2 oligonucleotides: 5'gatcccttaagtaaacagcatgagatc3',
356 5'gatctcatgctgtttacttaagggatc3' (Biomers).

357

358 **Kinase assay**

359 Recombinant Foxc2 (H00002303, Abnova) and Cdk5/p35 (14-477, Millipore) were incubated
360 with ^{32}P-ATP (Hartmann Analytic) with/without roscovitine (100 µM, R7772, Sigma-Aldrich).
361 SDS-PAGE and autoradiography were performed.

362

363 **Phosphate incorporation**

364 HUVECs or human LECs were transfected as indicated. Primary LECs were isolated from
365 embryo skin. 18h after transfection or isolation, cells were incubated with ^{32}P orthophosphate
366 (NEX053010MC, PerkinElmer) for 12h in phosphate-free medium (DMEM, 11971, Gibco).
367 Foxc2 immunoprecipitation, SDS-PAGE and autoradiography were performed.

368

369 **Statistics**

370 Numbers of independently performed experiments are indicated in the figure legends. Graph
371 data represent means ± SEM. Statistical analysis was performed using SigmaStat software
372 Version 3.1.

373

374

375 **Acknowledgements**

376 We thank Paul Greengard (Rockefeller University) for providing the floxed Cdk5 mice. We
377 thank Amelie Sabine for helping with valve quantification, Helene Maby-El Hajjami for the
378 LEC/BEC isolation protocol, and Cansaran Saygili for help with siRNA experiments (EPFL,
379 ISREC, University of Lausanne). We thank Ashok B. Kulkarni and Michaela Prochazkova
380 (NIH/NIDCR) for providing tissues from standard Cdk5 knockout embryos. We thank Cathrin
381 Pollmann (MPI Molecular Biomedicine, Münster, Germany) for help with lymphovenous valve
382 staining. We thank Kerstin Loske for mouse genotyping, Rita Socher and Anna Kulinyak for
383 preparing paraffin sections (Department of Pharmacy, LMU Munich). The animal facility of
384 the Department of Pharmacy, LMU Munich is gratefully acknowledged. This work was
385 supported by German Research Foundation (ZA 186/4-1, to S.Z.) and CRSII3_141811 (to
386 T.P.).

387

388

389 **Author contributions**

J.L. designed and performed experiments, analysed data and wrote the paper. M.M. designed experiments, provided deleterCre mice and wrote the paper. Y.A., S.Z. and B.H. performed experiments. J.A.B. provided floxed Cdk5 mice and wrote the paper. R.H.A. provided Cdh5(PAC)-CreERT2 mice and wrote the paper. N.M. provided anti-Foxc2 antibody. T.V.P. designed experiments and wrote the paper. A.M.V. and S.Z. supervised the project and wrote the paper.

Competing financial interests

None.

References

1. Tammela, T. & Alitalo, K. Lymphangiogenesis: Molecular mechanisms and future promise. *Cell* **140**, 460-476 (2010).
2. Yang, Y. *et al.* Lymphatic endothelial progenitors bud from the cardinal vein and intersomitic vessels in mammalian embryos. *Blood* **120**, 2340-2348 (2012).
3. Hagerling, R. *et al.* A novel multistep mechanism for initial lymphangiogenesis in mouse embryos based on ultramicroscopy. *EMBO J* **32**, 629-644 (2013).
4. Srinivasan, R. S. & Oliver, G. Prox1 dosage controls the number of lymphatic endothelial cell progenitors and the formation of the lymphovenous valves. *Genes Dev* **25**, 2187-2197 (2011).
5. Schulte-Merker, S., Sabine, A. & Petrova, T. V. Lymphatic vascular morphogenesis in development, physiology, and disease. *J Cell Biol* **193**, 607-618 (2011).
6. Makinen, T. *et al.* PDZ interaction site in ephrinB2 is required for the remodeling of lymphatic vasculature. *Genes Dev* **19**, 397-410 (2005).
7. Bazigou, E. *et al.* Integrin-alpha9 is required for fibronectin matrix assembly during lymphatic valve morphogenesis. *Dev Cell* **17**, 175-186 (2009).
8. Jurisic, G. *et al.* An unexpected role of semaphorin3a-neuropilin-1 signaling in lymphatic vessel maturation and valve formation. *Circ Res* **111**, 426-436 (2012).
9. Bouvree, K. *et al.* Semaphorin3A, Neuropilin-1, and PlexinA1 are required for lymphatic valve formation. *Circ Res* **111**, 437-445 (2012).
10. Petrova, T. V. *et al.* Defective valves and abnormal mural cell recruitment underlie lymphatic vascular failure in lymphedema distichiasis. *Nat Med* **10**, 974-981 (2004).
11. Dhavan, R. & Tsai, L. H. A decade of CDK5. *Nat Rev Mol Cell Biol* **2**, 749-759 (2001).
12. Liebl, J., Furst, R., Vollmar, A. M. & Zahler, S. Twice switched at birth: cell cycle-independent roles of the "neuron-specific" cyclin-dependent kinase 5 (Cdk5) in non-neuronal cells. *Cell Signal* **23**, 1698-1707 (2011).
13. Wang, Y. *et al.* Ephrin-B2 controls VEGF-induced angiogenesis and lymphangiogenesis. *Nature* **465**, 483-486 (2010).
14. Tang, Y., Harrington, A., Yang, X., Friesel, R. E. & Liaw, L. The contribution of the Tie2+ lineage to primitive and definitive hematopoietic cells. *Genesis* **48**, 563-567 (2010).

15. Pareek, T. K. *et al.* Cyclin-dependent kinase 5 activity is required for T cell activation and induction of experimental autoimmune encephalomyelitis. *J Exp Med* **207**, 2507-2519 (2010).
16. Chen, F., Wang, Q., Wang, X. & Studzinski, G. P. Up-regulation of Egr1 by 1,25-dihydroxyvitamin D3 contributes to increased expression of p35 activator of cyclin-dependent kinase 5 and consequent onset of the terminal phase of HL60 cell differentiation. *Cancer Res* **64**, 5425-5433 (2004).
17. Studzinski, G. P. & Harrison, J. S. The neuronal cyclin-dependent kinase 5 activator p35Nck5a and Cdk5 activity in monocytic cells. *Leuk Lymphoma* **44**, 235-240 (2003).
18. Chen, F. & Studzinski, G. P. Expression of the neuronal cyclin-dependent kinase 5 activator p35Nck5a in human monocytic cells is associated with differentiation. *Blood* **97**, 3763-3767 (2001).
19. Hess, P. R. *et al.* Platelets mediate lymphovenous hemostasis to maintain blood-lymphatic separation throughout life. *J Clin Invest* **124**, 273-284 (2014).
20. Turner, C. J., Badu-Nkansah, K., Crowley, D., van der Flier, A. & Hynes, R. O. Integrin-alpha5beta1 is not required for mural cell functions during development of blood vessels but is required for lymphatic-blood vessel separation and lymphovenous valve formation. *Dev Biol* (2014).
21. Bertozzi, C. C. *et al.* Platelets regulate lymphatic vascular development through CLEC-2-SLP-76 signaling. *Blood* **116**, 661-670 (2010).
22. Uhrin, P. *et al.* Novel function for blood platelets and podoplanin in developmental separation of blood and lymphatic circulation. *Blood* **115**, 3997-4005 (2010).
23. Fu, J. *et al.* Endothelial cell O-glycan deficiency causes blood/lymphatic misconnections and consequent fatty liver disease in mice. *J Clin Invest* **118**, 3725-3737 (2008).
24. Wei, G. *et al.* Ets1 and Ets2 are required for endothelial cell survival during embryonic angiogenesis. *Blood* **114**, 1123-1130 (2009).
25. Ivanov, K. I. *et al.* Phosphorylation regulates FOXC2-mediated transcription in lymphatic endothelial cells. *Mol Cell Biol* (2013).
26. Kriederman, B. M. *et al.* FOXC2 haploinsufficient mice are a model for human autosomal dominant lymphedema-distichiasis syndrome. *Hum Mol Genet* **12**, 1179-1185 (2003).
27. Fang, J. *et al.* Mutations in FOXC2 (MFH-1), a forkhead family transcription factor, are responsible for the hereditary lymphedema-distichiasis syndrome. *Am J Hum Genet* **67**, 1382-1388 (2000).
28. Finegold, D. N. *et al.* Truncating mutations in FOXC2 cause multiple lymphedema syndromes. *Hum Mol Genet* **10**, 1185-1189 (2001).
29. Iida, K. *et al.* Essential roles of the winged helix transcription factor MFH-1 in aortic arch patterning and skeletogenesis. *Development* **124**, 4627-4638 (1997).
30. Kume, T., Jiang, H., Topczewska, J. M. & Hogan, B. L. The murine winged helix transcription factors, Foxc1 and Foxc2, are both required for cardiovascular development and somitogenesis. *Genes Dev* **15**, 2470-2482 (2001).
31. Sabine, A. *et al.* Mechanotransduction, PROX1, and FOXC2 cooperate to control connexin37 and calcineurin during lymphatic-valve formation. *Dev Cell* **22**, 430-445 (2012).
32. Kanady, J. D., Dellinger, M. T., Munger, S. J., Witte, M. H. & Simon, A. M. Connexin37 and Connexin43 deficiencies in mice disrupt lymphatic valve development and result in lymphatic disorders including lymphedema and chylothorax. *Dev Biol* **354**, 253-266 (2011).
33. Norrmen, C. *et al.* FOXC2 controls formation and maturation of lymphatic collecting vessels through cooperation with NFATc1. *J Cell Biol* **185**, 439-457 (2009).
34. Hawasli, A. H. *et al.* Cyclin-dependent kinase 5 governs learning and synaptic plasticity via control of NMDAR degradation. *Nat Neurosci* **10**, 880-886 (2007).
35. Betz, U. A., Vosshenrich, C. A., Rajewsky, K. & Muller, W. Bypass of lethality with mosaic mice generated by Cre-loxP-mediated recombination. *Curr Biol* **6**, 1307-1316 (1996).

36. Liebl, J. *et al.* Cyclin-dependent kinase 5 regulates endothelial cell migration and angiogenesis. *J Biol Chem* **285**, 35932-35943 (2010).
37. Kerjaschki, D. *et al.* Lipoxygenase mediates invasion of intrametastatic lymphatic vessels and propagates lymph node metastasis of human mammary carcinoma xenografts in mouse. *J Clin Invest* **121**, 2000-2012 (2011).
38. Schoppmann, S. F. *et al.* Telomerase-immortalized lymphatic and blood vessel endothelial cells are functionally stable and retain their lineage specificity. *Microcirculation* **11**, 261-269 (2004).
39. Furst, R. *et al.* Atrial natriuretic peptide induces mitogen-activated protein kinase phosphatase-1 in human endothelial cells via Rac1 and NAD(P)H oxidase/Nox2-activation. *Circ Res* **96**, 43-53 (2005).

Figure Legends

Figure 1. Endothelial cell specific Cdk5 knockout mice. (**a**) Impaired survival of Cdk5$^{fl/fl}$Tie2Cre mice. 40% Cdk5$^{fl/fl}$Tie2Cre mice died during the first 2 days, 75% during the first 30 days after birth. 352 mice; 54 Cdk5$^{fl/fl}$Tie2Cre mice. (**b**) Reduced size of Cdk5$^{fl/fl}$Tie2Cre mice (d11). (**c**) Reduced body weight of Cdk5$^{fl/fl}$Tie2Cre mice. *p≤0.05; n≥4 per age and genotype. (**d**) Intestinal bleedings of Cdk5$^{fl/fl}$Tie2Cre mice (d20). (**e**) Embryonic lethality of Cdk5$^{fl/fl}$Tie2Cre embryos. Percent of living Cdk5$^{fl/fl}$Tie2Cre embryos at indicated stages. (**f**-**h**) Blood-filled leaky superficial capillaries, bleedings, and edema formation in EC-specific Cdk5 knockout embryos. (**f**) E15.5 and E16.5 Cdk5$^{fl/fl}$Tie2Cre embryos. (**g**) E16.5 Cdk5$^{fl/fl}$VECCre embryos. (**h**) E15.5 Cdk5$^{\Delta/fl}$Tie2Cre embryos. (**i**) Decreased Cdk5 levels in LECs (29%) and BECs (41%) of E16.5 Cdk5$^{fl/fl}$Tie2Cre embryos. *p≤0.001; n=8 per genotype. (**j**) Decreased Cdk5 levels in LECs (7.8%) and BECs (6.4%) of E15.5 Cdk5$^{\Delta/fl}$Tie2Cre embryos. *p≤0.001; n=3 per genotype.

Figure 2. Defective lymphatic vessel (LV) development and function in EC-specific Cdk5 deficient mice. (**a**) LVs of Cdk5$^{fl/fl}$Tie2Cre embryos are dilated and contain blood cells. Staining of E16.5 transverse sections for endomucin (green, blood vessels), Lyve1 (red, LVs) and Hoechst 33342 (blue) show superficial vessels in the skin. n=5 per genotype. Scale bar 20 µm. (**b**-**d**) Primary lymph sacs (LS) of Cdk5$^{fl/fl}$Tie2Cre embryos are dilated and filled with blood. (**b**) Haematoxylin/Eosin (H/E) staining of E16.5 transverse sections at jugular regions.

Scale bar 200 µm. (**c**) Transverse sections at jugular regions of E16.5 embryos were stained for Lyve1 (red). Scale bar 100 µm. (**b**,**c**) n=6 per genotype. (**d**) Quantification of LS length and width. *p≤0.05. n=3 per genotype. (**e**-**g**) Patterning defects and ectopic SMC coverage of Cdk5$^{fl/fl}$Tie2Cre LVs. (**e**) Whole mount staining of E16.5 skin for Prox1 (green), Lyve1 (blue), α-SMA (red). Scale bar 100 µm. (**f**) LV dilation of Cdk5$^{fl/fl}$Tie2Cre embryos indicated by an increased LV area. (**g**) Decreased LV branching of Cdk5$^{fl/fl}$Tie2Cre embryos. (**f,g**) *p≤0.01. n=9 per genotype. (**h**) Abnormal connection between LVs and blood vessels (BVs) in Cdk5$^{fl/fl}$Tie2Cre embryos. Intravenous injected FITC-lectin (green) exclusively stained BVs (CD31, red) of control embryos but labeled large collecting LVs (Lyve1, blue) in Cdk5$^{fl/fl}$Tie2Cre embryos. n=3 per genotype. Scale bar 20 µm. (**i**) Communication between lymphatic and blood vessels persisted in adult mice. Intravenous injected Evans blue dye exclusively labeled arteries (A) and veins (V) in control mice. In Cdk5$^{fl/fl}$Tie2Cre mice the dye also reached collecting mesenteric LVs (L). n=3 per genotype. Age: d20-25. Scale bar 2 mm. (**j**,**k**) Impaired LV draining function in Cdk5$^{fl/fl}$Tie2Cre mice. (**j**) Subcutaneously injected Evans blue was not removed from the injection site (asteriscs) in E16.5 Cdk5$^{fl/fl}$Tie2Cre embryos. n=3 per genotype. Scale bar 0.5 mm. (**k**) Subcutaneously injected Evans blue (hind paw) was not drained away from the injection site in Cdk5$^{fl/fl}$Tie2Cre mice, but labels tortuous LVs. n=3 per genotype. Age: d20-25. Scale bar 1 mm.

Figure 3. Defective lymphatic valve formation and maturation in endothelial-specific Cdk5 knockout embryos. (**a**) Cdk5 expression in lymphatic valves. Whole mount stainings of E18.5 mesenteric vessels show colocalization of Cdk5 (green) and Prox1 (red) (arrowheads). n=3. (**b**) Schematic illustration of the stages of lymphatic valve morphogenesis according to [31]. Stage 1: Initiation of lymphatic valve formation. LEC clusters express high levels of Prox1. Stage 2: Ring-like valve structures of Prox1-high-expressing LECs are established. Stage 3: Leaflet formation starts by invagination of cells into the lumen. (**c**-**f**) Cdk5 controls lymphatic valve formation. Stainings of (**c**) skin and (**d**) mesenteric vessels of E16.5 embryos for Prox1 (green), Foxc2 (blue) and α-SMA (red). Valve stages are indicated

549 by numbers. n=9 per genotype. Scale bar 50 µm. (**e**,**f**) Quantification of valves at specific
550 stages in E16.5 embryos. n=9 per genotype. Percentage of valves in respective stages are
551 indicated. (**e**) skin; *p≤0.001. (**f**) mesenteric vessels; *p≤0.001. (**g**-**j**) Cdk5 controls lymphatic
552 valve maturation. Stainings of (**g**) skin and (**h**) mesenteric vessels of E18.5 embryos for
553 Prox1 (green), Foxc2 (blue) and α-SMA (red). Valve stages are indicated by numbers. n=5
554 per genotype. Scale bar 50 µm. (**i**,**j**) Quantification of valves at specific stages in E18.5
555 embryos. Impaired valve maturation is indicated by reduced numbers of valves at stages 2
556 and 3. (**i**) skin; total *p≤0.05; stage 2 *p≤0.001; stage 3 *p≤0.05. (**j**) mesenteric vessels; total
557 *p≤0.05; stage 2 *p≤0.001; stage 3 *p≤0.05. (**i**,**j**) n=5 per genotype. Percentage of valves in
558 respective stages are indicated.
559
560 **Figure 4. Endothelial Cdk5 knockout embryos frequently show impaired**
561 **lymphovenous valve formation.** Sagittal views of control and Cdk5$^{fl/fl}$Tie2Cre embryos
562 (E12.5) wholemount immunostained for CD31 (green), VEGFR3 (blue) and PROX1 (red) are
563 shown (left panels). Two contact sites between pTD and CV that express high levels of
564 Prox1 indicate lymphovenous valves (arrowheads). Individual optical sections (right panels)
565 through the contact area of pTD and CV are shown. In the control, two areas with a double
566 layer of endothelial cells that express high levels of Prox1 indicate lymphovenous valves
567 (arrowheads). control: n=4. 3 out of 5 analyzed Cdk5$^{fl/fl}$Tie2Cre embryos showed defects in
568 lymphovenous valve formation.
569
570 **Figure 5. Cdk5 is not essential for valve maintenance.** (**a**) Normal lymphatic vessels in
571 postnatally induced endothelial Cdk5 knockout mice. Mesentery of d10 control and
572 Cdk5$^{fl/fl}$VECCre pups treated with tamoxifen (d1-d3). Lymphatic vessel (L), artery (A) and
573 vein (V) are indicated. n=2 per genotype. Scale bar 2 mm. (**b**) Normal lymphatic valves in
574 postnatally induced endothelial Cdk5 knockout mice. Staining of mesentery of d10 control
575 and Cdk5$^{fl/fl}$VECCre pups for Prox1 (green) and α-SMA (red). n=2 per genotype. Scale bar
576 50 µm.

577

578 **Figure 6. Cdk5 controls Foxc2 by phosphorylation.** (**a**) Cdk5 activates the Foxc2
579 luciferase reporter. Foxc2 reporter activity was analyzed after cotransfection of HepG2 cells
580 with empty vector, Foxc2, Cdk5/p35, or Foxc2 and Cdk5/p35. *p<0.05. n=5. (**b**,**c**) Interaction
581 of Cdk5 and Foxc2. Immunoprecipitations of Foxc2, Cdk5, and IgG of (**b**) hLECs
582 overexpressing Foxc2 and Cdk5/p35 or (**c**) untreated hLECs. (B,C) n=3. IP:
583 immunoprecipitation. SN: supernatant. (**d**) Cdk5 phosphorylates Foxc2 *in vitro*. Recombinant
584 Foxc2 and Cdk5/p35 were incubated with ^{32}P-ATP with/without the Cdk5 inhibitor roscovitine
585 (rosco, 100μM). SDS-PAGE and autoradiography were performed. n=2. (**e**-**g**) Cdk5
586 phosphorylates Foxc2 *in vivo*. (**e**) Cdk5 overexpression increases Foxc2 ^{32}P incorporation.
587 HUVECs overexpressing Foxc2 with/without Cdk5/p35. * p<0.01. n=3. (**f**) Cdk5
588 downregulation decreases Foxc2 ^{32}P incorporation. HUVECs transduced with non-targeting
589 (nt) or Cdk5 shRNA and transfected with Foxc2. *p<0.05. n=2. (**g**) Foxc2 ^{32}P incorporation in
590 E16.5 control and Cdk5$^{fl/fl}$Tie2Cre LECs. *p<0.05, n=3 per genotype. (**h**) Phosphorylated
591 ERK (pERK) and ERK are not changed in E16.5 Cdk5$^{fl/fl}$Tie2Cre LECs. n=2 per genotype. (**i**)
592 Levels of Cdks1, 2, 7, 8, 9 are not changed by Cdk5 silencing in hLECs. (**j**) Cdk5-mediated
593 phosphorylation controls Foxc2 transcriptional activity. Foxc2 reporter gene activity was
594 analyzed after cotransfection of HepG2 cells with empty vector, Foxc2, pmFoxc2, or Foxc2-
595 mutΔS219-366 (Foxc2-Δ), with/without Cdk5/p35. Cdk5 induces Foxc2 reporter activation
596 when coexpressed with Foxc2. When cotransfected with Foxc2 phosphorylation mutants
597 pmFoxc2 or Foxc2-Δ, Cdk5 did not induce Foxc2 reporter activation. * p<0.001. n=4. (**k**)
598 Interaction of Cdk5 with Foxc2 and Foxc2 phosphorylation mutants. Immunoprecipitations of
599 Cdk5 (or IgG as control) from hLECs overexpressing Cdk5/p35 together with either Foxc2,
600 pmFoxc2, or Foxc2-mutΔS219-366 were performed. Cdk5 coprecipitates with Foxc2, but not
601 with pmFoxc2, or Foxc2-mutΔS219-366. n=3. IP: immunoprecipitation. SN: supernatant.

602

603 **Figure 7. Cdk5 regulates Foxc2 downstream target expression.** (**a**) The Foxc2
604 downstream target connexin37 (Cx37) is decreased in LVs (L) but not arteries (A) of

605 Cdk5$^{fl/fl}$Tie2Cre embryos. Whole mount stainings of E16.5 mesentery for Cx37 (green), Prox1
606 (blue), and α-SMA. Lower panels show high magnification pictures. n=4 per genotype. Scale
607 bars 20 µm. (**b**,**c**) Cx37 mRNA is significantly decreased in (**b**) Cdk5$^{fl/fl}$Tie2Cre LECs but not
608 (**c**) BECs. *p≤0.001. n=5 per genotype. (**d**) Cdk5 silencing decreases Cx37 mRNA in hLECs.
609 *p≤0.05. n=4. (**e**) Cdk5 silencing decreases Cx37 protein in hLECs. n=2. (**f**,**g**) Expression of
610 the Foxc2 downstream target genes EPB41L5 and CSNK1G3 is decreased in Cdk5 siRNA
611 treated hLECs. (**f**) EPB41L5 *p≤0.05. n=4. (**g**) CSNK1G3 *p≤0.05. n=5. (**h**,**i**) Expression of
612 the Foxc2 downstream target genes (**h**) BMP4 and (**I**) MEF2C is not changed in Cdk5 siRNA
613 treated hLECs. (**h**,**i**) ns not significant, each n=3. (**j**) EPB41L5 mRNA is decreased in E16.5
614 Cdk5$^{fl/fl}$Tie2Cre LECs. *p≤0.001. n=4 per genotype.
615

Figure 1

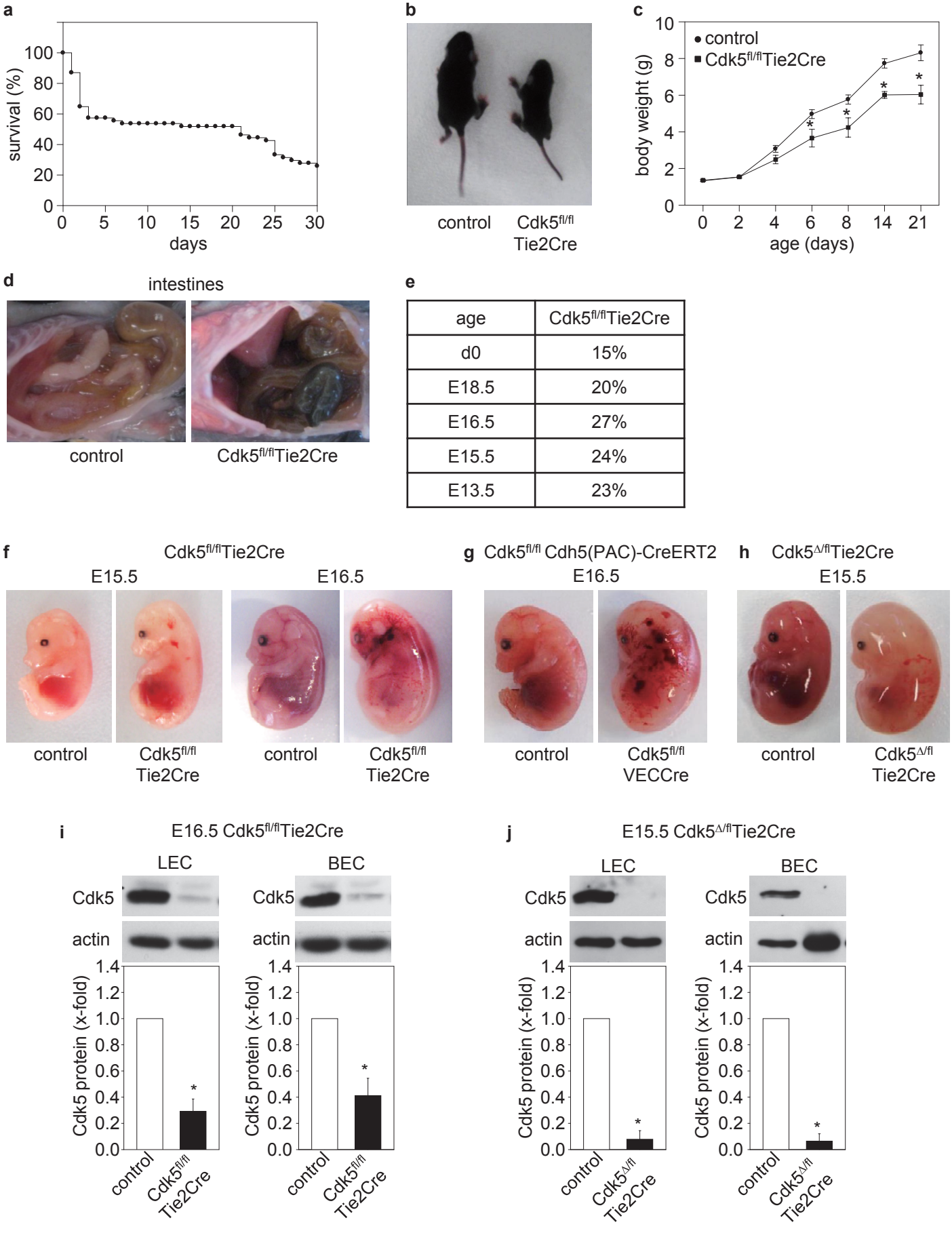

age	Cdk5fl/flTie2Cre
d0	15%
E18.5	20%
E16.5	27%
E15.5	24%
E13.5	23%

Figure 2

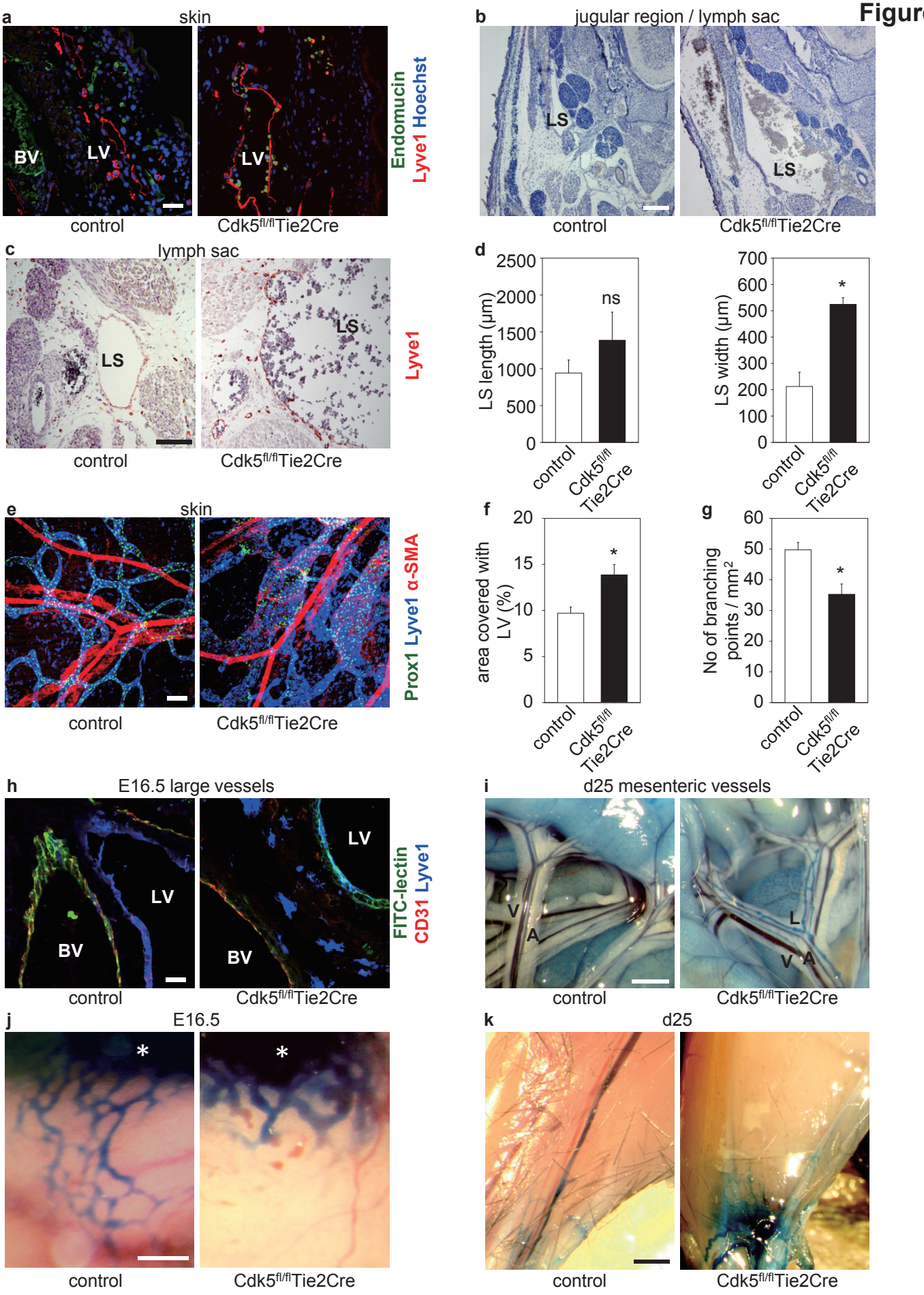
a
skin
BV
LV
LV
Endomucin
Lyve1 Hoechst
control
Cdk5fl/flTie2Cre
b
jugular region / lymph sac
LS
LS
control
Cdk5fl/flTie2Cre
c
lymph sac
LS
LS
Lyve1
control
Cdk5fl/flTie2Cre
d
LS length (µm)
2500
2000
1500
1000
500
0
ns
control
Cdk5fl/fl Tie2Cre
LS width (µm)
700
600
500
400
300
200
100
0
*
control
Cdk5fl/fl Tie2Cre
e
skin
Prox1 Lyve1 α-SMA
control
Cdk5fl/flTie2Cre
f
area covered with LV (%)
20
15
10
5
0
*
control
Cdk5fl/fl Tie2Cre
g
No of branching points / mm2
60
50
40
30
20
10
0
*
control
Cdk5fl/fl Tie2Cre
h
E16.5 large vessels
LV
LV
BV
BV
FITC-lectin
CD31 Lyve1
control
Cdk5fl/flTie2Cre
i
d25 mesenteric vessels
V
A
L
V A
control
Cdk5fl/flTie2Cre
j
E16.5
*
*
control
Cdk5fl/flTie2Cre
k
d25
control
Cdk5fl/flTie2Cre

Figure 3

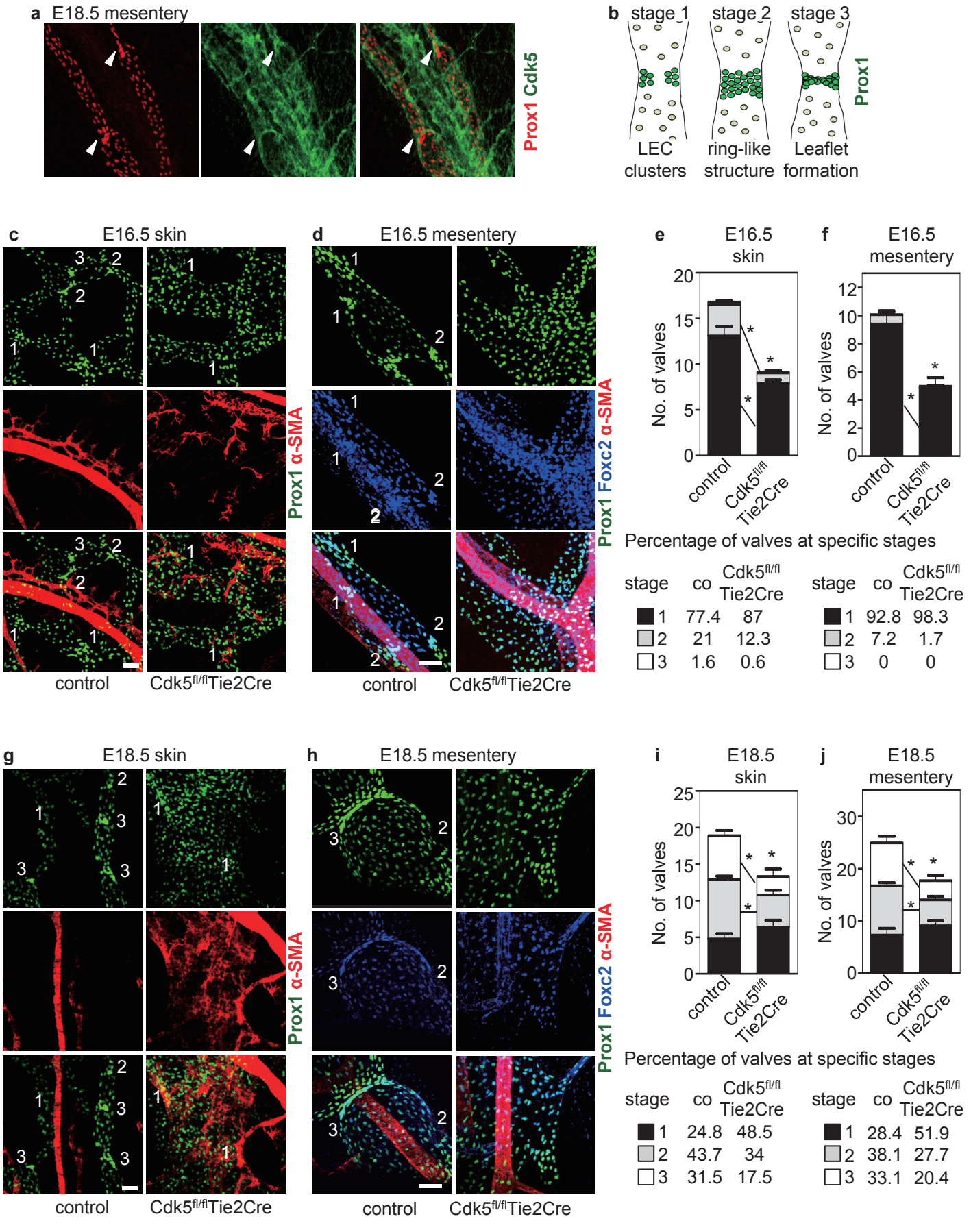
a E18.5 mesentery
Prox1 Cdk5
b stage 1
stage 2
stage 3
Prox1
LEC clusters
ring-like structure
Leaflet formation
c E16.5 skin
Prox1 α-SMA
control
Cdk5fl/flTie2Cre
d E16.5 mesentery
Prox1 Foxc2 α-SMA
control
Cdk5fl/flTie2Cre
e E16.5 skin
No. of valves
control
Cdk5fl/fl Tie2Cre
f E16.5 mesentery
No. of valves
control
Cdk5fl/fl Tie2Cre
Percentage of valves at specific stages
stage co Cdk5fl/fl Tie2Cre
1 77.4 87
2 21 12.3
3 1.6 0.6
stage co Cdk5fl/fl Tie2Cre
1 92.8 98.3
2 7.2 1.7
3 0 0
g E18.5 skin
Prox1 α-SMA
control
Cdk5fl/flTie2Cre
h E18.5 mesentery
Prox1 Foxc2 α-SMA
control
Cdk5fl/flTie2Cre
i E18.5 skin
No. of valves
control
Cdk5fl/fl Tie2Cre
j E18.5 mesentery
No. of valves
control
Cdk5fl/fl Tie2Cre
Percentage of valves at specific stages
stage co Cdk5fl/fl Tie2Cre
1 24.8 48.5
2 43.7 34
3 31.5 17.5
stage co Cdk5fl/fl Tie2Cre
1 28.4 51.9
2 38.1 27.7
3 33.1 20.4

Figure 4

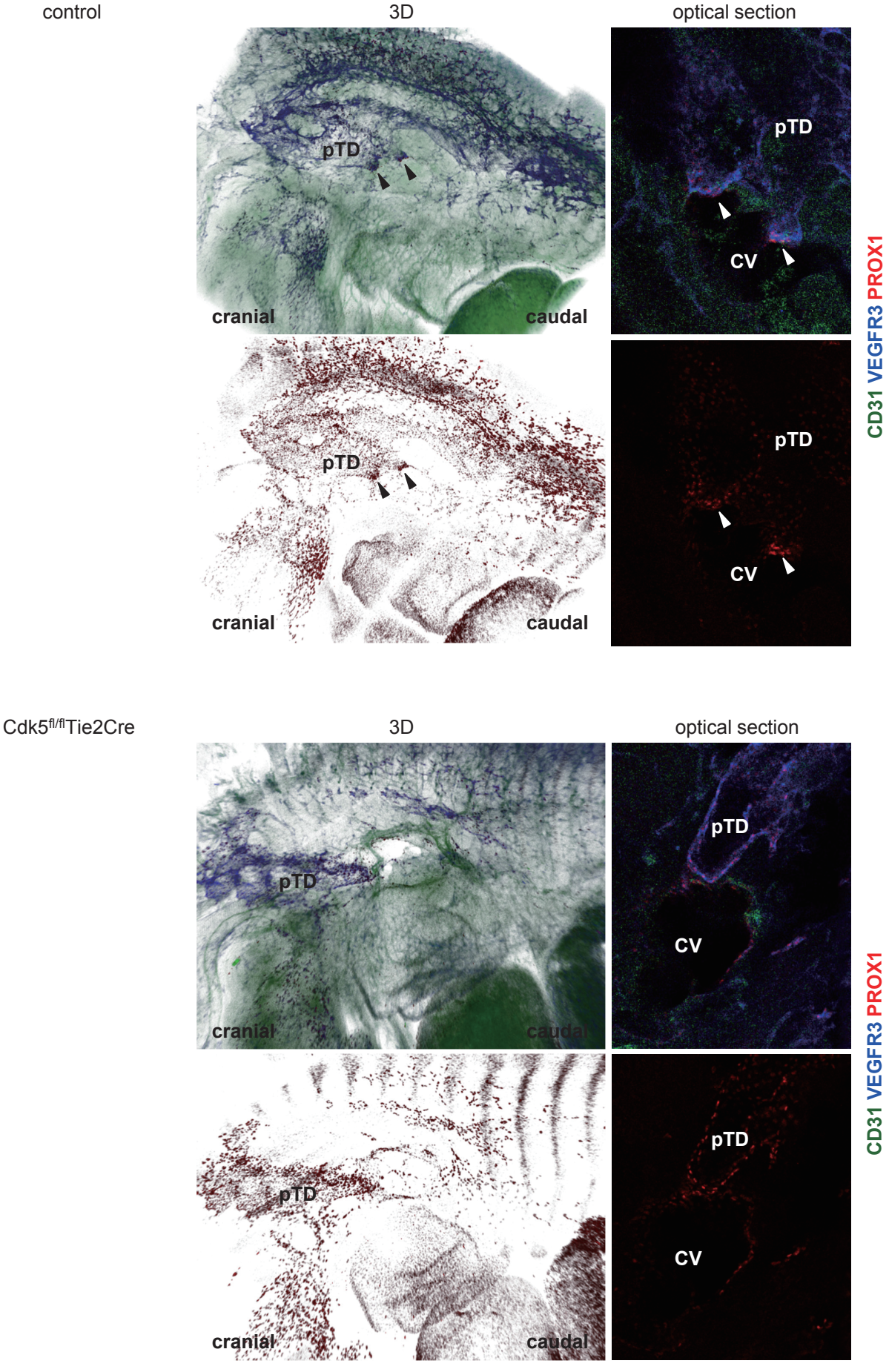
control
3D
optical section
pTD
cranial
caudal
CV
CD31 VEGFR3 PROX1
Cdk5fl/flTie2Cre
3D
optical section
pTD
cranial
caudal
CV
CD31 VEGFR3 PROX1

Figure 5

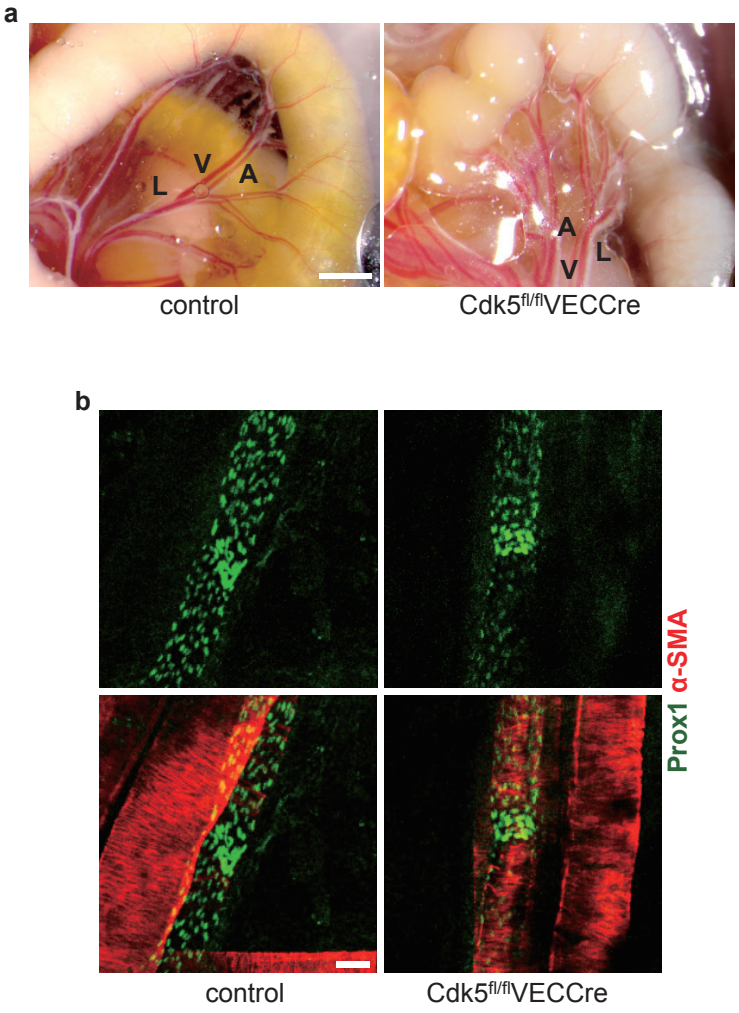
a
L
V
A
A
V
L
control
Cdk5fl/flVECCre
b
Prox1 α-SMA
control
Cdk5fl/flVECCre

Figure 6

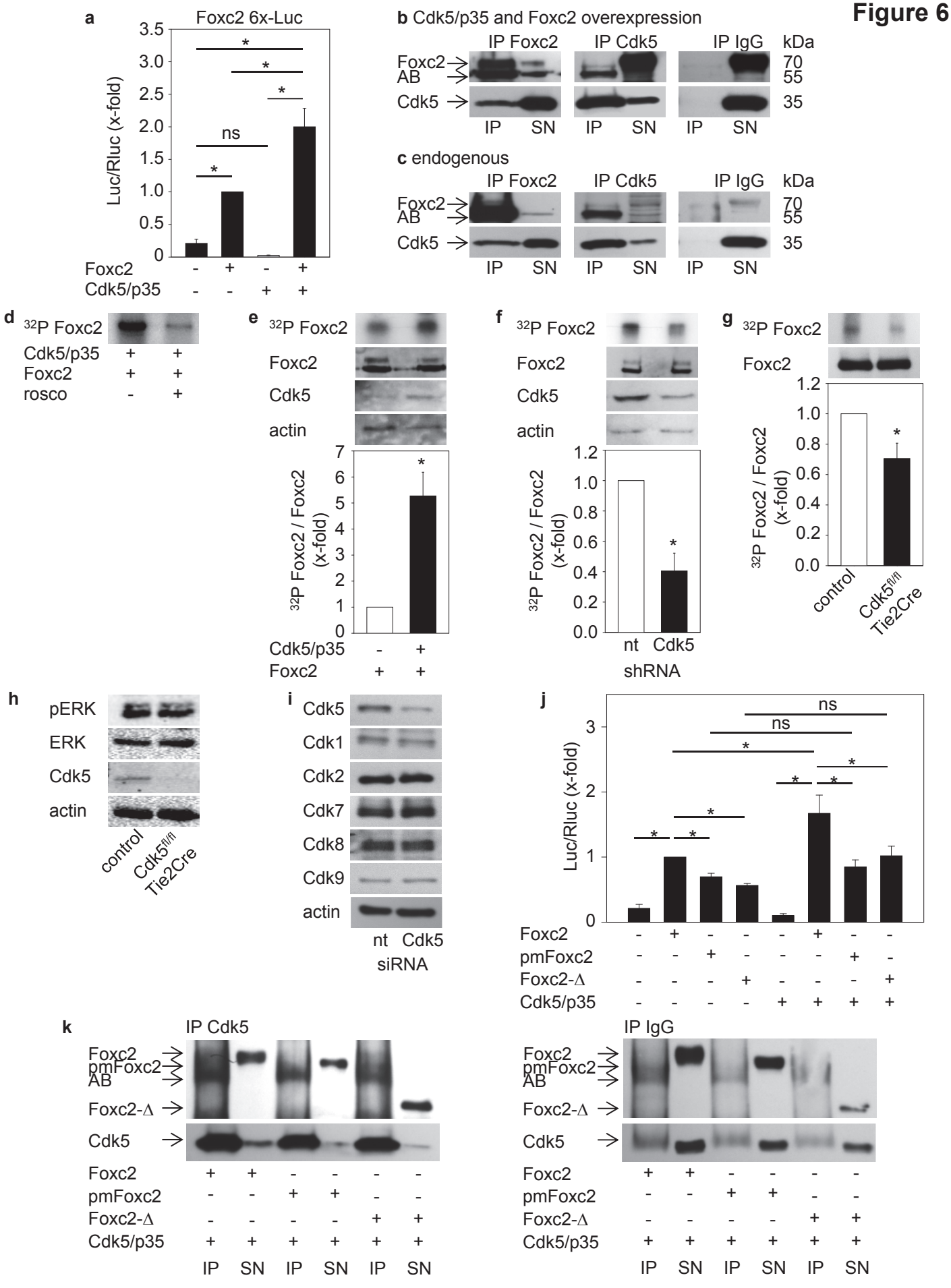
a
Foxc2 6x-Luc
Luc/Rluc (x-fold)
Foxc2
Cdk5/p35
b Cdk5/p35 and Foxc2 overexpression
IP Foxc2
IP Cdk5
IP IgG
kDa
Foxc2 AB
Cdk5
IP SN IP SN IP SN
c endogenous
d
32P Foxc2
Cdk5/p35
Foxc2
rosco
e
32P Foxc2
Foxc2
Cdk5
actin
32P Foxc2 / Foxc2 (x-fold)
f
32P Foxc2
Foxc2
Cdk5
actin
32P Foxc2 / Foxc2 (x-fold)
nt Cdk5 shRNA
g
32P Foxc2
Foxc2
32P Foxc2 / Foxc2 (x-fold)
control
Cdk5fl/fl Tie2Cre
h
pERK
ERK
Cdk5
actin
control
Cdk5fl/fl Tie2Cre
i
Cdk5
Cdk1
Cdk2
Cdk7
Cdk8
Cdk9
actin
nt Cdk5 siRNA
j
Luc/Rluc (x-fold)
ns
Foxc2
pmFoxc2
Foxc2-Δ
Cdk5/p35
k
IP Cdk5
IP IgG
Foxc2
pmFoxc2
AB
Foxc2-Δ
Cdk5
Foxc2
pmFoxc2
Foxc2-Δ
Cdk5/p35
IP SN IP SN IP SN

Figure 7

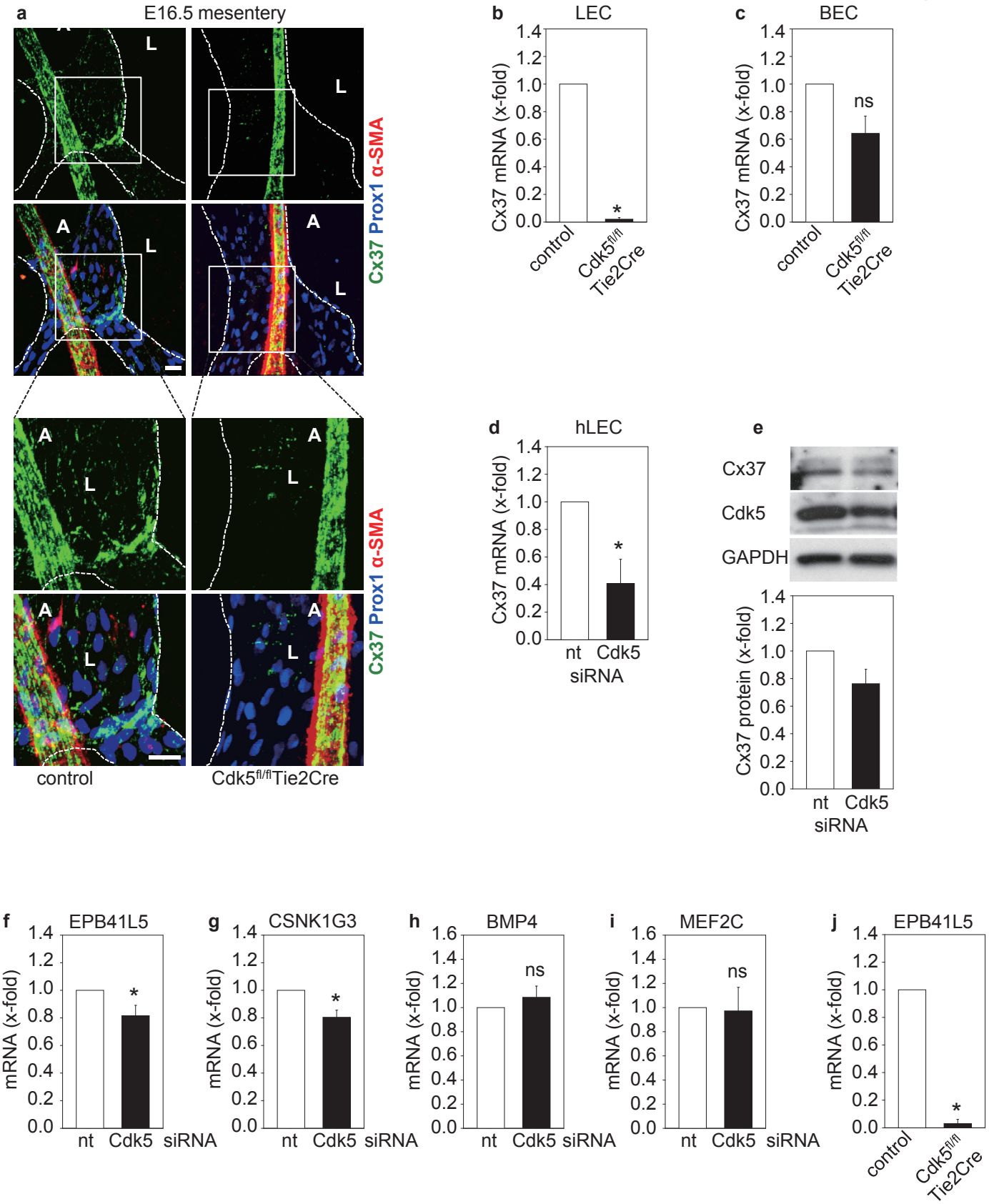
a
E16.5 mesentery
L
A
Cx37 Prox1 α-SMA
control
Cdk5fl/flTie2Cre
b
LEC
Cx37 mRNA (x-fold)
control
Cdk5fl/fl Tie2Cre
c
BEC
ns
d
hLEC
nt Cdk5 siRNA
e
Cx37
Cdk5
GAPDH
Cx37 protein (x-fold)
f
EPB41L5
g
CSNK1G3
h
BMP4
i
MEF2C
j
EPB41L5
mRNA (x-fold)

Supplementary Figure Legends

Supplementary Figure S1. Expression of Cdk5 in the mouse endothelium. (**a**,**b**) Cdk5 is ubiquitously expressed in the endothelium. Transverse sections of E16.5 embryos were stained for Cdk5 (green) and CD31 (red) or Lyve1 (red). Cdk5 is expressed in endothelial cells of (**a**) large arteries, veins, blood vessel capillaries (arrowheads), and (**b**) large collecting lymphatic vessels and lymphatic capillaries (arrowheads). n=3. Scale bar 20 µm. (**c**,**d**) p35 is ubiquitously expressed in the endothelium. Transverse sections of E16.5 embryos were stained for p35 (green) and CD31 (red) or VEGFR3 (red). p35 is expressed in endothelial cells of (**c**) large arteries, veins, blood vessel capillaries (arrowheads) and (**d**) lymphatic vessels. n=3.

Supplementary Figure S2. Knockdown of Cdk5 in the mouse endothelium. (**a**) Gene targeting strategy. (**b**) PCR genotyping of Cdk5 wildtype (wt; 392 bp) and floxed (fl; 464 bp) alleles. (**c**) Cdk5 expression is decreased in liver sinusoidal endothelial cells (LSECs) from adult endothelial-specific Cdk5 knockout mice ($Cdk5^{fl/fl}$Tie2Cre genotype). Western blots for Cdk5 and actin. *p≤0.001. n=8 per genotype. (**d**) Cdk5 expression is decreased in LSECs from adult inducible endothelial-specific Cdk5 knockout mice ($Cdk5^{fl/fl}$VECCre; $Cdk5^{fl/fl}$Cdh5(PAC)-CreERT2 genotype) after tamoxifen treatment. Western blots for Cdk5 and actin. *p≤0.01. n=5 per genotype. (**e**) Images show bleedings (arrows) in the skin and intestines of newborn $Cdk5^{fl/fl}$Tie2Cre pups.

Supplementary Figure S3. Downregulation of Cdk5 in the mouse endothelium. (**a**,**b**) Cdk5 is expressed in blood (**a**) and lymphatic (**b**) vessel ECs of control embryos and is decreased in the endothelium of $Cdk5^{fl/fl}$Tie2Cre embryos. Transverse sections of E16.5 embryos were stained for Cdk5 (green) and CD31 (red) or Lyve1 (red). Insets are presented in higher magnification on the right. n=3 per genotype. Scale bars 20 µm. (**c**) Cdk5 expression is decreased in BECs and LECs of E14.5 $Cdk5^{fl/fl}$Tie2Cre embryos. Actin indicates equal loading. n=2 per genotype.

Supplementary Figure S4. Blood vessel phenotype of endothelial Cdk5 knockout embryos. (**a**-**d**) Arterial and venous cell fate specification in Cdk5$^{fl/fl}$Tie2Cre embryos. Transverse sections of control and Cdk5$^{fl/fl}$Tie2Cre embryos at (**a**,**b**) E13.5 and (**c**,**d**) E16.5 were stained for the arterial marker ephrinB2 together with CD31 or the venous marker EphB4 and CD31. Arteries of control and Cdk5$^{fl/fl}$Tie2Cre embryos show comparable expression of ephrinB2 (**a**,**c**), veins show comparable expression of EphB4 (**b**,**d**). (**a**-**d**) n=3 per genotype each. Scale bar 20 µm. (**e**-**g**) Coverage of blood vessels with SMC is not changed in Cdk5$^{fl/fl}$Tie2Cre embryos. (**e**) Transverse sections of E13.5 embryos were stained for α-SMA and endomucin. n=3 per genotype. Scale bar 50 µm. (**f**) Transverse sections of E16.5 embryos were stained for α-SMA and endomucin. n=3 per genotype. Scale bar 50 µm. (**g**) Whole mount stainings of dorsal skin of E16.5 embryos for α-SMA and CD31. n=9 per genotype. Scale bar 50 µm.

Supplementary Figure S5. Abnormal development, non-separation, and dysfunction of lymphatic vessels in EC-specific Cdk5 deficient mice. (**a**) Dilated vessels in the skin of EC-specific Cdk5 knockout embryos. Haematoxylin/Eosin (H/E) staining of transverse paraffin sections of E16.5 embryos was performed. Scale bar 100 µm. n=6 per genotype. (**b**) Lymphatic vessels (LV) of Cdk5$^{fl/fl}$Tie2Cre embryos are dilated and contain blood cells. Staining of E16.5 transverse sections for endomucin (green, blood vessels), Lyve1 (red, lymphatic vessels) and Hoechst 33342 (blue). Large collecting lymphatic vessels of E16.5 control and Cdk5$^{fl/fl}$Tie2Cre embryos are shown. n=5 per genotype each. Scale bar 20 µm. (**c**) Abnormal connection between LVs and blood vessels (BVs) in Cdk5$^{fl/fl}$Tie2Cre embryos. Single channels referring to Fig. 2h. Intravenous injected FITC-lectin (green) exclusively stained BVs (CD31, red) of control embryos but labeled large collecting LVs (Lyve1, blue) in Cdk5$^{fl/fl}$Tie2Cre embryos. n=3 per genotype. Scale bar: 20 µm. (**d**,**e**) Superficial lymphatic capillaries of both control littermates and Cdk5$^{fl/fl}$Tie2Cre embryos are not reached by

intravenously injected (**d**) FITC-lectin (scale bar: 20 µm) or (**e**) Evans blue. Scale bar 1 mm. n=3 per genotype each.

Supplementary Figure S6. Endothelial knockdown of Cdk5 does not induce apoptosis, but leads to lymphatic vessel hyperplasia. (**a**-**d**) Apoptosis is not changed in Cdk5$^{fl/fl}$Tie2Cre mice. TUNEL staining of transverse paraffin sections of E16.5 embryos. (**a**) Staining of E16.5 skin for TUNEL (green), Collagen IV (red), Hoechst 33342 (blue). 3 mice per genotype. Staining of rat mammary gland sections served as a positive control. Scale bar 20 µm. (**b**-**d**) Numbers of TUNEL-positive cells in (**b**) liver, (**c**) brain, and (**d**) spinal column. (**b,c**) 4 mice per genotype. (**d**) 3 mice per genotype. ns: not significant. **(e-h)** Lymphatic vessel hyperplasia in endothelial Cdk5 knockout mice. Quantification of Prox1 positive cells in **(i)** E16.5 skin (t-test, *p≤0.05, n=9 per genotype) **(j)** E16.5 intestines (t-test, *p≤0.05, control: n=10, Cdk5$^{fl/fl}$Tie2Cre n=9), **(k)** E18.5 skin (ns, control: n=6, Cdk5$^{fl/fl}$Tie2Cre n=5), and **(l)** E18.5 intestines (ns, n=5 per genotype). ns: not significant.

Supplementary Figure S7. Defective lymphatic valve formation and maturation in EC-specific Cdk5 knockout embryos. (**a**-**d**) Defective valve formation and maturation in Cdk5$^{fl/fl}$Tie2Cre embryos. Staining of (**a**) E16.5 skin and (**b**) mesenteric vessels, as well as (**c**) E18.5 skin and (**d**) mesenteric vessels for Prox1 (green), Foxc2 (blue; strong phenotype) or LYVE1 (blue, mild phenotype), and α-SMA (red). Overview pictures. Scale bars 100 µm. Numbers indicate valve stages. (**a**,**b**) n=9 per genotype. (**c**,**d**) n=5 per genotype. (**e**) Defective valve formation in Cdk5$^{fl/fl}$VECCre embryos. Whole mount staining of E16.5 skin for Prox1 (green) and α-SMA (red). Scale bar 100 µm. Numbers indicate valve stages. n=2 per genotype.

Supplementary Figure S8. Expression of LEC specific genes is not influenced by Cdk5 knockdown. (**a**) Immunoblots show expression of Foxc2, Ets1, Ets2, Lyve1, Podoplanin, Prox1, and VEGFR3 in LECs from E14.5 embryos with control and Cdk5$^{fl/fl}$Tie2Cre

phenotype. n=2 per genotype. (**b**) Whole mount stainings of E16.5 mesenteries show expression of Foxc2, Ets1, Ets2, Podoplanin, Prox1, and VEGFR3 in control and $Cdk5^{fl/fl}$Tie2Cre embryos. Cdk5 is decreased in E16.5 $Cdk5^{fl/fl}$Tie2Cre embryos. Scale bar 50µm. n=2 per genotype and staining.

Supplementary Figure S9. Cdk5 does not influence Foxc2 expression. (**a**-**d**) Foxc2 mRNA is not decreased in (**a**) LECs and (**c**) BECs of E16.5 $Cdk5^{fl/fl}$Tie2Cre embryos. ns: not significant. n=5 per genotype. Decreased Cdk5 mRNA in (**b**) LECs and (**d**) BECs of E16.5 $Cdk5^{fl/fl}$Tie2Cre embryos. *p≤0.001. n=5 per genotype. (**e**,**f**) Foxc2 mRNA is slightly decreased in hLECs treated with Cdk5 siRNA. (**e**) Foxc2 mRNA. *p≤0.05. n=4. (**f**) Reduced Cdk5 mRNA. *p≤0.05. n=4. (**g**,**h**) Foxc2 mRNA is not decreased in HUVECs treated with Cdk5 siRNA. (**g**) Foxc2 mRNA. ns: not significant. n=3. (**h**) Decreased Cdk5 mRNA. *p≤0.001. n=3. (**i**) Foxc2 protein is not decreased in LECs and BECs from E16.5 $Cdk5^{fl/fl}$Tie2Cre embryos. Western blots for Lyve1 and Prox1 confirm LEC identities. Cdk5 expression is reduced. Actin indicates equal loading. Quantitative evaluation is displayed. ns: not significant. n= 4. (**j**) Foxc2 protein is not decreased in standard Cdk5 knockout embryos. Western blots for Foxc2, Cdk5 and actin (loading control) from lysates from wildtype (Cdk5+/+) and standard Cdk5 knockout (Cdk5-/-) embryos at E16.5. Quantitative evaluation is displayed. 2 embryos per genotype. (**k,l**) Cdk5 siRNA does not decrease Foxc2 protein in (**k**) hLECs and (**l**) HUVECs. Western blots for Foxc2, Cdk5, and actin are displayed. Quantitative evaluations are shown. ns: not significant. n=3 each. (**m**) Cdk5 silencing does not influence Foxc2 localization. HUVECs treated with non-targeting (nt) or Cdk5 siRNA were stained for Foxc2 (green). Hoechst33342 staining shows nuclei (blue). Scale bar 20 µm. n=2.

Supplementary Figure S10. Cdk5 does not influence binding of Foxc2 to naked DNA, but regulates Foxc2 reporter activation and target expression. (**a**,**b**) Foxc2 binding to naked DNA is not changed by Cdk5 silencing. (**a**) Foxc2 electromobility shift assays (EMSA) from HUVECs treated with non-targeting (nt) or Cdk5 siRNA. Foxc2 supershift indicates

specificity. n=5. (**b**) Transfection control: Western blots from HUVECs treated with non-targeting (nt) or Cdk5 siRNA. (**c**) Transfection control to Fig. 6a. Western blots from HepG2 cells after cotransfection with empty vector, Foxc2, or Cdk5/p35. (**d**) Transfection control to Fig. 6j. Western blots from HepG2 cells after cotransfection with empty vector, Cdk5/p35, Foxc2, pmFoxc2, or Foxc2-mutΔS219-366 (Foxc2-mutΔ). (**e**) Prox1 mRNA is decreased in LECs of $Cdk5^{fl/fl}$Tie2Cre embryos. *p≤0.01. n=5 per genotype. (**f**) Cdk5 silencing downregulates Prox1 mRNA in hLECs. Prox1 mRNA expression in hLECs treated with non-targeting (nt) or Cdk5 siRNA is shown. *p≤0.05. n=4. (**g,h**) Expression of VE-Cadherin is not changed in $Cdk5^{fl/fl}$Tie2Cre embryos. (**g**) VE-Cadherin (VEC) mRNA is not significantly reduced in E16.5 $Cdk5^{fl/fl}$Tie2Cre embryos. n=5 per genotype. (**h**) Whole mount stainings of E16.5 skin reveal no obvious change in VE-cadherin (green) expression in lymphatic vessels of $Cdk5^{fl/fl}$Tie2Cre embryos. Scale bar 20 µm. n=3 per genotype.

Supplementary Figure S1

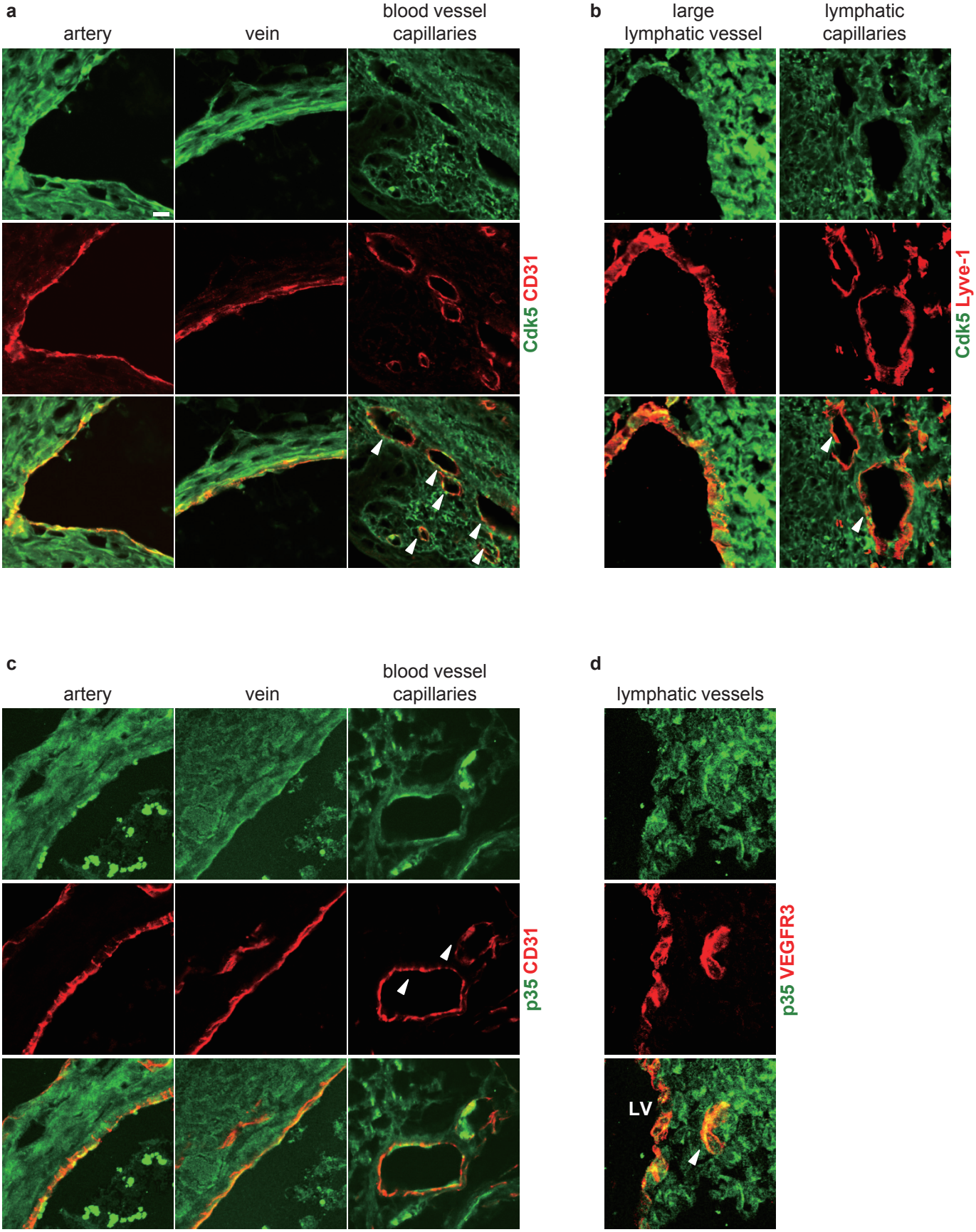

Supplementary Figure S2

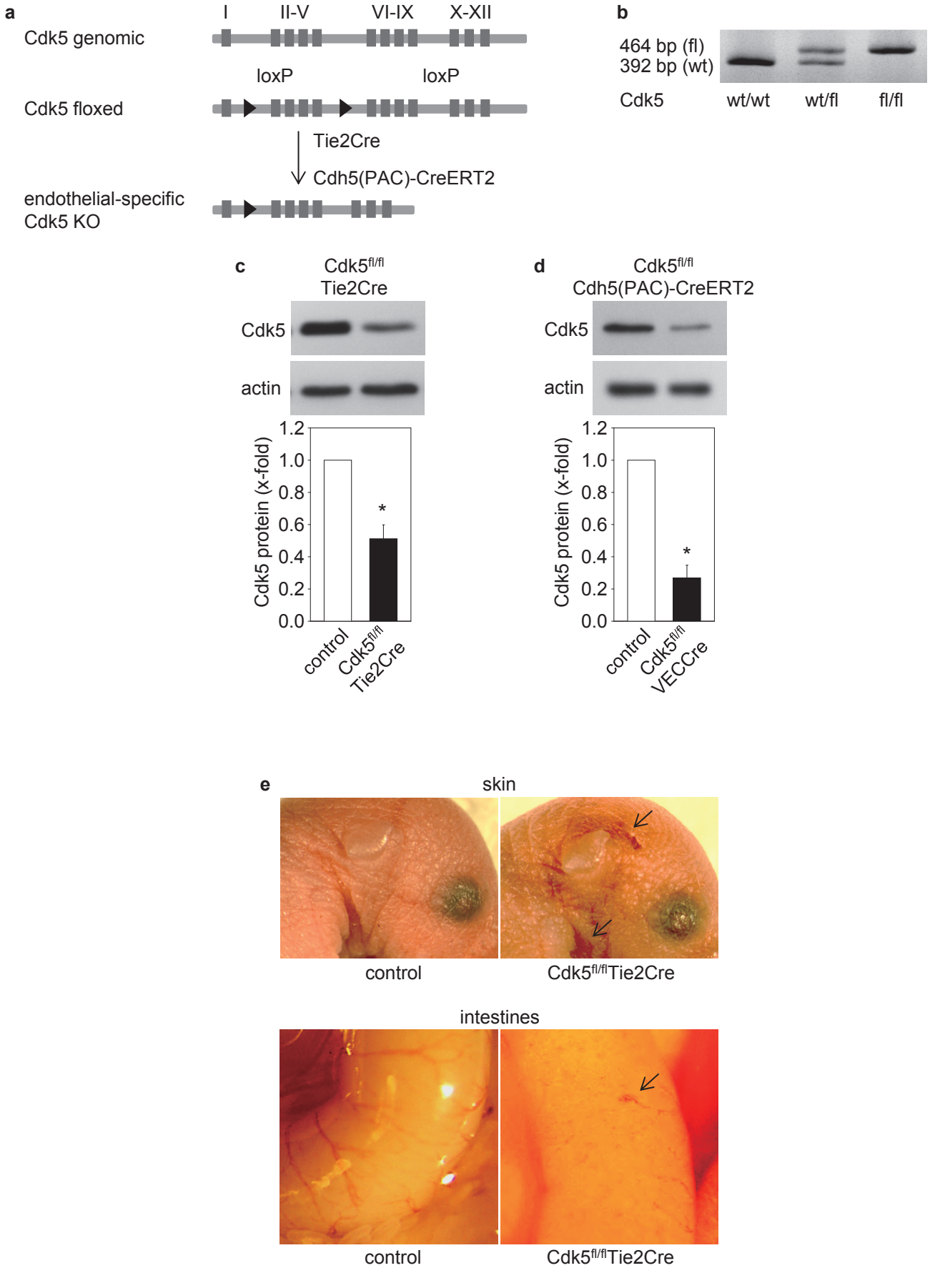

Supplementary Figure S3

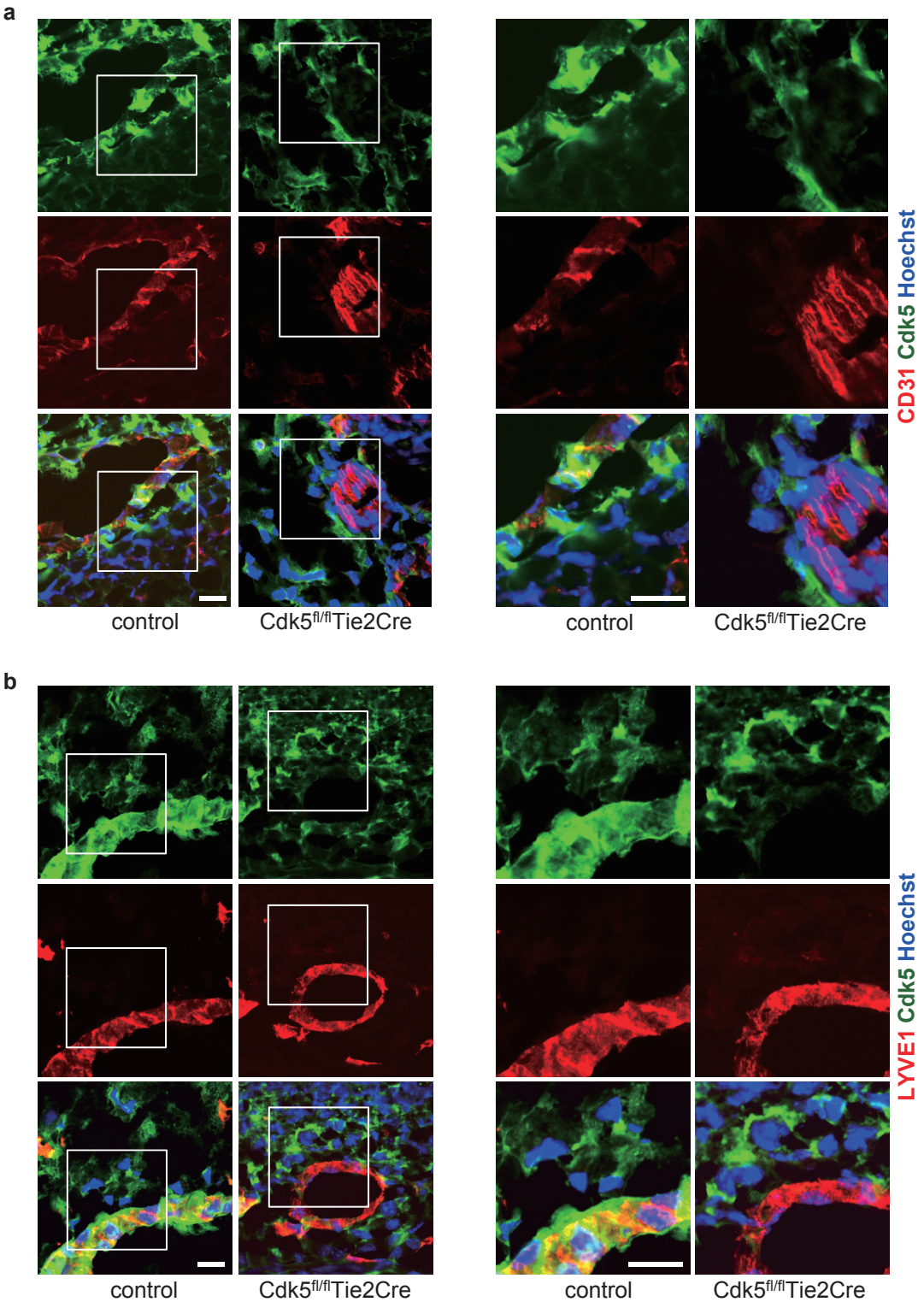

Supplementary Figure S4

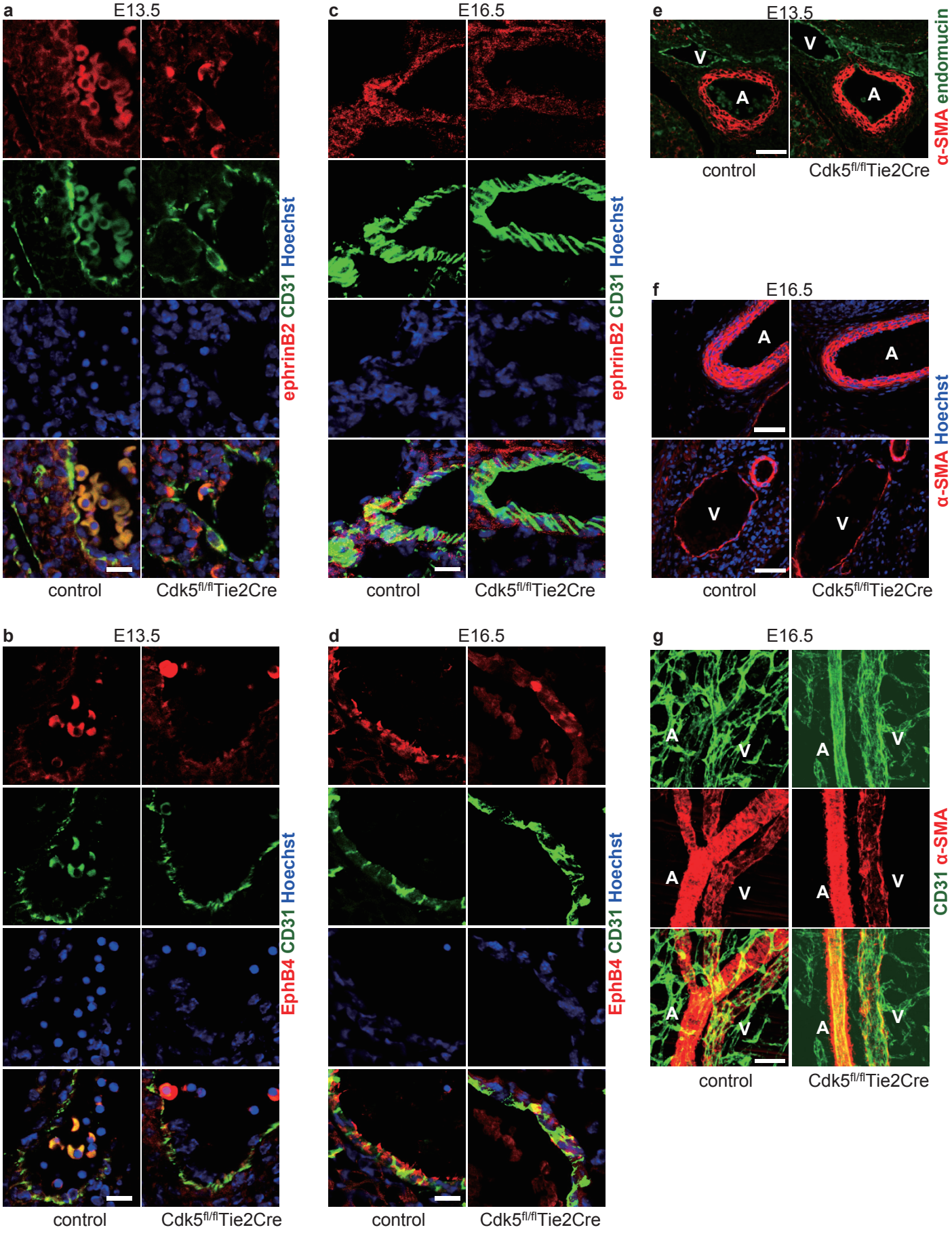

Supplementary Figure S5

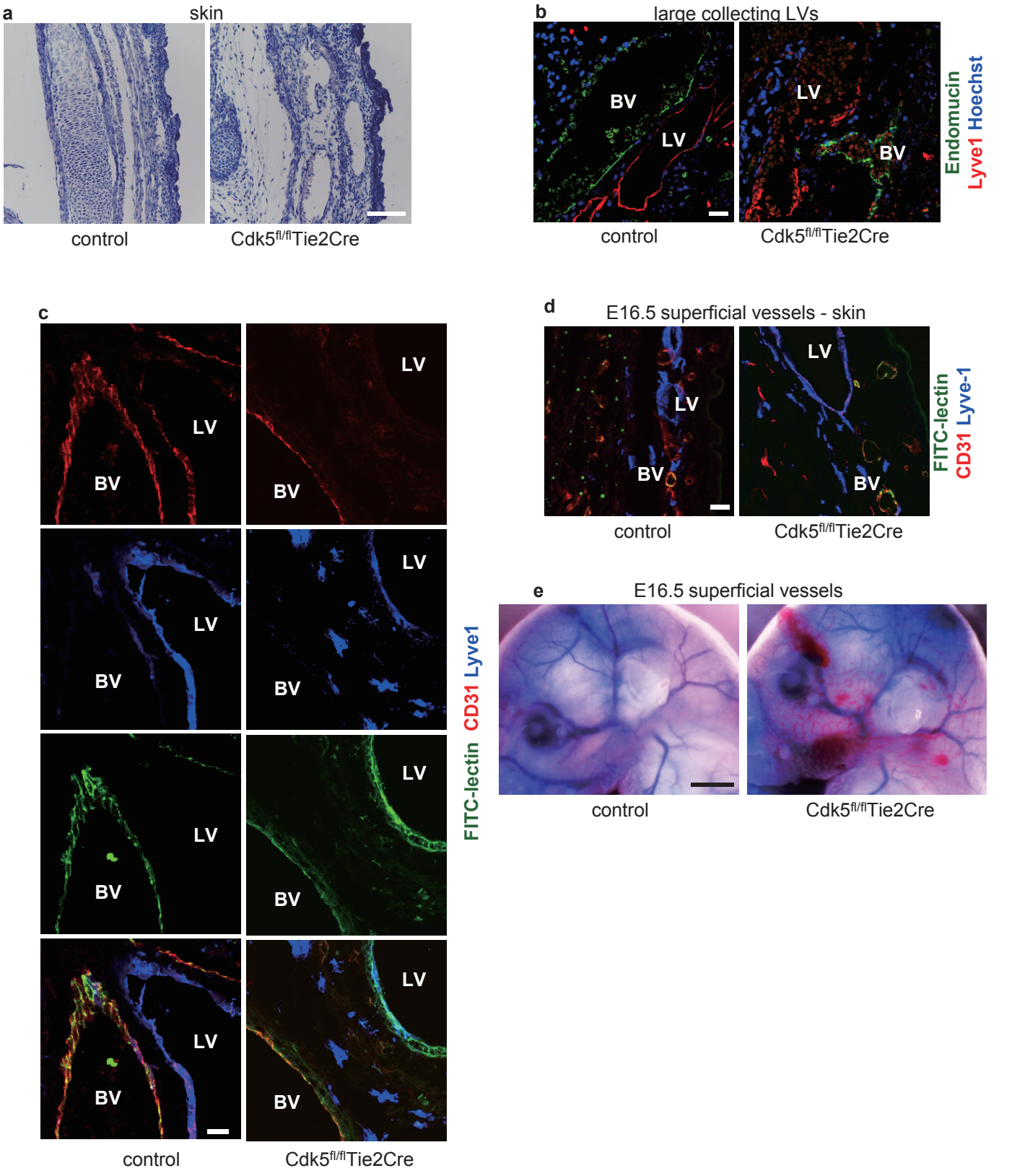

Supplementary Figure S6

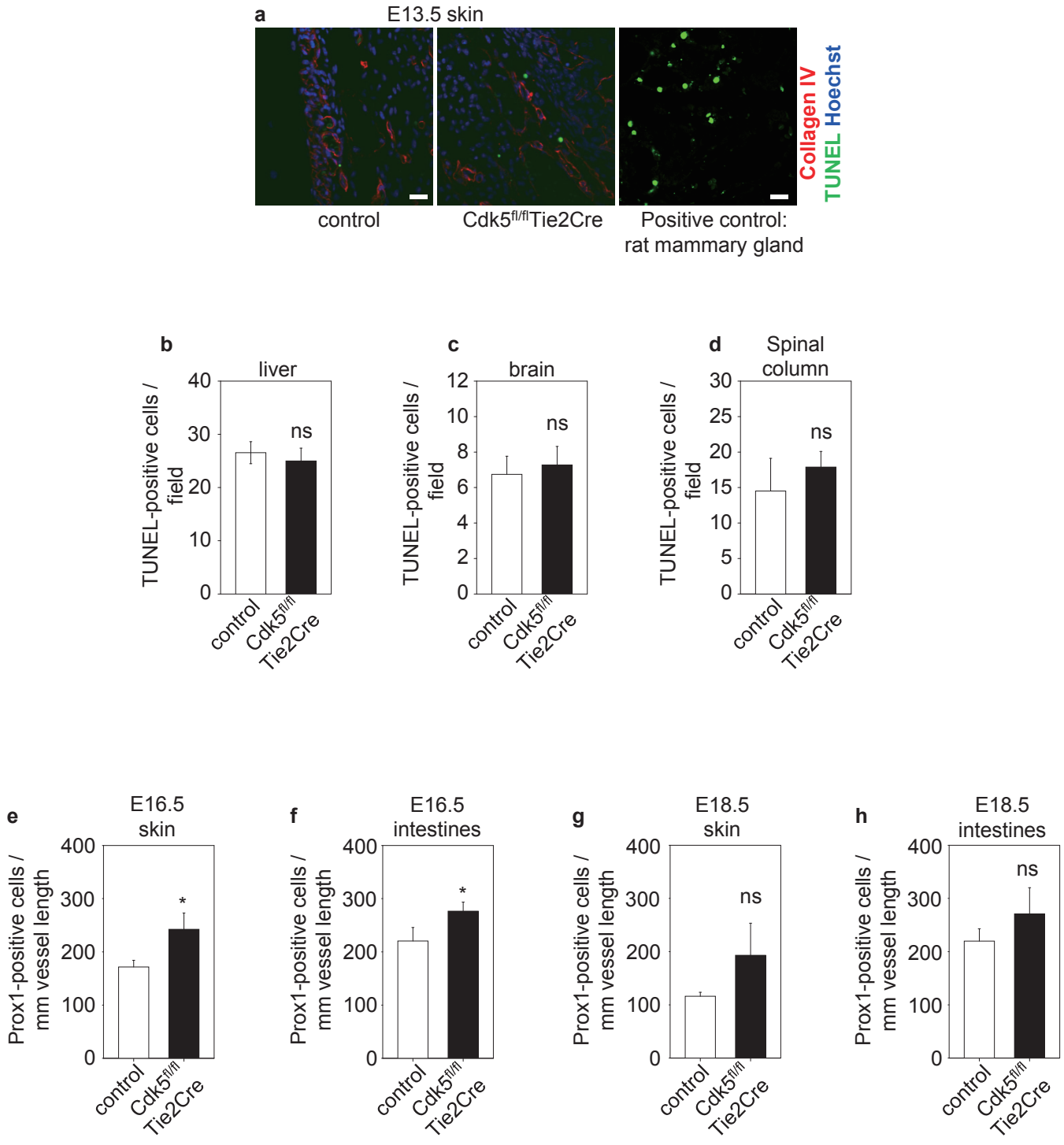

Supplementary Figure S7

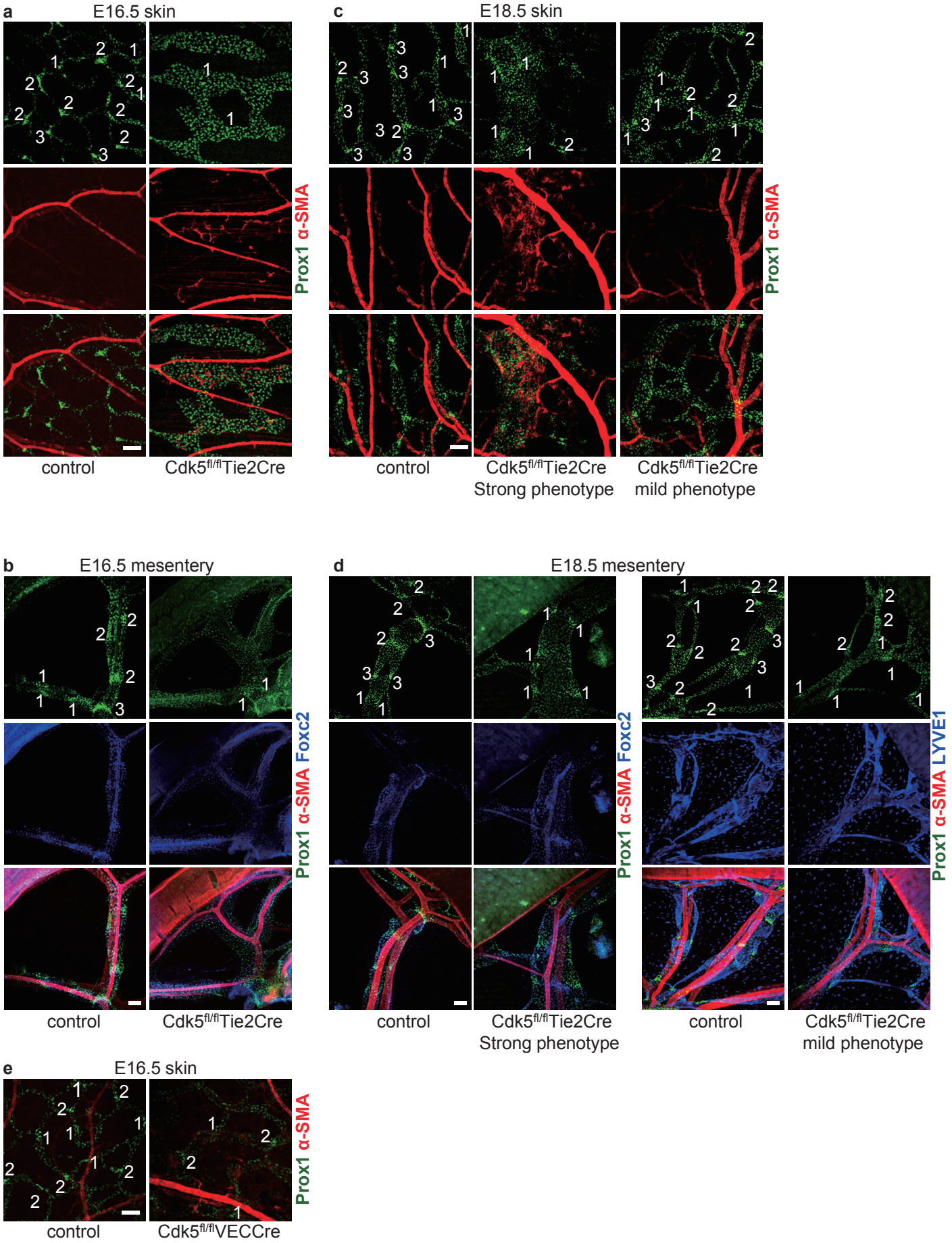

Supplementary Figure S8

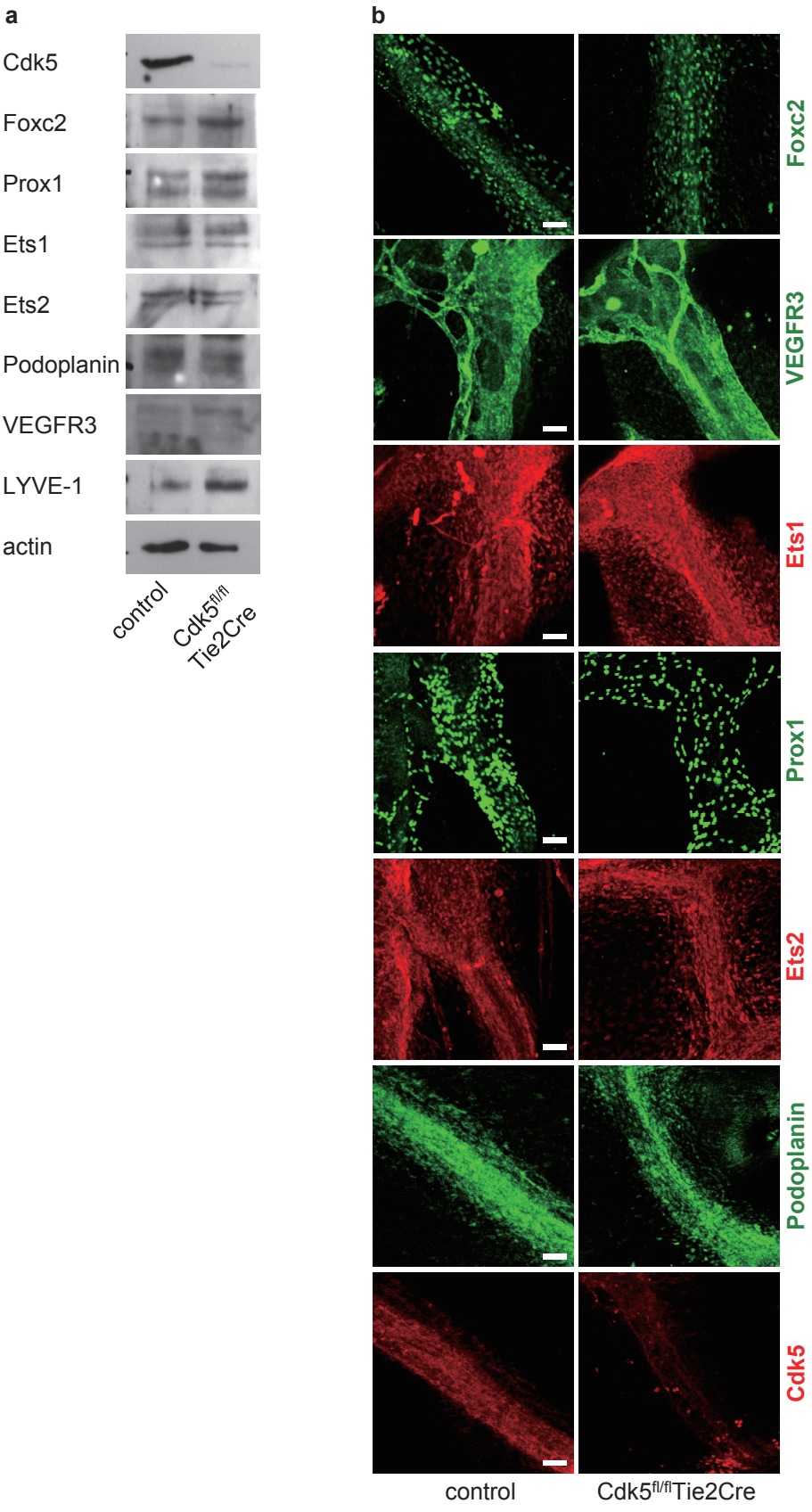

Supplementary Figure S9

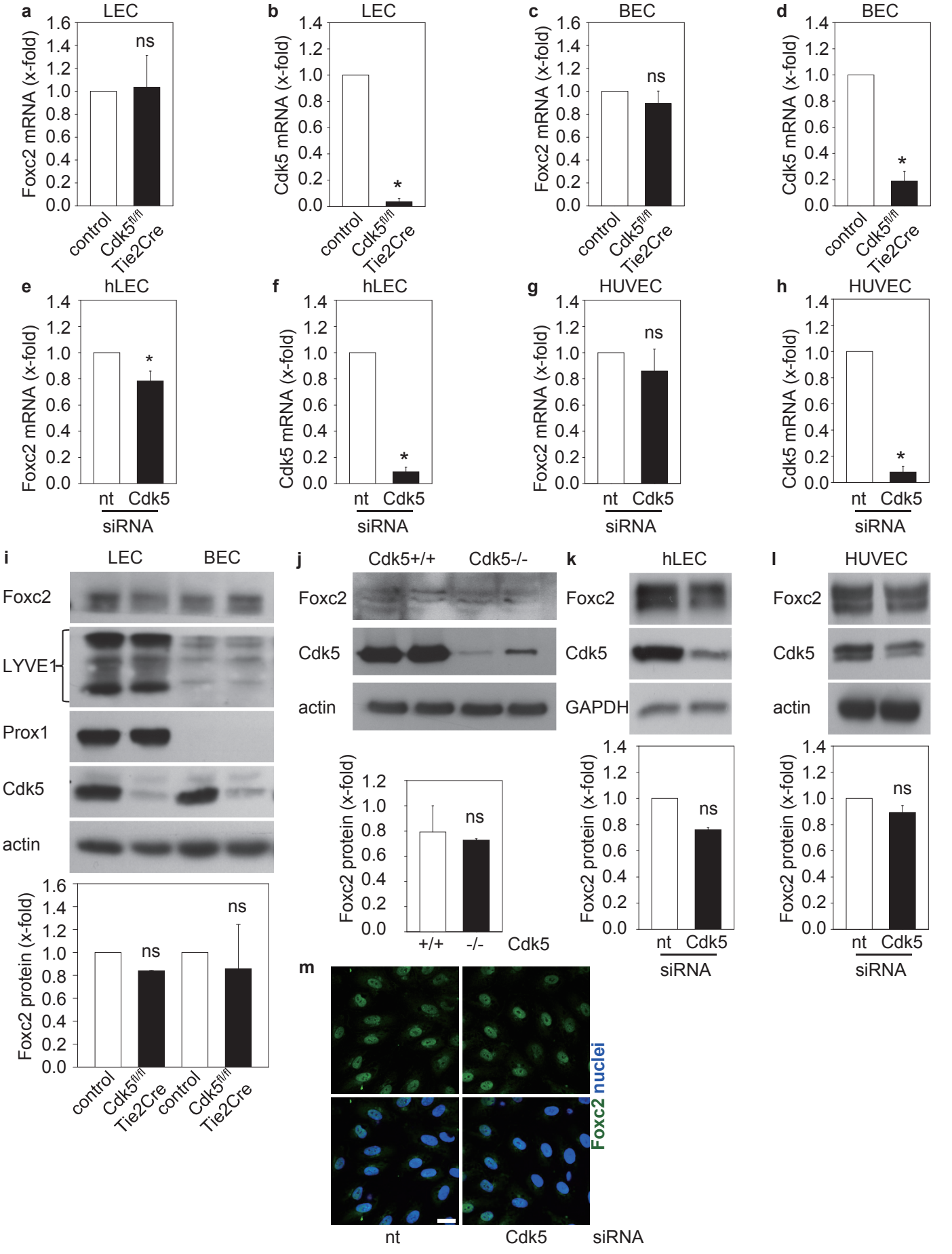

Supplementary Figure S10